Spray Pyrolysed Tin Chalcogenide Thin Films: Optimization of optoelectronic properties of SnS for possible photovoltaic application as an absorber layer

Thesis Submitted to

Cochin University of Science and Technology

in partial fulfillment of the requirements

for the award of the degree of

Doctor of Philosophy

in

Physics

by

T. H. SAJEESH

Department of Physics
Cochin University of Science and Technology
Cochin- 682 022, Kerala, India

May 2012

Spray Pyrolysed Tin Chalcogenide Thin Films: Optimization of optoelectronic properties of SnS for possible photovoltaic application as an absorber layer

Ph.D thesis in the field of Thin Film Photvoltaics

Author

T. H. Sajeesh
Thin film photovoltaic division
Department of Physics
Cochin University of Science and Technology
Cochin- 682 022, Kerala, India
E-mail : sajeeshth@gmail.com

Guide:

Dr. K. P. Vijayakumar
Professor
Cochin University of Science and Technology
Cochin- 682 022, Kerala, India
E-mail : kpv@cusat.ac.in

Department of Physics
Cochin University of Science and Technology
Cochin- 682 022, Kerala, India

May 2012

Front cover: Energy band level scheme of SnS deduced from the work, XPS depth profile pattern of SnS and Herzenbergate orthorhombic structure of SnS.

Department of Physics
Cochin University of Science and Technology
Cochin- 682 022, Kerala, India

Dr. K. P. Vijayakumar
Professor

Mob: 9847322577
E-mail : kpv@cusat.ac.in

Certificate

Certified that the work presented in this thesis entitled "Spray Pyrolysed Tin Chalcogenide Thin Films: Optimization of optoelectronic properties of SnS for possible photovoltaic application as an absorber layer" is based on the authentic record of research done by Mr. T. H. Sajeesh under my guidance in the Department of Physics, Cochin University of Science and Technology, Cochin – 682 022, India and has not been included in any other thesis submitted for the award of any degree.

Dr. K. P. Vijayakumar
(Supervising Guide)

Declaration

I hereby declare that the work presented in the thesis entitled "Spray Pyrolysed Tin Chalcogenide Thin Films : Optimization of optoelectronic properties of SnS for possible photovoltaic application as an absorber layer" is based on the original research work done by me under the guidance of Dr. K. P. Vijayakumar, Professor, Department of Physics, Cochin University of Science and Technology, Cochin – 682 022, India and has not been included in any other thesis submitted for the award of any degree.

Cochin 682 022 *T. H. Sajeesh*


Dedicated to
അച്ഛനും അമ്മയ്ക്കും.....

Acknowledgements

This dissertation would not have been possible without the guidance and the help of several individuals who in one way or another contributed and extended their valuable assistance in the preparation and completion of this study. I dedicate this page to each and everyone who helped me to explore and relish in the sea of knowledge.

First and foremost, I take immense pleasure in expressing my sincere and deep sense of gratitude to my supervising guide and mentor, Dr. K.P. Vijayakumar, Professor, Dept.of Physics, Cochin University of Science and Technology for his sustained interest, creative suggestions, motivation and exemplary guidance throughout the course of this work. I extend my profound thanks to Prof. C. Sudha Kartha for the moral support I got. I have always admired her ability to view any dilemma in true light and give right focus to work. Her suggestions and criticism helped me improve in many ways. The encouragement and ideas given by her during our lab meetings is worth mentioning here.

I extend my sincere thanks to The Head, Department of Physics, Cochin University of Science and Technology and all other former Heads of the Department for allowing me to use the facilities. I greatly acknowledge the help and guidance of all the faculty members of the Department of Physics throughout my research work.

I thank all the non-teaching office staffs of our department- present and past for the care and help extended to me.

I am grateful to Prof. Y. Kashiwaba and Abe, Department of Electrical and Electronic Engineering, Iwate University, Japan for XPS measurements and the support they have extended to me for completing my Ph.D work. I am also thankful to

Dr. K.B. Jinesh, Energy Research Institute, Nanyang Technological University for inspiring me to work in a different and interesting pace.

I would like to thank my seniors Dr. Teny Theresa John, Dr. Ratheesh Kumar, Dr. Beena Mary John, Dr. A. Sreekumar, Dr. R. Sreekumar, Dr. Kishore, Dr. Deepa, Dr. Tina Sebastian, Dr. Meril Mathew, Dr. Pramitha, Dr. Anita, and Dr. Vimalkumar for their love and support.

I would always remember with love and affection, my colleagues and juniors Mrs. Angel Susan Cherian, Mr. Rajesh M.R., Mr. Rajesh C.S, Mr. Sreeroop S.S, Mr. Subin Thomas, Mr. Subramanian V, Mr. Rajeshmon V.G, Mr. Aneesh George, Mrs. Poornima N, Mr. Anaswalih P. K, Mr. Santhosh M.V, Ms. Nithya P, Mr. Bijesh K, Ms. Jalaja M. A, Mr. Deepu D. R and Mr. Sreejith M. S for the fun filled days in this department and in the campus. Words are inadequate to thank them for the timely and invaluable support. It was very enjoyable to work with the younger generation of the lab - Ms. Gincy, Mrs. Jisha, Ms. Aswathi, Mr. Anshad, and Ms. Geethu.

I would like to name many more research scholars of this University, who had always been there to support me in this journey and whose friendship I would like to maintain for a lifetime. I fondly remember the wonderful chats we used to have at the corridors, while taking break from the research and the badminton/cricket games we used to play in the department courtyard. I especially thank all my friends in the department for going out of their way to help me out whenever I needed them.

I thank all the teachers of my school days, graduation and post-graduation for inspiring and encouraging me in all endeavours.

I greatly acknowledge Kerala State Council for Science Technology and Environment for providing fellowship for the initial two years and University Grants

Commission for providing me fellowship through RFSMS scheme for the remaining years during the course of my work.

I specially thank Mr. Anoop. V, my cousin for designing the cover page of the thesis.

My deepest gratitude goes to my family for their unflagging love and support throughout my life; this dissertation would have been simply impossible without them. I am indebted to my achan, for his care and love. As a typical father in an Indian family, he worked industriously to support the family and spared no effort to provide the best possible atmosphere for me to grow up and earn the education. He never complained in spite of all the hardships in his life. I have no suitable word that can fully describe amma's everlasting love to me. I remember her constant support when I encountered difficulties. I cannot ask for more from my vallyamma, as she is simply perfect. I also remember my brother Mr. T. H. Sandeep with affection.

There are so many others whom I may have inadvertently left out and I sincerely thank all of them for their help.

T.H. Sajeesh

Preface

In the early 19th century, industrial revolution was fuelled mainly by the development of machine based manufacturing and the increased use of coal. Later on, the focal point shifted to oil, thanks to the mass-production technology, ease of transport/storage and also the (less) environmental issues in comparison with the coal!!

By the dawn of 21st century, due to the depletion of oil reserves and pollution resulting from heavy usage of oil the demand for clean energy was on the rising edge. This ever growing demand has propelled research on photovoltaics which has emerged successful and is currently being looked up to as the only solace for meeting our present day energy requirements. The proven PV technology on commercial scale is based on silicon but the recent boom in the demand for photovoltaic modules has in turn created a shortage in supply of silicon. Also the technology is still not accessible to common man. This has onset the research and development work on moderately efficient, eco-friendly and low cost photovoltaic devices (solar cells). Thin film photovoltaic modules have made a breakthrough entry in the PV market on these grounds.

Thin films have the potential to revolutionize the present cost structure of solar cells by eliminating the use of the expensive silicon wafers that alone accounts for above 50% of total module manufacturing cost.

Well developed thin film photovoltaic technologies are based on amorphous silicon, CdTe and $CuInSe_2$. However the cell fabrication process using amorphous silicon requires handling of very toxic gases (like phosphene, silane and borane) and costly technologies for cell fabrication. In the case of other materials too, there are difficulties like maintaining stoichiometry (especially in large area films), alleged environmental hazards and high cost of indium. Hence there is an urgent need for the

development of materials that are easy to prepare, eco-friendly and available in abundance.

The work presented in this thesis is an attempt towards the development of a cost-effective, eco-friendly material for thin film solar cells using simple economically viable technique. Sn-based window and absorber layers deposited using Chemical Spray Pyrolysis (CSP) technique have been chosen for the purpose.

Chapter 1 of the thesis outlines some general aspects of photovoltaics, with an elaborate description of thin film solar cells. Role of different layers of thin film solar cell has been described here in detail. This chapter gives a vivid description of various absorber layers which are presently in the frontier areas of thin film based photovoltaic devices, both at research and lab level. The necessity for finding out new and better alternatives for these materials has been discussed in this chapter. Following this, a review giving the importance, applications and history of Tin Sulfide thin films is also presented.

Chapter 2 deals with various material characterization techniques which have been used for the work, giving a concise account on the relevant theory behind each technique. This chapter also consists of a brief description on the fabrication, standardization and working principle of the indigenously developed automated coating unit used for depositing thin films for the work along with a note on the versatility of CSP technique. A brief note on the thermal evaporation technique is also included in this chapter as it has been employed in the work for the electrode deposition and ex-situ metal diffusion.

In **Chapter 3**, deposition of uniform p-type and n-type SnS films using CSP technique has been elaborated. Optimization of various deposition parameters like distance between the spray head and the substrate, substrate temperature, spray rate, concentration of the anionic and cationic precursor solutions, their molarity, and atomic ratio for obtaining single-

phase, p-type, stoichiometric, SnS films with direct band gap have been discussed in detail. By adjusting certain deposition parameters we could also obtain n-type SnS thin films which facilitate the possibility of fabrication of SnS homojunction. Conditions required for the deposition of highly photosensitive SnS thin films are also described under this section. Here we have comprehensively evaluated the results obtained from structural, optical, electrical, transport, compositional and morphological analyses of these samples employing various techniques. This chapter also includes surface scanning of the samples performed using photo thermal deflection analysis. The optimized deposition parameters required for growth of other binary sulfide phases of tin such as SnS_2, Sn_2S_3 are also included in this chapter.

Chapter 4 deals with the engineering of structural, optoelectronic and morphological properties of SnS films so as to make it more suitable for photovoltaic device fabrication. Two entirely different techniques have been adopted for this purpose. The first one is an 'ex-situ' technique called "Ex-situ diffusion" in which Sn atoms were thermally diffused into the SnS films. This was done by depositing a layer of Sn metal over SnS films followed by annealing of the Sn/SnS bilayer at 100˚C in high vacuum for 30 min. The key achievement of this work is that, without altering the band gap, properties could be optimized for proposed photovoltaic application. Second half of this chapter deals with improvisation of properties of SnS films employing an 'in-situ' technique (by controlling the pH of the precursor by adding NH_4Cl) where we have avoided all the post deposition treatments. From this study we could understand that there is an optimum value for pH (~2) to obtain device quality SnS thin film. The remarkable achievements include band gap engineering and reduction of resistivity by three orders (to ~$6x10^{-2}$ Ω.cm) with considerable enhancement in the crystallinity.

Exploiting the potential of a new material for photovoltaic applications requires an extensive (and mandatory too) analysis of the

defect levels. In **Chapter 5**, Photoluminescence (PL) technique has been employed to probe in detail, the origin of various defect levels in the SnS thin films. Various defect levels within the band gap could be identified and we could propose a comprehensive energy band diagram of SnS thin films for the first time. The potential of these tailored SnS films for fabricating photovoltaic junction was demonstrated through trials on junction fabrication having the structure, ITO/n-type Window layer/p-SnS/electrode. The work has been found to be promising as we could obtain photovoltaic shift when illuminated with sunlight.

Chapter 6 gives in a nutshell**,** the main results and conclusions arrived at. The future outlook has also been briefly discussed.

Publications

Part of the thesis has been published in the following internationally referred journals

PUBLICATIONS IN INTERNATIONAL JOURNALS

1. **T. H. Sajeesh,** A. R. Warrier, C. S. Kartha and K.P. Vijayakumar "*Optimization of parameters of chemical spray pyrolysis technique to get n and p-type layers of SnS*", ***Thin Solid Films*** 518 (2010) 4370–4374.

2. **T. H. Sajeesh**, N. Poornima, C. S. Kartha, and K. P. Vijayakumar "*Unveiling the defect levels in SnS thin films for photovoltaic applications using photoluminescence technique*" ***Phys. Status Solidi A*** 207 (2010) 1934–1939.

3. **T. H. Sajeesh**, C. S. Kartha, C. Sanjeeviraja, Y. Kashiwaba and K. P. Vijayakumar "*Ex-situ Sn diffusion: a well suited technique for enhancing the photovoltaic properties of the SnS absorber layer*" ***J. Phys. D: Appl. Phys*** 43 (2010) 445102-445108.

4. **T. H. Sajeesh**, A. S. Cherian, C. S. Kartha, and K. P. Vijayakumar "*Engineering Structural and Opto-Electronic Properties of SnS Films Deposited using Chemical Spray Pyrolysis Technique by Controlling pH of the Precursor Solution*" ***Energy Procedia*** 15 (2012) 325-33.

5. **T. H. Sajeesh**, K. B. Jinesh, C. S. Kartha, K. P. Vijayakumar "Role of pH of precursor solution in taming the material properties of spray pyrolysed SnS thin films" **Applied Surface Science** Early view (2012) DOI: 10.1016/j.apsusc.2012.03.121.

6. **T. H. Sajeesh**, K. B. Jinesh, M. Rao, C. S. Kartha, and K. P. Vijayakumar "*Defect levels in SnS thin films prepared using chemical spray Pyrolysis*" **Phys. Status Solidi A** (2012) DOI:10.1002/pssa.201127442.

7. **T. H. Sajeesh**, C. S. Kartha, K. P. Vijayakumar "*Versatility of Chemical Spray Pyrolysis to obtain Sn_xS_y thin fiilms*" *submitted to* ***Journal of Thermal Spray Technology***.

8. A. R. Warrier, **T. H. Sajeesh**, C. S. Kartha, and K. P. Vijayakumar, "*Determination of thermal and electronic carrier transport properties of SnS thinfilms using photothermal beam deflection technique*" **Journal Material Research Bulletin** (Under review).

CONFERENCE PUBLICATIONS

International:

1. **T. H. Sajeesh**, C. S. Kartha, and K. P Vijayakumar "*Raman and XPS analysis of spray deposited Tin- Chalcogenide thin films for Photovoltaic applications*" **PVSEC-21** Fukuoka Sea Hawk, Japan December 2011.

2. **T. H. Sajeesh**, A. S. Cherian, C. S. Kartha, and K. P. Vijayakumar "*Engineering structural and opto-electronic properties of SnS films deposited using CSP technique by controlling pH of the precursor solution*" **ICMAT** NUS, Singapore June2011

3. **T. H. Sajeesh**, C. S. Kartha, and K. P Vijayakumar "*Preparation and Charecterization of Sn_xS_y films by chemical spray pyrolysis*" **IC-SOLACE** CUSAT, India January 2008.

4. **T. H. Sajeesh**, N. Poornima, C. Sudha Kartha, and K .P Vijayakumar "*Unveiling defect levels in sprayed SnS thin films with the help of Photoluminescence*" **XVIII International Materials Research Congress** Cancunn, Mexico August 2009.

National:

1. **T. H. Sajeesh**, C. S. Kartha, and K. P. Vijayakumar *"Effect of Spray rate and Precursor Concentration Ratio on the properties of SnS thin films prepared by Chemical Spray Pyrolysis"* **DAE-SSPS**, Mysore December 2007.
2. **T. H. Sajeesh,** K. P. Vijayakumar, and C. S. Kartha *"Characterization of p-type thin films prepared using CSP Technique"* **MRSI-AGM** Delhi February 2007.
3. **T. H. Sajeesh,** C. S. Kartha, and K. P. Vijayakumar *"Structural and Optoelectronic Properties of Spray Pyrolysed SnS Thin Films and fabrication of thin film solar cell using it* **Kerala Science Congress** Kollam January 2009.
4. **T. H. Sajeesh**, C. S. Kartha, K. P. Vijayakumar *"Development of all sprayed Thinfilm solarcells using SnS as the absorber layer"* **MRSI-AGM,** Kolkata February 2009.
5. **T. H. Sajeesh**, C. S. Kartha, and K. P Vijayakumar *"Structural and Optoelectronic Properties of Spray Pyrolysed SnS Thin Films"* **PSG Conference** Coimbatore 2009.
6. **T. H. Sajeesh**, C. S. Kartha, K. P. Vijayakumar *"Deposition and Charecterisation of SnS_2 thin films for photovoltaic applications"* **HTFT Conference** Cochin 2011.
7. P. K. A. Swalih, **T. H. Sajeesh**, C. S. Kartha, K. P. Vijayakumar, *"Evaluation of transport properties of spray deposited SnS thin films using photothermal beam deflection technique"*, **HTFT Conference** Cochin 2011.

.....ഇഒര....

Contents

Chapter - **6**

.....ꕥ.....

Chapter 1

SIGNIFICANCE OF ABSORBER LAYER IN THIN FILM SOLAR CELLS

Contents

1.1 Introduction

Life of the sun can be practically considered to be infinite and it is radiating its energy in all possible directions. A part of this energy is falling on our earth too. When sunlight strikes a solar cell, the incident energy is directly converted into clean electricity without any mechanical movement, any fuel and any exhaust or other byproducts. Interest in photovoltaics has grown rapidly during the past few decades. The importance of alternative / renewable energy sources is being fully accepted due to its significance as energy source in replacing oil and coal and the ecological reasons. Because of these reasons there is very strong and focused research and development works in the field of photovoltaics going on all over the world.

Solar cell or photovoltaic cell is nothing but a p-n junction. When photons with energy greater than or equal to the band gap of absorber material impinges on the cell, electrons are excited from the valence band to the conduction band in the absorber. Once electron-hole pairs are created, the electrons cross the junction to go from p to n region while the holes move from n to p region, releasing their energy before recombining with each other. In other words, the electron-hole pairs, which are within one-diffusion-length from the built-in electric field of the junction, are separated giving rise to a 'photo voltage' and photo current. The junction can be usually homojunction, hetero junction or Schottky barrier [1].

Performance of any solar cell is intimately related to the properties of the material of which they are made [2]. Even though materials that exhibit properties suitable for photovoltaic applications are many, environmental friendly material or devices capable of converting solar power to electrical energy with moderate efficiency at low cost and possessing high stability under operation are very few.

History of photovoltaics goes back to the nineteenth century, when Becquerel discovered (in 1839) photo voltage produced by the action of light on an electrode in an electrolyte solution [3]. Table 1.1 shows the notable events in the history of photovoltaics since then.

Table 1.1 Notable events in the history of photovoltaics.

Year	*Scientist/ group*	*Country*	*Achievement*	Ref.
1839	Becquerel	*France*	Discovers photovoltaic effect in liquid electrolytes	3
1873	Smith	UK	Discovers photoconductivity of solid Se	4
1877	Adams and Day	UK	The first observation of PV effect in solids	5
1883	Fritts	USA	makes first large area solar cell using Se film	6
1954	Bell Lab	USA	First 6% efficient solar cells : Si	7
1954	Air Force	USA	First thin film solar cells : Cu_2S/CdS	8
1955	Hoffman Electronics	USA	2% efficient Si PV cells at $1500/W	9
1955	RCA	USA	GaAs cell with 6% efficiency	10
1958	NASA	USA	Launches Vanguard satellite with Si backup solar array	9
1960	Hoffman Electronics	USA	offers 10% efficient Si PV cells	9
1963	Sharp Corp	Japan	produces first commercial Si modules	9
1966	NASA	USA	Launches satellite with 1 kW solar cell array	9
1970	Alferov, Andreev	USSR	First GaAs heterostructure solar cells	11
1972	IEEE		First PV conference with a session on terrestrial applications	9
1973	University of Delaware	USA	World's first solar powered residence built with Cu_2S (not c-Si!) solar modules	9
1974		Japan	Project Sunshine initiated in Japan to foster growth of PV industry and applications;	9
1974	Tyco	USA	grows 2.5 cm wide Si ribbon for photovoltaics, first alternative to Si wafers	9
1975	Hovel	USA	First book dedicated to PV science and technology	9
1979		USA	First thin-film solar cell $>$ 10% using Cu_2S/CdS	12
1981		KSA	350 kW Concentrator array installed	9
1982		CA,USA	First 1 MW utility scale PV power plant with Arco Si modules on 2-axis trackers	9
1984		CA, USA	6 MW array installed in Carrisa Plains	9
1985	UNSW	Australia	Si solar cell exceeds 20% efficiency under standard sunlight	13
1985	Stanford Univ.	USA	high-efficiency Si solar cells: Si solar cell $>$ 25% under 200X concentration	9
1986	Arco Solar	USA	First commercial thin-film power module, the a-Si G4000	9
1987		Australia	Fourteen solar powered cars complete the 3200 km World Solar Challenge race with the winner averaging 70 kph	9
1988	IBM	USA	GaAs heterostructure cells having 13% efficiency reported	14
1994	NREL	USA	GaInP/GaAs 2-terminal concentrator $>$ 30%	9
1996	EPFL	Switzerland	Photoelectrochemical —Dye-sensitized solid/liquid cell achieves 11%	15
2005			CIGS introduces in the market	16
2007	U niversity of Delaware		claims to achieve new world record in Solar Cell Technology without independent confirmation - 42.8%	9
2011	Baden-Wuerttemberg	Germany	Cu(InGa)Se_2 thin-film solar cell reaches 20.3% efficiency	17
2010	Solar Impulse	Switzerland	Aircraft completes first solar-powered night flight	18
2012	NREL	USA	Certified World Record for Polymer Solar Cell Efficiency (8.6%)	19

Apart from all the aforesaid efforts and initiatives, electricity from solar cells is still unaffordable for the common man. In this scenario the thin film solar cells made of eco-friendly and cost effective novel and abundant materials can make significant contribution and hence needs treatment with due importance.

1.2 Thin film solar cells

1.2.1 Why thin film solar cells

Over recent years, the photovoltaic market has been booming enormously with sales almost completely dominated by crystalline silicon similar to that of micro / digital electronics. Wafer costs account for over 50% of the total module cost. One way of eliminating this major cost component is to replace wafers by thin films of semiconductors deposited onto a supporting substrate (more commonly, glass). The sustained boom (10 years of 40%/annum compounded growth) is causing demand for Si wafers to outstrip the capacity to supply, creating a market entry opportunity for a number of competing thin film technologies [20]. These (thin film semiconductors) fall into two main classes; one based on Si in amorphous, nanocrystalline and polycrystalline phases and the other based on polycrystalline chalcogenide (Group VI) semiconducting compounds [21].

Since the volumes associated with the wafer based approaches are increasing rapidly, thin film technologies have to grow quickly just to maintain their present market share (total combined share is less than 10%). There is a higher barrier for market entry for thin-film technologies due to higher capital costs per unit output for thin film manufacturing facilities. Manufacturing of the conventional wafer based modules is

commonly divided in to four separately financed operations: Si purification, crystal growth and wafering, cell processing, and cell encapsulation. However, in a thin film operation, all these operations effectively are 'bundled' into one process [20].

Rapidly escalating demand for Si wafers is creating a supply shortage that will moderate the growth of the wafer-based output over the coming 2 years at least. This gives thin film products an opportunity to increase market share and to establish its credentials on a market previously not all that interested in such devices, at least partly due to the undeniably superb reliability and durability demonstrated by the wafer based approach [20].

Although the basic physics of thin film devices is the most complex, they offer two main advantages [22]. (1) as the thickness of the active layers will be less than that of crystalline Si device by two or three orders due to high optical absorption, the material cost shall remain a small part of the total cell cost and (2) thin film deposition process can be easily adapted for large area deposition, without affecting the continuous 'production line' processing. The tasks of developing large-scale procedures and building the machines to produce thin film solar cell arrays in a continuous process are formidable (as these are not available 'off-the-shelf' as in the case of Si technology), once the process and technology are developed, these machines should be able to provide enormous output and hence result in low unit cost.

1.2.2 Structure of thin film solar cells

Thin film solar cell can be fabricated using different materials deposited in thin film form [22]. In general, thin film solar cell consists of a

substrate, transparent conducting oxide (TCO), buffer layer, absorber layer, anti reflection coating and metal contact. Each of these layers has different physical and chemical properties and hence affects the overall performance of the device in some form or other. Since each layer has different crystal structure, microstructure, lattice constant, electron affinity/work function, thermal expansion coefficient, diffusion coefficient, chemical affinity, carrier mobility, mechanical adhesion, etc; there can be stress, defects and interface states, surface recombination centers, inter diffusion and chemical changes at the interface causing electrical and opto-electronic property changes [1]. Therefore utmost care has to be taken in order to select materials for these layers. A brief description on the function of various layers of a thin film solar cell is given below.

1.2.2.1 Absorber layer

Performance of hetero junction thin film solar cell is basically dependent on the choice of the optimum absorber material because light absorption and the generation of the carriers take place in the absorber layer material. Band gap of the absorbing material must be small enough to allow absorption of an appreciable portion of solar spectrum and at the same time large enough to minimize the reverse saturation current density. Direct band gap semi conductors (1.2-1.7 eV) with high absorption coefficient are preferred for the purpose [2]. Also the diffusion length of the minority carriers must be large enough so that the generated carriers can reach the contacts without much loss. Therefore, in general, p-type semiconductors are used as absorber layers.

Present thin film modules are based on amorphous Si (either in a single junction or multiple junction configurations), as well as on the

chalcogenide compounds CdTe or $CuInS_2$ (CIS). Thin film modules based on polycrystalline Si is a more recent market entrant. The module efficiency of various thin film modules [25] in 2006 (the year we took up the present study) is shown in Figure 1.1

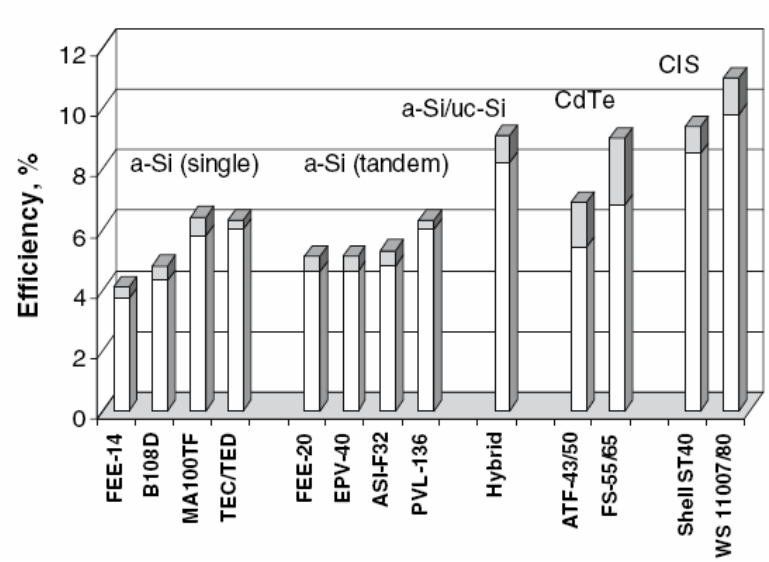

Figure.1.1 : Nominal energy conversion efficiency range of various thin-film modules (data from [25]) darker top region indicates range for product meeting specifications.

1.2.2.2 Buffer Layer

Primary function of a buffer layer in a hetero junction is to form a junction with the absorber layer and at the same time it should be capable of admitting maximum amount of light to the junction. Minimal absorption and recombination losses and transportation of the photo generated carriers with minimum electrical resistance are the key functions of this layer [24]. Some of the requirements to be satisfied by a material to be qualified for the selection as buffer layer are listed below.

1) Wider band gap for maximum transmission in the visible region
2) Minimum lattice mismatched crystal structure
3) Optimal band discontinuities resulting virtually no band offset
4) Capability to hold larger doping density

1.2.2.3 TCO

The front contact in a solar cell must be able to carry the current of the solar cell and at the same time it must be transparent for most of the incident radiation. In most thin film solar cells a wide band gap semiconductor is used as front / top layer [23]. Usually it is one of so called TCOs, such as ZnO, In_2O_3/SnO_2 (ITO), or SnO_2:F (FTO). In order to be transparent for visible light the front contact required to have a band gap of more than about 3.3 eV which is the case for the mentioned TCOs. Absorption in the infrared is an important issue for TCOs because of free carrier absorption just like in metals.

A general requirement for the front contact is that its sheet resistivity should be below 10 Ω/□ (specific area resistance).

1.2.2.4 Anti-reflective coatings:

"Reflection" losses are introduced by partial coverage of the front surface by non-transparent contacts (i.e., metal contact fingers) or by reflection at material interfaces. Experimentally, these losses are minimized by the application of anti-reflective coatings. Coatings or treatments for reducing the surface reflectance loss are referred to as anti reflecting layers. They are formed by interposing a layer of intermediate index of reflectance between the high and low index materials.

1.3 State of art of various Absorber layers

1.3.1 Silicon based Absorber layers

1.3.1.1 Single-junction amorphous silicon (a-Si) :

a-Si solar cells have been used in consumer products such as calculators and digital watches since the early 1980s. Although attempts have been made to launch outdoor power modules in the market since the mid-1980s only after 2000 that several companies, notably Kaneka and Mitsubishi of Japan, have supplied single junction a-Si power modules in appreciable quantities [26,27]. a-Si is deposited at low temperature in a way that allows about 10% (atomic) H incorporation, the secret to this technology's success [28]. Hydrogen greatly improves quality of the material. A p-i-n junction structure is used with the n and p-type regions creating a field in the intrinsic layer (i-layer) due to their work-function difference [29]. Since the a-Si is not very conductive, a key feature of the technology is the use of a transparent conductive SnO_2 layer between the Si and the glass. The strength of a-Si technology is its simplicity combined with the use of benign and abundant Si. The technology also is able to capitalize on equipment development in the active matrix display area, where similar deposition equipment is used. One factor that explains the relatively slow uptake of a-Si technology, given its early potential, is the light-induced degradation of material quality. Manufacturers now rate product in terms of ''stabilized'' performance, which is obtained after a field exposure of a month or two. However, stabilized module efficiency is quite low, generally in the 4–6% range, as apparent from Figure 1.1.

1.3.1.2 Multiple junction amorphous silicon devices

One way of accommodating the decreased material quality under light exposure is to use thinner layers of a-Si. This is possible if two or

more cells are stacked on top of one another. If the band gaps of the lower cells are smaller than that of the upper cells, this also gives a performance boost. The earliest approach to reduce the band gap from the quite high values (typical value of hydrogenated a-Si 1.7 eV) was by alloying with germanium. The US company 'United Solar' is the most successful current proponent of this approach, marketing a module based on a 3-cell stack with the two underlying cells made from a-Si alloyed with germanium. This gives nominal module performance in the 6–7% range, comparable to the best of the single junction a-Si approaches. A more recent approach is to combine an a-Si top cell with a bottom cell consisting of a two-phase mixture of amorphous and microcrystalline silicon. Band gap of the lower cell is determined by the crystalline regions in this mixed phase, and is similar to that of wafer-based cells (1.1 eV). Apart from the use of two cells, which improves module performance to the 8–10% range, the technology otherwise resembles that of a-Si, with its associated strengths and weaknesses. Although these hybrid cells are not presently manufactured, Japanese manufacturers, Kaneka and Sharp have announced plans to supply such modules in the open market soon.

1.3.1.3 Crystalline silicon on glass (CSG)

There is also an alternative Si-based technology that involves high temperature processing to convert an initially a-Si layer to a polycrystalline layer. The resulting films have properties similar to those of the polycrystalline wafers that now dominate the commercial solar module market. The better quality of this material makes it more conductive, eliminating the need for a TCO (reducing the cost) and eliminating the a-Si stability problem [30]. Crystalline Si on glass (CSG) technology includes several other features that further improve the

ruggedness of the technology, including a fault tolerant metallization approach and the use of higher grade borosilicate float glass, as compared to the soda-lime glass used in normal modules. Accelerated life testing has shown exceptional durability potential for this approach, even as compared to the wafer-based approach [31,32].

1.3.2 Compound semiconductor based thin film solar cells

1.3.2.1 Cu_xS cells

Stability and long term operation has proven to be a real problem for several thin film technologies. The original 'all thin film solar cell' consisting of a junction between Cu_xS/CdS showed promise of reasonable efficiency and ease of preparation [33-37]. For a period of almost 20 years dating from the late 50's, this photovoltaic system was the only 'all-film cell' available. Solar cells with efficiency of ~10 % were also made with $Cu_xS/Cd_{1-y}Zn_yS$ thin films (y= 0.10, 0.16).

The complexity of this system arises from the variety of Cu_xS phases that may exist at room temperature with quite different photovoltaic properties and from the ability to change from one phase to another during cell operation due to interaction with atmosphere or diffusion of Cu onto the CdS. Optical degradation process was also reported on this type of cells due to reversible photo-induced defect reaction, caused by photo-excitation after Cu diffusion into CdS [38].

Many attempts to produce a stable cell rectifying these problems looked promising but proved unsuccessful and further work on the system was finally abandoned.

1.3.2.2 Cu_2O cells

Even though, Cu_2O has a larger direct band gap compared to the optimum value, due to its very low production cost [22] and non toxic nature it has been thought attractive in spite of its low efficiency. Although it was suggested that efficiencies of 10% could be achieved by careful cell design, actual cell parameters were typically V_{oc} = 370 mV, J_{sc} = 7.7 mA/cm^2, FF= 57%, and efficiency = 1.6%. Just as the simple fabrication process of the Cu_xS/CdS cell could not make that cell practically useful because of its inherent instabilities, the cost effective and simple fabrication process of Cu/Cu_2O cell could not make that cell practically useful.

1.3.2.3 CdTe Cells

When research work on thin film Cu_xS/CdS cells came to an end because of the unavoidable degradation associated with the Cu diffusion, the question naturally arose as to what other p-type material could form useful hetero junction with CdS. In the most efficient CdTe cells , $CdSnSO_4$ is used as TCO and Zn_2SnO_4 buffer layer is included to improve quality of interface. Presently, two companies (First Solar and Antec Solar) manufacture CdTe based modules.

A heterojunction device having n-type CdS window on top of p-type CdTe base, appeared to be an attractive structure for photovoltaic conversion because both materials lend themselves to different thin film technologies, and their band-gaps (at 2.4 eV and 1.5 eV respectively) are well suited for solar energy conversion. In spite of the fact that the CdS-CdTe pair has a crystal mismatch of 9.7%, it appears to be the best available combination of the II-VI semiconductors for photovoltaic conversion [39]. Deposition of the CdTe cell can be done by variety of

techniques including close-spaced sublimation (CSS), vapour transport, chemical spraying, or electroplating. A summary of the general properties of CdTe is available in reference [40].

In all the thin film solar cells based on junctions involving p-CdTe polycrystalline thin films, three problems appear to be dominant: recombination losses associated with the junction interface, difficulty in doping the p-CdTe, and difficulty in obtaining low resistive contacts to the p-CdTe [2]. Another key disadvantage associated with CdTe is the potential health and safety issues that arise because of the toxic nature of Cd, both in connection with manufacturing as well as large scale field use [41]. Although Cd-based modules are apparently banned in some countries such as Netherlands, Japan, etc., proponents point out that the required Cd is a by-product of Zn mining. Concentrating Cd in the photovoltaic modules is thereby argued to be a positive step for the environment. Others point out this argument can only be true if the Cd is used in a closed cycle [42]. Two of the former key players in the CdTe area, BP Solar and Matsushita, have both abandoned the technology, citing the effect of these environmental concerns. The lack of abundance of Te is also pulling back this technology from taking up the challenge of future energy source.

1.3.2.4 Cu (In,Ga)Se_2 cells

As photovoltaic research extended beyond the simple group IV elemental Si, to group III-V compounds like GaAs, and then to group II-VI compounds like CdTe, it moved to I-III-VI_2 compounds like $CuInSe_2$ (CIS) with one more step of complexity. With the introduction of Ga to CIS to get Cu(In,Ga)Se_2 (CIGS) the performance of the device enhanced considerably (which resulted in widening of band gap to 1.3 eV and

improvement on material quality). As of now, CIGS is a star performer in the laboratory with 20.3% efficiency demonstrated for small cells [17], but the module efficiency is only 13.4%. The main manufacturers of CIGS cells are Wurth Solar, Avancis Solar (formerly Shell Solar) and Globel Solar. There are several inherent difficulties for this material to commercialize. Unlike other thin film technologies, which are deposited onto a glass superstrate, CIS technology generally involves deposition onto a glass substrate structure. An additional glass top-cover is then laminated to the cell/substrate combination. Present designs require a thin layer of CdS deposited from solution. Considerable effort is being directed for replacing this layer due to the issues associated with the use of Cd, as previously noted and also to avoid the wet process which is a bunch process not suitable in a production line.

Fabrication and use of CIS solar cell raises several questions in the areas of health and safety and the supply of key elements [43]. Hazardous chemicals like H_2Se and Cd are involved in the fabrication and structure of these cells. H_2Se is a highly toxic gas and it can be used safely only with certain safety precautions. To minimize the risk associated with it, the gas produced onsite should be recycled after use.

If cells enter into large scale production, availability of In might become an issue. [44,45] Although it appears that there is sufficient quantity of In to meet the growing demand of an effective solar cell market, there could be a conflict between supply and demand. It will be interesting to note that, all known reserves of indium is only sufficient to produce solar cells that can provide electrical energy equal to that presently produced by the whole available wind generators.

1.3.2.5 Cu_2ZnSnS_4 Cells

Cu_2ZnSnS_4 (CZTS) is a novel p-type semiconductor that has been receiving immense consideration nowadays because of its high latent potential. CZTS containing only abundant and non-toxic elements is reported to have a band gap between 1.45 and 1.6 eV [46-48] and a band edge absorption coefficient above 10^4 cm^{-1} [49]. Katagiri and co-workers [50] prepared 6.78% efficient CZTS cells through sputtering process followed by annealing in H_2S. Later by vacuum processing CZTS solar cells with 8.4% efficiency, has been achieved by Shin *et al.* [51]. This is the highest efficiency reported for pure sulfide CZTS prepared by any method. With the introduction of Se to CZTS ($Cu_2ZnSn(S,Se)_4$), scientists in IBM have come up with an efficiency of 10.1% very recently.

1.3.2.6 Other Emerging Solar cell technologies

Apart from the activity outlined above with cell technologies based on inorganic material, recent years have seen a burst of activity with organic and mixed organic-inorganic cells. One general strand of activity in this category is based on dye-sensitization of porous Titania films [52]. Attempts to commercialize dye-sensitized cell were initially spearheaded by the firm 'Sustainable Technologies International' of Queanbeyan, New South Wales [53], with small numbers of modules appearing in some attractive building-integrated systems. Presently the work at the laboratory level targets the replacement of the liquid required in present devices by solid-state material. The inverse light conversion process is fundamentally more challenging with organic material, although laboratory progress is being reported. Main challenge is to improve the energy conversion efficiency of the experimental devices while simultaneously improving the stability and durability.

1.4 Major challenges in thin film solar cell technology: Significance of research on novel thin film photovoltaic materials & Tin Chalcogenides alternatives

To achieve cost-effective thin film solar cells for large-scale production of solar energy, the absorbing semiconductor material used in the device needs to satisfy many requirements. First, the constituent elements should be inexpensive, non-toxic, and abundant. Second, to obtain high energy conversion efficiency, the material should have appropriate optical and electrical properties such as a suitable optical band gap, a high optical absorption coefficient, a high quantum yield for the excited carriers, a long carrier diffusion length, and a low recombination velocity [2].

As we found in the previous sections, there were many thin film materials which are being investigated worldwide to compete with c-Si as a solar energy conversion material. We saw that, the two main forerunners alongside a-Si today are CdTe and CIGS. But there were material disadvantages in the toxicity of Cd and the rarity of indium and tellurium. Although tellurium is currently in low demand, up-scaled production of CdTe could potentially produce a price spike that would exclude CdTe from being an economic solar energy conversion material. In a-Si technology, the source material is abundant, and unlike the case of c-Si, relatively inexpensive low-temperature fabrication processes are available; however, the PV conversion efficiencies in a-Si are limited to less than 10%, a fraction of what CIGS can achieve. Toxicity is another major concern in the production of a-Si due to the usage of poisonous gasses. CIGS is not, however, without disadvantages as well. Indium is often cited as a material that may cause CIGS to suffer a material supply issue because of the

recently accelerated use of indium in opto-electronics for LCD displays. Moreover, the deposition processes that produce the best efficiencies in chalcopyrite films are difficult to control and scale up. For example, the process that has produced the world record CIGS cells is a vacuum-based co-evaporation fabrication method [17] involving a complex 3-stage procedure that is difficult to monitor and control. Scaling this process up to a manufacturing level may require new and more sophisticated techniques than currently being employed. Alternative non-vacuum processes have been developed to deposit CIGS on a manufacturing scale, but they are also not without problems nor do they produce the same quality of film [54]. Typical commercial polycrystalline silicon solar cell modules operate at or below 15% energy conversion efficiency [54]. As with any new technology, questions about lifetime, durability and material safety still exist which are reasons why currently thin-film solar cells only fill about 6% of the worldwide photovoltaic market.

However, the roadblock to a substantial improvement of the above mentioned aspects has prompted the research workers to take up two major challenges:

a) to develop new photovoltaic materials which are also cheap, nontoxic and easy to manufacture

b) to fabricate low-cost high-performance solar cells for commercial mass production using non vacuum and simple techniques

Currently efforts are being made at various laboratories all over the world to develop new solar cell materials to improve the cell properties either by its own merit or by improving cell deposition process/cell

structure like the tandem structure. Careful selection of suitable alternative materials for the existing technology is inevitable to bring thin film solar cells to the 'driving seat'. Factors that should be considered in developing new semiconductor materials include

(i) a suitable energy band gap that matches the solar spectrum to maximize absorption of the incident solar radiation,

(ii) ability to fabricate cells having acceptable efficiency using the material using a low cost and /or eco-friendly deposition method such that the "energy payback time" and the "energy pay back ratio" are acceptable,

(iii) abundance of the elements in the material and

(iv) low environmental cost when a "cradle to grave" life cycle analysis is made with respect to the extraction of the elements [2].

Theoretically maximum possible conversion efficiency that can be achievable for different materials as a function of optical band gap is shown in Figure 1.2. This was proposed by Leffersky *et al.* [55]. For this, he used theories dealing with photovoltaic effect as well as electromagnetic wave interacting with semiconductors to predict the characteristics of a semiconductor which would operate with an optimum efficiency as a photovoltaic solar energy converter. Existence of such an optimum material results from the interaction between the optical properties of the semiconductor which determine what fraction of the solar spectrum is utilized and its electrical properties which determine the maximum efficiency of conversion into electricity. Considerable attention is devoted to the effect of the forbidden energy gap of the semiconductor.

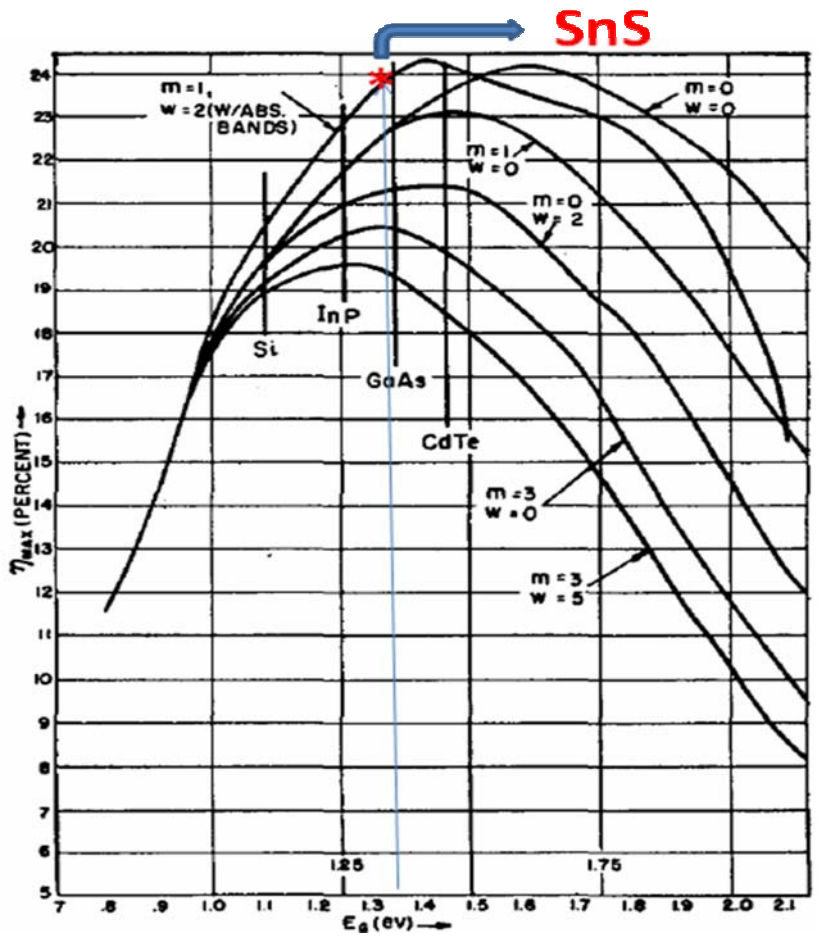

Figure 1.2: Band gap Vs theoretically achievable maximum conversion efficiency.

From Figure 1.2, we can perceive that one of the Sn-chalcogenide, SnS is occupying the apex position. The other suitable properties of Sn chalcogenide for photovoltaic applications are investigated in the following section.

Among the tin chalcogenide thin films, SnS and SnS_2 are of most importance because of suitable opto-electronic properties for photovoltaic applications. Owing to optimum band gap, high absorption coefficient and p-type conductivity SnS is a suitable candidate for absorber layer in thin film

solar cells whereas because of the wider band gap and n-type conductivity, SnS_2 is a competitive nontoxic substitute for window layer.

Despite of these promising properties, solar cells based on SnS absorbers have not achieved conversion efficiency higher than 1.3% [56] while theoretically such cells should be able to reach 24% efficiency [55]. This poor performance may be due to defects and/or impurities in SnS layers that result from the preparation methods used to make the films for cell fabrication. In the present work, we are investigating these aspects (along with the possibility of using CSP technique to deposit the film) in order to bring this material in to the frontier area of photovoltaic research.

A brief review on the works done so far on SnS thin films is presented below.

1.5 Review of SnS thin films

The goal of this section is to present a state of the art of SnS absorber layers. However, in order to conceptualize the cell operation with such absorbers, firstly the structural, electrical and optical properties of single crystal and thin film SnS should be recalled.

Works on SnS dates back to the beginning of the twentieth century. SnS was first reported by a German mineralogist Herzenberg in 1932 [57]. Since then, reports are available on the various structural, optical and electronic properties of the material.

1.5.1 Structure of SnS

IV-VI group compound semiconductors fascinated attention in the beginning mainly due to their unmatched applications in producing

infrared rays and detection. Among the IV-VI semiconducting compounds, tin chalcogenides exhibit orthorhombic structure with eight atoms per unit cell [58-60] forming double layer planes normal to the longest axis. SnS and SnSe are isomorphous and crystallize in an orthorhombic layer structure [61].

According to Hofmann, SnS has orthorhombic structure that may be described as pseudo-tetragonal as shown in the Figure. 1.3. Every Sn atom is surrounded by three S atoms. The bond angles are nearly 90˚. Figure 1.3 also shows clearly that SnS has a layer structure with double layers perpendicular to the c-axis. SnS has unit cell with lattice parameters of a = 4.334 Å, b = 11.200 Å, and c = 3.987 Å, which can be viewed as a distorted rock salt (NaCl) structure. It is composed of double SnS layers perpendicular to the b-axis with Sn and S atoms covalently bonded within the layers and weak van der Waals bonds between the layers. The double layer held by van der Waals forces in SnS is expected to give a chemically inert surface with few surface states. This defect-tolerant surface might reduce the carrier recombination loss due to defects at p-n junctions and at grain boundaries.

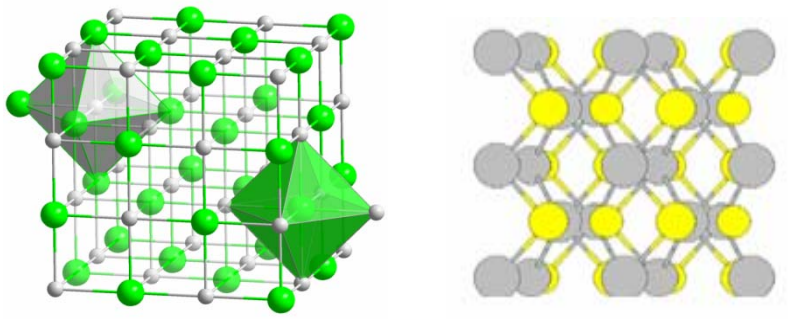

Figure 1.3: (Left) distorted rock salt (NaCl) structure of SnS (Right) Layered structure of tin chalcogenides.

1.5.2 Phase diagram of Sn-S system:

An exhaustive report on various SnS minerals can be found in the report by Kissin *et al.* [62]. A p-T-x diagram of the SnS system was determined by Albers *et al.* especially in the region of the compound SnS and is shown in Figure 1.4 [63]. This diagram is quite helpful in understanding the feasibility of formation of binary sulfides of Sn like SnS, Sn_2S_3, SnS_2 even at low temperatures and suitable Sn:S ratio.

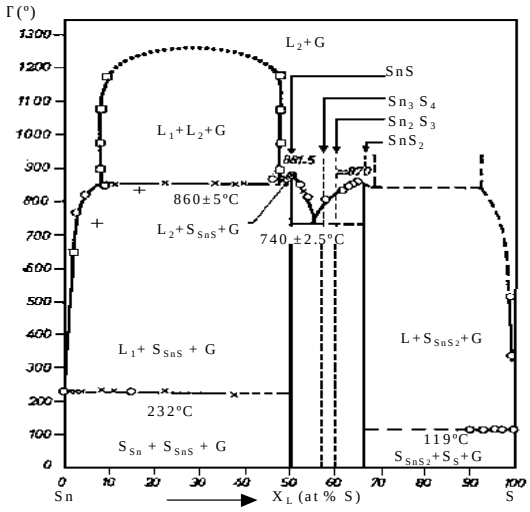

Figure 1.4: p-T-x diagram of Sn-S system

1.5.3 SnS single crystals

Conventionally SnS single crystals have been prepared using direct vapor transport technique [64], stoichiometric composition technique [65], Physical vapor transport method [66] or Bridgman-Stockbarger technique [67].

In the year 1961, Hass *et al.* [68] quantified some of the different physical constants of p-type SnS single crystals by analyzing IR reflection spectrum. From the analysis, they could measure the refractive index

(n_0 = 3.6±0.1), dielectric constant (19.5± 2), effective charge on the atoms (e* = 0.7 e) and the effective mass of hole as m*= 0.20m_0 of the SnS single crystals. A dissociation energy of 3 eV was reported for the SnS molecule by Ram *et al.* in 1973 [69]. In 1977, the results of Raman scattering and infrared reflectivity measurements on SnS were published by Chandrasekhar *et al.* [70]. Later, Chamerlain *et al.* [71,72] reported (as two letters to the editor) the direct and indirect band gap of SnS single crystals deduced from infrared photoconductivity studies. They observed an indirect energy gap at 1.13± 0.02 eV and 1.22 ± 0.02 eV and a direct band gap of 1.43 ± 0.2 eV.

In year 1977 some important works on the Raman analysis of layered SnS compound were reported. The zone centre phonons in the layer crystal SnS was studied employing Raman scattering technique and concluded that SnS behaves approximately like a two dimensional crystal [73, 74]. To follow, a few reports on the detailed Raman analysis of various binary sulfides of Sn were published [75, 76].

A detailed account of photo-acoustic and thermo acoustic of SnS single crystal oriented in (0 0 1) plane was given by Nikolic *et al.* who reported the phonon relaxation time and free carrier concentration of SnS single crystals [77]. The influence of temperature and pressure on electronic transitions in SnS was reported by Parenteau *et al.* [78]. In 1989 Elkorashy determined the optical constants of SnS single crystals like, absorption coefficient, refractive index, extinction coefficient, dielectric constants and reflectance [79]. A very important work carried out by Ettema *et al.* in 1992 that resulted in the deduction of electronic structure of SnS [80]. Nassary reported the electrical conductivity and Hall Effect

results of SnS single crystals grown using Bridgemann method over the temperature range 141-521 K. Several physical parameters like thermo electric power, ratio of mobilities, effective mass, relaxation time, diffusion length and diffusion coefficient for majority and minority carriers were successfully determined in this work [81].

A few material properties of SnS single crystal has been summarized from the afore mentioned references and are given in Table 1.2.

Table 1.2: Material properties of SnS single crystals.

Conductivity type	Usually p- type, S vacancies n-type, Sb doped n-type
Structure	Orthorhombic Hergenbergite polycrystalline a= 4.33 nm, b= 3.98 nm, c= 11.18 nm
Indirect band gap	1.13 ± 0.02 eV and 1.22 ± 0.02 eV
Direct band gap	1.43 ± 0.2 eV.
Carrier concentration	$5x10^{17}$ cm^{-3}
Refractive index	3.5
Resistivity	0.06 Ω.cm
Hole mobility	54 $cm^2V^{-1}s^{-1}$ (300 K); 2000 $cm^2V^{-1}s^{-1}$ (77 K)
Effective mass of hole	0.4 m_0
Dielectric constant	14-19
Activation energy	0.28-0.3 eV
Absorption coefficient	$2x\ 10^4cm^{-1}$
Density	5 g/cm^3
Melting point	1154 K

1.5.4 SnS Thin films

A review on the major works done so far on SnS thin films deposited using different deposition techniques is outlined in chronological order in

the following paragraphs. With the help of this information, performance of the devices with SnS absorbers will finally be summarized.

1.5.4.1 Preparation techniques

SnS thin films could be prepared through various physical and chemical means of thin film deposition such as vacuum evaporation [82], radio frequency sputtering [83], electrochemical deposition [84,85], atmospheric pressure chemical vapor deposition [86], plasma enhanced chemical vapor deposition [87], brush plating [88], dip deposition [89], chemical bath deposition [90] and chemical spray pyrolysis (CSP) [91]. Property of the material is found to vary drastically depending on the mode of deposition and the deposition parameters. Some of them are discussed below in brief.

(a) Thermal Evaporation

Thin films of SnS were prepared using thermal evaporation by El-Nahass *et al.* In the work they investigated structural transformation upon annealing in the temperature range of 432-573 K. An exhaustive report on the various optical properties of SnS films was also included in this paper [92].

The substrate often plays a critical role in determining the properties of the film deposited, especially when the deposition technique is thermal evaporation. In a very significant work published in a couple of international journals, Devika *et al.* have studied the effect of substrate surface on the physical properties of vacuum evaporated SnS thin films. The substrates investigated include, Corning 7059 glass, ITO coated glass, Si-wafer, and Ag coated glass substrates. Over ITO, SnS films had very high roughness, grain size and good electrical conductivity [93, 94]. In the same year, they investigated effect of annealing on the vacuum evaporated

SnS thin films and found that with increase in the annealing temperature, the composition of the film changed due to re-evaporation of Sulfur [95].

Co-evaporation technique has been employed to deposit SnS films and the material properties of the films were characterized by Reddy *et al.* in the year 2006. They deposited SnS at different substrate temperature and the films had grain size = 120 nm, resistivity = 6.1 Ω.cm and activation energy = 0.26 eV. These films crystallized in orthorhombic crystal structure with orientation along (0 4 0) plane. The films deposited at T_S =300˚C were highly crystalline and exhibited a dominant SnS phase along with traces of SnS_2 and Sn_2S_3 phases. They were also successful in depositing nearly stoichiometric, low resistive and single phase SnS films with an optical band gap of 1.37 eV [96].

Miles *et al.* also deposited films of SnS on glass and SnO_2: coated glass substrates using thermal evaporation with the aim of optimizing the properties of the film for using in solar cells. In particular they investigated the effects of source temperature, substrate temperature, deposition rate and film thickness on the chemical and physical properties of the films [97].

Polycrystalline SnS thin films, having thickness around 650 nm, were grown out of high purity SnS powder at a substrate temperature of 250˚C. These films were then annealed at 200°C and 300°C for 2, 4, and 6 hours, and at 400°C for 2 and 4 hours in argon ambience [98]. The direct band gap of all these films was between 1.33 and 1.53 eV. They observed that except for annealing at 400°C all the films were nearly stoichiometric in nature, suggesting lower rate of desulfurization in that ambient. Carrier concentration and mobility of these films were found to be ranging from 10^{15}-10^{16} cm^{-3} and 0.8-31.6 cm^2 V^{-1} s^{-1} respectively.

(b) Two-step process

This is a comparatively novel deposition technique. The basic principle here is the sulfurization of thin metallic tin precursor layers**.**

Reddy *et al.* reported a detailed study of the structural properties of the SnS thin films deposited using the two-step process. Here the sulfurization was done in vacuum furnace using a graphite box and the Sn precursors layers were annealed at different temperatures (100-400˚C) in excess S ambience [99].

Later, Gordillo *et al.* synthesized SnS:Bi thin films out of this technique [100]. The films were characterized through spectral transmittance and XRD measurements to determine both, the optical constants and structural properties. The studies revealed that the SnS:Bi films tend to grow with a mixture of the SnS and Bi_2S_3 phases. It was also found that the SnS:Bi films present an absorption coefficient greater than 10^4 cm^{-1} and an energy band gap ranging from 1.37 to 1.47 eV, indicating that this compound has good properties required for an absorber layer in thin film solar cells.

Sn_xS_y thin films were prepared by depositing Sn thin films using vacuum deposition technique on glass substrates and then the films were vulcanized for 45 min at 210°C, 240°C, or 270°C [101]. Optical and electrical properties of the films vulcanized at different temperatures were studied. With increasing vulcanization temperature, the direct energy gap, hall mobility and carrier concentration of the films increase but the resistivity reduced. However, the vulcanization temperature has little effect on the conduction type and all the films showed p-type conduction. Films vulcanized at 240°C, which are polycrystalline orthorhombic SnS

films preferentially growing in the {111} direction, exhibited the best performance. The films, with direct energy gap of 1.46 eV and a resistivity of 25.54 Ω.cm (thickness in the range of 200-800 nm), were highly uniform and showed strong bonding to the substrates.

(c) Atomic Layer Deposition (ALD)

ALD is one of the techniques in demand for depositing thin films of a few mono layers. Homogeneous and ultra thin films of various materials can be coated on a variety of substrates using this technique. SnS was grown using sequential exposures of Sn(II) 2,4-pentanedionate ($Sn(acac)_2$) and H_2S. In situ quartz crystal microbalance (QCM) studies showed that the SnS ALD mass gain per cycle was 11-12 ng/cm^2 at 175°C on gold-covered QCM sensor [102]. The growth rate was in the range 0.22-0.24 Å/cycle and ratio of mass loss to mass gain $|\Delta m_2/\Delta m_1|$ from the H_2S and $Sn(acac)_2$ reactions was ~0.32 at 175°C. Value of this ratio is close to the predicted ratio from the proposed surface chemistry for SnS deposited by ALD. The SnS ALD growth rate was also independent of substrate temperature from 125-225°C. X-ray fluorescence studies confirmed that Sn/S atomic ratio was ~1.0 for the SnS films. XPS measurements revealed that the films contained oxygen impurities at 15-20 atomic percentage after air exposure. The films had a band gap of ~1.87 eV which was higher than the value of the bulk (~1.3 eV).

(d) Chemical Bath Deposition (CBD)

CBD is a simple and very popular technique for thin film deposition, especially for the deposition of chalcogenide thin films. Pramanik *et al.* [103] developed this method for the deposition of SnS thin films on glass substrate at room temperature. The deposited films were amorphous and

possessed n-type conductivity with an optical band gap of 1.51 eV. Latter, Ristov *et al.* in 1989 [104] prepared p-type SnS thin films from $SnCl_2$ and Na_2S precursors. An interesting observation they made was that, on annealing this film for a short while above 280˚C the conductivity changed to n-type without any detectable change in the composition.

Lokhande *et al.* [105] reported the procedure for depositing various metal chalcogenide thin films including SnS by employing CBD technique. A much simplified technique for preparing good quality SnS films was reported by Nair *et al.* [106]. Employing the process, they were able to deposit uniform p- type films having thickness up to 1.2 μm. These films exhibited slight photosensitivity as well. In the same year, the same groups highlighted the application of these SnS films as tubular solar collectors owing to its high absorbance [107].

SnS thin films with porous structure were deposited by Leion *et al.* on glass using Triethonalamine (TEA), Thioacetamide, $SnCl_2 \cdot H_2O$ and aqueous ammonia as reactants and aqueous NH_4Cl solution as buffer. The samples were characterized using XRD and SEM. XRD results suggested that the samples were polycrystalline with orthorhombic structure unit while SEM results indicated that the film surface had bamboo leaf-shaped morphology. These porous structures developed by them are in principle much suitable for third generation photovoltaic devices [108].

Akkari *et al.* investigated the influence of TEA concentration on the properties of SnS films and optimized the deposition parameters [109]. These films were characterized with XRD, SEM and spectrophotometric measurements. The obtained thin films with TEA concentration equal to 13.5M exhibited orthorhombic structure and direct band gap about 1.65eV.

Hankare *et al.* [110] deposited SnS films on non-conducting glass substrate at room temperature. $SnCl_2$ and $Na_2S_2O_3.5H_2O$ were used as source materials to obtain SnS films. These films were uniform, well adherent and brown in color and were characterized using XRD, optical absorption, electrical conduction measurements and SEM techniques. Optical band gap of the samples was 1.0 eV. The films exhibited p-type conductivity with an activation energy of 0.62 eV.

By employing multi deposition runs SnS thin films having the zinc blend structure were deposited using CBD technique by Akkari *et al.* [111]. The precursors were aqueous solution containing 30 ml TEA, 10 ml Thioacetamide, 8 ml Ammonia solution and 10 ml of Sn^{2+} (0.1 M). XRD, SEM, and spectrophotometric measurements were done on these films. Crystallinity of the films improved with film thickness and band gap energy was about 1.76 eV for film prepared after six deposition runs.

Guneri *et al.* [112] deposited SnS on glass substrates using CBD at room temperature by keeping the substrates in the bath for 24 hours. Crystallite size, lattice parameters, defective location, and texture coefficient of the films were calculated from the XRD data. EDAX analysis revealed that the films were nearly stoichiometric (Sn/S, 54.13/45.8). From Hall measurements, it was found that the films exhibited p-type conduction. Its resistivity and mobility were calculated to be 2.53×10^5 Ω.cm and 8.99×10^5 cm^2/Vs respectively. The activation energy was calculated to be 0.527 eV in temperature range from 353-573 K by Arrhenius equation. Optical band gap values of direct and indirect transitions were estimated to be 1.37 eV and 1.05 eV, respectively. After this work, they reported the effect of deposition time on the structural,

electrical and optical properties of SnS thin films at different deposition times (2, 4, 6, 8 and 10 h) at 60°C [113]. All deposited films were polycrystalline and had orthorhombic structure with small crystal grains. But the microstructures had changed with deposition time, and were nearly stoichiometric. Hall measurements showed that the obtained films had p-type conduction and resistivity values of SnS films changed with deposition time. Band gap measurement indicated that allowed direct, allowed indirect, forbidden direct and forbidden indirect transitions, band gap values varied in the range 1.30-1.97 eV, 0.83-1.36 eV, 0.93-1.49 eV and 0.62-1.23 eV, respectively for these set of samples.

Influence of the pH value (pH 1.5, 2.5 and 3.5) in CBD technique on the growth and properties of SnS thin films were investigated by Kassim *et al.* [114] They could obtain relatively uniform grain size, good coverage and thicker films for lower pH value such as pH 1.5. Band gap values were found to be 1.2-1.6 eV for the films deposited under various pH values.

(e) Close-spaced vapor transport (CVT) method

In the year 2001, Yanuar et al. [115] made use of CVT for the first time to deposit SnS thin films. The films were crystalline with an energy band gap of 1.32 eV. These films exhibited p-type conductivity with hole density $10^{17}/cm^3$.

(f) Chemical Spray Pyrolysis (CSP) Technique

Thankaraju *et al.* [116] deposited n-type SnS films by CSP technique using $SnCl_2$ and Thio-Urea on glass and FTO substrates at 350˚C. But these films were highly resistive and amorphous. They observed an indirect band gap of 1 eV for these films. Interestingly their SnS films exhibited

some photoconductivity (10 times the dark conductivity) as well. But since then no further reports are available on the application level of this photosensitive films deposited using spray technique.

Sn_2S_3 thin films were deposited by Salah *et al.* using CSP technique. $SnCl_2$ and thio-urea were used as the precursor solutions and they investigated the effect of substrate temperature on the material properties of these films [91].

Reddy *et al.* [117] reported spray pyrolytic deposition of Sn_xS_y films on Sb doped SnO_2 glass substrates. They have deposited films at different substrate temperatures and investigated its physical properties. They found that films formed in the temperature range 300-375˚C were nearly stoichiometric, single phase SnS with average grain size of 0.36 μm. The resistivity of the films was 30 Ω.cm, band gap was 1.32 eV and net carrier concentration was $2x10^{15}$ cm^{-3}. In another publication, the same group reported effect of variation of the concentration of the precursor solution on spray pyrolysed SnS thin films. They observed that, when molarity of the precursor was in the region 0.09-0.13M, the films were nearly stoichiometric and had a resistivity of 32 Ω.cm [118].

Again, CSP technique was used by Rodriguez *et al.* to deposit SnS films. $SnCl_2$ and N,N-Dimethylthiourea were used as precursors [119]. They deposited films at different substrate temperatures and these films were characterized using several techniques. XRD studies showed that substrate temperature affects the crystal structure of the deposited material as well as the optoelectronic properties. The calculated optical band gap value for films deposited at 320-396°C was 1.70 eV. Additional

phases of SnS_2 at 455°C and SnO_2 at 488°C were also observed. The measured electrical resistivity value for SnS films was ~1×10^4 Ω.cm.

(g) Chemical Vapor Deposition (CVD)

Price *et al.* [120] deposited SnS films employing atmospheric pressure CVD technique using Tri-n-Butyltin Trifluoroacetate and H_2S as precursors at 350 600˚C under nitrogen. Exhaustive Raman analysis was performed on the samples and the results were discussed.

Baron *et al.* employed Aerosol assisted CVD to deposit SnS thin films. In this work, they used $(PhS)_4Sn$ as the precursor solution and H_2S as the co-reactant. They found that at 500˚C, uniform films of SnS was deposited [121]. In the work they mainly investigated the mechanism of decomposition of $(PhS)_4Sn$ and the structure of the precursors.

Juarez *et al.* [122] deposited SnS thin films with the help of "Plasma Enhanced Chemical Vapour Deposition (PECVD)" technique in the year 2002. Electrical and optical characterizations of the Sn_xS_y thin films were reported. They investigated effect of relative concentration of the precursor vapour $SnCl_2$ and H_2S, keeping all the other deposition parameters as constant. They reported activation energy of 0.15 eV for the films.

Using simple tin Thiosemicarbazone complexes of the type $Bz_3SnCl_{(L)}$ (L=Thiosemicarbazones of Salicylaldehyde and 4-chlorobenzaldehyde) Bade *et al.* deposited SnS thin films using aerosol-assisted CVD technique [123]. XRD pattern of these films revealed the formation of SnS regardless of growth temperature and precursor type. SEM images showed that the films had wafer-like morphology and the growth temperatures did not have a profound effect on morphology.

(h) Electro deposition

SnS films for PV application were successfully deposited employing electrochemical deposition technique and a detailed report on results of electrical characterization were given by Sato *et al.* [124]. Works are also available on the deposition of SnS thin films over flexible metallic substrates. Khel *et al.* deposited SnS thin films on Al sheet through electro chemical deposition (ECD) technique from aqueous solutions containing $SnSO_4$ and $Na_2S_2O_3$. The films were polycrystalline and orthorhombic in structure. Composition was found to be S-rich in acidic pH and Sn-rich at higher pH values. Relation between film properties and deposition parameter was studied in this work to optimize the deposition condition. [125]

SnS thin films were synthesized by Zaina *et al.*, in aqueous media in the presence of Triethanolamine using ECD method [126]. Effect of deposition potential, Triethanolamine concentration, and deposition time on the properties of SnS films was studied. The presence of Triethanolamine showed improvement in reproducibility, adherence and crystallinity of the films. XRD studies indicated formation of polycrystalline compounds. Properties of the films varied with variation in deposition parameters. The highest photo response was obtained for the film deposited at -0.80 V in the presence of 0.06 M Triethanolamine. Films deposited at longer deposition time showed higher photo response. Absorbance study revealed that the band gap energy was about 1.20 eV with indirect transition.

Jain *et al.* cathodically electrodeposited SnS thin films on SnO_2-coated conducting glass substrates, from an aqueous solution containing $SnCl_4$

and $Na_2S_2O_3$ [127]. The films had Herzbergite orthorhombic crystal structure. Flakes/needle-like crystal structures present in as-deposited samples was due to the anisotropic growth of various crystal planes. Interestingly they could observe that annealing of these needle-like structures resulted in the growth of platelet-like structures. These films were polycrystalline with an optical energy band gap of 1.4 eV. Using a different set of deposition conditions Chen *et al.* reported the deposition of SnS thin films onto the ITO glass substrates by employing the same technique. Here aqueous solution containing $SnSO_4$ and $Na_2S_2O_3$ with pH = 2.7, $Sn^{2+}/S_2O_3^{2-}$ = 1/5, deposition potential E = -0.72~-0.75 V (vs. SCE), and the bath temperature at 30°C -50°C were used. They found that, with increase in bath temperature, the films became more compact with stronger XRD peaks. At the same time, the light absorption range of the films shifted towards the longer wavelength side with the increase in bath temperature [128].

Pulse-form electro-deposition technique was used by Cheng *et al.* to deposit SnS films on ITO-coated glass substrates. The potential applied to the substrates was of pulse-form with V_{on} -0.75 V (vs. SCE) and off potential, V_{off} was varied from -0.1-0.5 V [129]. Films were characterized using XRD, EDAX, SEM and optical measurements. When V_{off} was in the range 0.1-0.3 V, the SnS films had the best uniformity and adhesion. Band gap (direct) of the films was in the range, 1.23-1.33 eV. These films exhibited p-type or n-type conductivity and their resistivity was measured to be 16.8-43.1 Ω.cm. Effect of annealing on the SnS thin films deposited using pulse electro-deposition method were studied by Yue *et al.* [130]. The films were annealed at different temperatures in air for 1 hour. The XRD pattern showed that the film were decomposed and oxidized

completely at 250°C. Surface morphology and grain size changed with annealing temperature. The magnitude of the direct energy gap changed with the annealing temperature. They observed that annealing at 100°C, resulted in good crystallinity and strong blue-UV emission. SnS thin films of different thicknesses were deposited on TCO-coated glass substrates using pulse electro-deposition by Anaya *et al.* [131]. The applied potential pulses were -0.95V (V_{on}) and +0.1V (V_{off}). Crystal structure of the deposited films was orthorhombic with lattice parameters similar to that of the mineral herzenbergite. A systematic increase in the band gap was observed with increase in the film thickness. Dark conductivities of 60 and 510 nm thick films were 3.8 × 10-8 $(\Omega.cm)^{-1}$ and 6.72 × 10-7 $(\Omega.cm)^{-1}$ respectively. They observed that the structural parameters such as lattice constants and grain size showed a systematic change with film thickness. Yue *et al.* prepared SnS films on ITO-coated glass with average grain size of about 10 nm. [132]. These films had randomly oriented needle-like crystallites of nearly equal sizes. The EADX analysis indicated that the atomic ratio of Sn to S is 50.6:49.4.

I) Successive Ionic Layer Adsorption and Reaction (SILAR)

SnS nanocrystallites thin films were synthesized using SILAR technique by Mondal *et al.* [133]. The films were phase pure and polycrystalline with crystallite size approximately ranging between 8-11 nm. They noticed complete oxidation to SnO_2 due to heat treatment at 400°C in air for one hour and attributed the activation energy of 0.28 eV obtained to that associated with deep acceptor levels due to excess tin atoms. A modified SILAR technique was used by Gao *et al.* in which a certain quantity of NH_4Cl was added to the precursor solution to deposit SnS thin films having zinc blende structure [134]. These films were slightly

Sn-rich and small amount of O impurity was present in them. No other impurity such as nitrogen or Cl was found in the films. Dark conductivity of the films was about 10^{-6} $(\Omega.cm)^{-1}$.

J) Other chemical/physical routes

Both p-type and n- type SnS thin films were deposited using sputtering method for photovoltaic application in 1994 by Guang-pu *et al.* [135]. Nano crystallites of SnS was fabricated by employing mild solution routes by Qing Li *et al.* [136]. They investigated reaction of thiourea with different tin sources in different organic solvents. Thin films of p-SnS were brush plated on to SnO_2 coated glass substrate from aqueous solution containing $SnCl_2$ and $Na_2S_2O_3$ by Subramanian *et al.* [88].

Cifuentes *et al.* [137] deposited polycrystalline SnS thin films on glass substrates using a novel procedure involving a chemical reaction between the precursor's species evaporated simultaneously. XRD measurements indicated that the synthesized samples grew in several phases (SnS, SnS_2 and Sn_2S_3) depending upon the deposition conditions. However, through an exhaustive study, they found conditions to grow thin films predominantly in the SnS phase with orthorhombic structure. Employing microwave assisted chemical solution technique; deposition of SnS thin was reported by Jayaprakash *et al.* The deposition was carried out in the range of microwave power output from 160 to 720 W [138].

Thin films of SnS were prepared through nano-multilayer method on glass substrate followed by rapid thermal processing at 300˚C for 5 min in Ar atmosphere [139]. These stoichiometric films had prominent orientation along (0 4 0) plane. The film had optical energy band gap of

1.44 eV and p-type electrical conductivity with resistivity of 500 Ω.cm. The activation energy of the material was 0.035 eV.

1.5.4.2 Characterization of SnS thin films

In an important work published in Physical Review B in 1991, by employing Mossbauer spectroscopy, Lefebvre *et al.* convincingly concluded that, two oxidation numbers, II and IV existed for Sn in its binary compounds. The difference between Sn^{II} and Sn^{IV} was identified as mainly corresponding to the variation of about 0.7 Sn 5s electrons. [140]. Nair *et al.* reported the results of detailed XPS analysis performed on the SnS films. They also found that annealing of these films at higher temperature for some long period resulted in the conversion of SnS to SnO_2 phase [141].

Adsorption and sensing properties of micro porous SnS films have been reported by Jiang *et al.* [142]. They found that electrical and optical responses with respect to adsorption of specific guests, such as NH_3, H_2S and alcohols, show high sensitivity, reversibility and fast reaction times that are comparable to some commercial semiconductor sensors. This made micro porous layered SnS potentially interesting in environmental, industrial and biomedical monitoring. As a continuation of this work, they (Jiang *et al.*) tried to highlight Meso-SnS as a new class of thermo-tropic liquid crystals. [143]. In an another report, they reported the characterization results by employing tools like XRD, SEM, TEM, MAS-NMR, Raman spectroscopy, UV-Vis spectroscopy, Mossbauer spectroscopy, thermo gravitometry (TG), Differential Scanning Calorimetry (DSC) and temperature varied XRD. [144]

The dispersion parameters of SnS films were determined and reported by Safak *et al.* [145]. In this work, they could confirm that the

parameters obtained by using unpolarized light were in agreement with those reported for polarized cases. Moreover, a close similarity were observed with E//b polarization for SnS.

An in-depth characterization of the Sn-S system deposited using CVT technique was undertaken by Cruz *et al.* using XRD, XPS, and ^{119}Sn NMR characterization tools and the results were discussed. [146]. A study of electron momentum density distribution in SnS by means of Compton profiles was presented by Sharma *et al.* Ionic model calculations for a number of configurations of $Sn_{+x}S_{-x}$ ($0.0 \leq x \leq 2$) were also performed utilizing free-atom profiles [147].

With growing interest in SnS for solar photovoltaic device fabrication, the barrier characteristics of this semiconductor with respect to different metal contacts became increasingly important. Ghosh *et al.* [148] studied barrier characteristics of polycrystalline SnS thin films metalized with In, Al, Cu and Ag under different annealing conditions. Indium formed ohmic contact to p-SnS under all annealing conditions. With the other three metals, Schottky diodes were obtained and subsequently the contact parameters were studied under forward bias using In top contact under different annealing conditions. Although aluminum formed Schottky contact to polycrystalline SnS, annealing at 350˚C rendered it ohmic. EDAX analysis confirmed desulfurization from SnS thin films due to annealing. Breakdown voltage of the Al/SnS Schottky barrier diode was determined and it decreased with higher annealing temperature, supporting the increase in the doping profile with annealing temp. They also studied the Photoluminescence spectra of SnS films and correlated to surface trap centers generated due to annealing.

Optical properties of SnS thin films grown on a glass substrate with the help of CBD technique were investigated using Photo thermal deflection spectroscopy [149]. The experimentally normalized amplitude curves of the photo thermal signal *vs.* wavelength were compared to the corresponding theoretical ones and hence determined the optical absorption spectrum.

Mathew *et al.* [150] studied electrical transport and activation energy of the traps in the forbidden band of SnS. Charge transport is controlled by both diffusion and recombination at the depletion region. Two traps with activation energies 0.036 and 0.133 eV were detected at a particular applied bias. The traps showed a bias dependence for the activation energy; the zero field values of the ionization energies were estimated at 0.14 and 0.27 eV respectively.

1.5.4.3 Doping

Resistivity of pure SnS thin film deposited using vacuum evaporation is too high to make solar cell. In order to solve this problem, doped SnS thin films were fabricated using dopants like Sb, Sb_2O_3, Se, Te, In, and In_2O_3 [151]. From the experimental results, Sb was found as the best dopant source, as it reduced resistivity of SnS thin films reduced by four orders of magnitude, and the photosensitivity was double. In addition, the influence of Sb doping percentage on the electrical properties of doped SnS thin films was also investigated and found that optimum doping percentage of Sb was 1.3% ~1.5% in weight. After this work, effect of doping of Sb_2O_3 on vacuum evaporated SnS thin films was studied in detail by the same group [152]. They annealed the Sb_2O_3 doped SnS thin films in hydrogen atmosphere at different temperatures and for different

durations. Optimum doping content of Sb_2O_3 was found to be 0.2% in weight and the resistivity of the doped SnS film was 42 Ω.cm while that of pure-SnS film was 99 Ω.cm. In addition, the resistivity of Sb_2O_3 doped SnS film decreased as low as 24 Ω.cm on annealing at 400°C and 3 hour.

Thin films of lead tin sulfide ($PbSnS_2$) were deposited on glass substrates at 100°C using thermal evaporation method [153]. SEM and XRD studies revealed that the films were monophase and polycrystalline, with average particle size approximately 28 nm and fundamental absorption edge at 1.65 eV (direct allowed transition). Thermoelectric measurements showed the materials to be p-type in nature.

Ag doped SnS thin films were deposited on ITO coated glass using pulse electro-deposition by Yang *et al.* [154]. The doped films exhibited good crystallinity with larger grain size and optical gap of 1.66-1.89eV and high absorption coefficient ($\alpha > 5 \times 10^4$ cm^{-1}). By silver doping the resistivity could be brought down to the order of 10^{-3} Ω.cm and carrier concentration of 10^{19} cm^{-3} could be obtained. Jia *et al.* [155] employed a different technique for doping Ag in to the SnS matrix. SnS and Ag films were deposited on glass substrates by vacuum thermal evaporation technique successively and then the films were annealed at different temperatures (up to 300°C) in N_2 atmosphere for 2 hours in order to obtain silver doped SnS (SnS:Ag) films. With increase in annealing temperature, the carrier concentration and mobility of the films first rose and then dropped, whereas their resistivity and direct band gap showed the opposite trend. Annealing at 260°C yielded SnS:Ag films with the superior properties; these samples had direct band gap was 1.3 eV, carrier concentration up to 1.132×10^{17} cm^{-3} and the resistivity of about 3.1 Ω.cm.

Copper doped SnS films with thickness of about 300 nm had been grown on glass substrates using thermal evaporation technique by Zhang *et al.* [156]. Different Cu doped SnS films were obtained by controlling the Cu evaporation time to roughly alter Cu doping concentration in the SnS films (from 5.7 to 23 atomic %). Then they were annealed at (temperature of 250°C and pressure 5.0×10^{-3} Pa) for 90 min. With increase in Cu-doping concentration, grain size of the films became larger but the roughness decreased. Carrier concentration of the films increased sharply while resistivity decreased with respect to the variation in doping concentration.

1.5.4.4 Nano materials of SnS

Semiconductor nano crystals are of great interest because they provide an opportunity to observe the evolution of material properties with crystal structure, size and shape [157]. Semiconducting SnS nano wires, nano rods, and nano particles were prepared by employing a chemical technique by appropriately choosing different alkaline solution as reaction media by Changhua An *et al.* [158].

SnS particles in the size range of 5.0-6.5 nm were prepared by Li *et al.* [159]. Resorcinol-formaldehyde solution was added to these SnS nano particles after which the mixture was spin-coated on a Cu foil and carbonized at 650°C to prepare a net-like SnS/Cu composite thin-film electrode for Li-ion batteries.

Growth of SnS films with large surface area was accomplished by depositing it in a uniform nano wall structure over the entire substrate using CBD method [160]. Photoconductivity increased with the increase in film thickness for these 'nano wall' SnS thin films. Nano crystalline SnS of

various morphologies were prepared by Niwate *et al.* employing thermal and solvothermal decomposition of $Bz_3SnCl_{(L)}$ (L = benzaldehyde thiosemicarbazone) [161] TEM and SEM images revealed that morphologies of SnS depend on the method of preparation and the growth temperature.

Thin films and lawns of $Sn_{1-x}Pb_xS$ nano rods were produced using 'hot wall vacuum deposition method (HWVD)' by Bente *et al.* [162]. Roughness of the films measured by AFM was in the range 49.5-86.3 nm depending on Pb concentration. The rods were about 500 nm high and 300 nm in diameter. They observed that the droplet at the tip of rods consisted of tin and therefore it was concluded that the rods grew via a self-consuming vapor-liquid-solid mechanism.

1.5.4.5 SnS solar cells

This section deals with the brief review of the works where SnS thin films have been used for photovoltaic applications.

Ristov *et al.* deposited photovoltaic cells based on p-type SnS layer by employing chemical routes. Using chemical deposition method from two separate solutions, complete preparation of three types of cells was done with SnS as the base layer. Difference among the three types was in the window layer electrode. They employed chemical deposition technique to deposit CdO and Cd_2SnO_4. The third cell was purely Schottky barrier cell in which the window electrode was SnO_2:F, prepared using CSP technique. From the I-V, C-V and spectral characteristics measurements, they observed that the cell structure, with Cd_2SnO_4 film as the window electrode, exhibited better performance [163].

Sharon *et al.* reported conversion efficiency of 0.6% for a PEC cell prepared using SnS films grown by passing H_2S through an acidic solution of $SnCl_2$ [164]

Noguchi *et al.* [165] successfully deposited SnS thin film by vacuum evaporation technique and fabricated ITO/n-CdS/p-SnS/Ag structure. It exhibited short circuit current density (J_{sc}) of 7mA/cm^2, an open circuit voltage (V_{OC}) of 0.2 V, fill factor of 0.35 and a conversion efficiency of 0.29%

Another photovoltaic structure, SnO_2:F/CdS/SnS/(CuS)/Ag, with V_{OC} >300 mV and $J_{sc} \leq 5$ mA/cm^2 under an illumination of 850 W/m^2 using a halogen lamp, was reported by Avellaneda *et al.* [166]. Photovoltaic behavior of the structure varied on heating: $V_{OC} \approx 400$ mV and $J_{sc} < 1$ mA/cm^2, when heated at 423 K in air, but V_{OC} decreases and J_{sc} increases when heated at higher temperatures. They claimed that these photovoltaic structures were stable over at least one year.

Gunasekaran *et al.* reported fabrication of solar cells with SnS using photo chemically deposited CdS and $Cd_{1-x}Zn_xS$ as buffer layer. [167,168]. SnS absorber layer was deposited employing three-step pulse ECD technique. For the CdS/SnS structure, the best cell showed an efficiency of about 0.2%, while for the $Cd_{1-x}Zn_xS$/SnS structure, an efficiency of 0.7% was obtained.

Reddy *et al.* deposited SnS films by CSP and successfully fabricated ITO/n-CdS/p-SnS polycrystalline thin film heterojunction solar cell with 0.5% efficiency. Mathews *et al.* fabricated CdS/SnS heterojunctions by depositing SnS using pulse ECD while CdS was deposited using CBD technique. This cell had V_{OC} of 110 mV, J_{SC} of 0.72 mA/cm^2 and fill factor of 0.32 [169].

SnS/ZnO heterojunction was fabricated by Wu *et al.* using Al as the contact electrode [170]. Wide band gap InS-based thin film ($InS_xO_y(OH)_z$) was deposited onto SnO_2:F-coated glass through ECD technique from an aqueous solution using a two-step periodic-pulse voltage. This film was then used along with SnS thin film to fabricate a novel heterojunction. [171]. Performance parameters of these two structures were found to be rather poor. Miyawaki *et al.* fabricated ZnS/SnS heterojunction cells, in which, ZnS was deposited on p-type (electrochemically deposited) SnS thin films. The heterojunction cells showed rectification properties with very poor light activity [172].

SnS_2 and SnS nano particles were prepared via hydrothermal method, and solar cells were fabricated with the help of dip-coating technique using synthesized nano particles. Direct and indirect band gaps of SnS_2 thin film were 2.6 eV and 2.2 eV, respectively and those of SnS thin film were 1.2 eV and 1.0 eV, respectively. The solar cells produced J_{sc} of 1.1 $\mu A/cm^2$ and an V_{OC} of 25 mV [173].

SnS thin films with two different crystal structures, (orthorhombic ($SnS_{(OR)}$) and Zn-blende ($SnS_{(ZB)}$)) were synthesized using CBD technique by Avellaneda *et al.* [174]. These films possessed p-type electrical conductivity with band gaps of 1.2 and 1.7 eV respectively. The photovoltaic structure, SnO2:F/CdS/$SnS_{(ZB)}$/$SnS_{(OR)}$ with evaporated Ag-electrode exhibited an open-circuit voltage of 370 mV, a short-circuit current density of 1.23 mA/cm^2, fill factor of 0.44 and conversion efficiency of 0.2% under 1 kW/m^2 illumination. Improvement in the light generated current density when the two types of SnS absorber films were used was also presented in the paper. They also tested different evaporated

electrode materials and Ag-electrode was chosen for the future device fabrication.

Photovoltaic properties of the SnS/ZnO heterojunction were investigated by Ghosh *et al.* [175]. In another report the same group reported details of synthesis of SnS thin films via "galvanostatic electro deposition" and fabricated CdS/SnS heterostructure for photovoltaic applications [176]. They observed that the ITO/SnS/In structure exhibited linear current-voltage characteristics, establishing ohmic nature of both ITO/SnS and SnS/In junctions. Heterostructure ITO/CdS/SnS/In was characterized under dark and illuminated conditions. They also calculated several junction parameters like barrier height, diode ideality factor and series resistance of the heterostructure were estimated using Cheung model.

The n-type ZnO and p-type SnS were used to fabricate solar cells with the structure of ITO/ZnO/SnS/Al. The cell parameters were, J_{SC} = 1.38 mA/cm^2, V_{OC} = 0.42 V, FF = 0.40. [177]. Heterostructure solar cells were fabricated by depositing SnS on $ZnS_{0.8}O_{0.3}$ by electro deposition. The cell showed photovoltaic properties, although the efficiency was low [178].

The CdS nano-layer used as buffer layer of ZnO nano wire arrays/CdS/SnS thin film solar cells was prepared through thermal evaporation method [179]. They showed that CdS nano-layer plays a key role in reducing the leakage current.

Although several research groups fabricated SnS-related solar cells, the reported efficiencies were low. There is not much analysis available in literature about the low efficiency of the SnS based solar cells. A few repots

available on the failure analysis of the SnS based heterojunction are given below.

One of the reasons for this low efficiency is the mismatch at the band edges in the heterojunction. Sugiyama *et al.* reported the band discontinuities of CdS/SnS and SnS/SnO_2 hetero interfaces which were measured using XPS and C-V measurements [180]. The valence band offsets were determined to be approximately 1.5 eV for CdS/SnS and 3.5 eV for SnS/ SnO_2 interfaces whereas the conduction band discontinuities for these junctions were respectively found to be 0.4 eV and 1.0 eV. Using these values and the energy band gaps of the corresponding layers, the energy band diagram was developed and it was considered to be a TYPE-II heterostructure. The Fermi level was found to be much closer to the valence band maximum for SnS, whereas it appeared in the upper half of the band gap for both CdS and SnO_2. Energy band discontinuities in SnS/ZnMgO thin film heterojunction were reported by Reddy *et al.* recently [181].

Using single-phase SnS films, band discontinuities at SnS/CdS and SnO_2/SnS hetero-interfaces were measured employing XPS by Sugiyama *et al.* [182]. Valence band offsets were detected to be approximately 1.5 eV for SnS/CdS and 3.5 eV for SnO_2/SnS interfaces. Using these values and the energy band gaps of the corresponding layers, the energy band diagram was developed. It indicated that the SnS/CdS heterojunction is of TYPE-II form of heterostructure. This result indicated that SnS-related solar cells with CdS as window layer do not have an ideal band structure that could give high conversion efficiency.

Some of the cell performance parameters of SnS based heterojunctions reported by various groups have been tabulated below.

Table 1.3: Performance parameters of SnS based heterojunctions.

Heterojunctions	V_{OC} (mV)	I_{SC} (mA/cm^2)	FF	η (%)	Ref.
ITO/SnS	471	0.30	0.71	0.1	Wang *et al.*, *2010*
ZnO/SnS	120	0.04	0.33	0.003	Ghosh *et al*, 2009
SnO_2:F/CdS/SnS/Cu_2SnS_3	340	6.00	------	------	Avellaneda *et al.*, 2007
$Cd_{0.87}Zn_{0.13}S$/SnS	288	9.16	0.27	0.71	Gunasekaran *et al.*, 2007
CdS/SnS	260	9.6	0.53	1.30	Reddy *et al.*, 2006
SnS_2/SnS	350	1.5	------	------	Sánchez-Juárez *et al.*, 2005
CdO/SnS	200	0.054	------	------	Ristov *et al.*, 2001
Cd_2SnO_4/SnS	230	0.039	------	------	Ristov *et al.*, 2001
SnO_2:F/SnS	152	0.123	------	------	Ristov *et al.*, 2001

References

[1] J. Nelson, The Physics of Solar Cells Imperial College Press London (2003).

[2] R. H. Bube, Photovoltaic Materials, Series on Properties of Semiconductor Materials Vol. 1 Imperial College Press London (1998).

[3] E. Becquerel, Comptes Rendus **9** (1839) 561–567.

[4] Effect of Light on Selenium during the passage of an Electric Current (News) *Nature* **7**, 303-303 (1873).

[5] http://www.californiasolarcenter.org/history_pv.html

[6] C. Fritts, Proc. Am. Assoc. Adv. Sci. **33** (1883) 97.

[7] D. Chapin, C. Fuller, G. Pearson, J. Appl. Phys. **25** (1954) 676-677.

[8] D. Reynolds, G. Leies, L. Antes, R. Marburger, Phys. Rev. **96** (1954) 533-534.

[9] A. Luque, S. Hegedus, Handbook of photovoltaic science and engineering, John Wiley and Sons Chichester (2003).

[10] D. Jenny, J. Loferski, P. Rappaport, Phys. Rev. **101** (1956) 1208-1209.

[11] Z. Alferov, Fiz. Tekh. Poluprovodn. **4** (1970) 2378.

[12] R. B. Hall, J. D. Meakin, Thin Solid Films **63** (1979) 203-211.

[13] M. A. Green, High Efficiency Si solar cells Trans Tech publications Switzerland (1987).

[14] D. Sumner, C. Whitaker, L. Schlueter, in: Proceedings of 20th IEEE Photovoltaic Specialist Conference (1988) 1289–1292.

[15] A. J. McEvoy, M. Grätzel, Solar Energy Mater. **32** (1994) 221.

[16] M. Powalla, B. Dimmler, K. H. Gross, in: Proceedings of the 20th European Photovoltaic Solar Energy Conference Edited by W. Palz, H. A. Ossenbrink, P. Helm Munich Germany 1689 (2005).

[17] P. Jackson, D. Hariskos, E. Lotter, S. Paetel, R. Wuerz, R. Menner, W. Wischmann,, M. Powalla, Progress in Photovoltaics: Research and Applications **19** (2011) 894–897.

[18] http://www.reuters.com/article/2010/07/08/us-swiss-solar-aircraft-idUSTRE6671WK20100708

[19] L. Dou, J. You, J. Yang, Chun-Chao Chen, Y. He, S. Murase, T. Moriarty, K. Emery, G. Li , Y. Yang, Nature Photonics **6** (2012) 180–185.

[20] M. A. Green, Mater Electron **18** (2007) S15–S19.

[21] R. A. Smith, Semiconductors Academic Publishers Calcutta (1989).

[22] K. L. Chopra, Thin film solar cells Plenum press New York (1983).

[23] H. L. Hartnagel, A. L. Dawar, A. K. Jain, C. Jagadish, Semiconducting Transparent Thin Films, IOP Publishing Philadelphia (1995).

[24] M. Mathew, Engineering the Properties of Indium Sulfide for Thin film Solar Cells by doping PhD Thesis Cochin University of Science and Technology (2009).

[25] M. Schmela, Photon Int. **2** (2006).

[26] M. Schmela, Photon Int. February 2, (2006)

[27] M. Schmela, Photon Int. March Issue, 3 (2004) 46–53.

[28] M. A. Green, Thin-Film Photovoltaics, in : Advances in Solar Energy An Annual Review of Research and Development Edited by D. Y. Goswami, American Solar Energy Society, Inc. New York 187–214 (2003).

[29] A. Shah, Thin-Film Silicon solar Cells, Taylor and Francis group New York (2010).

[30] M. A. Green, P. A. Basore, N. Chang, D. Clugston, R. Egan, R. Evans, J. Ho, D. Hogg, D. Jarnason, M. Keevers, P. Lasswell, J. O'Sullivan, U. Schubert, A. Turner, S. R. Wenham, T. Young, Sol. Energy **77** (2004) 857–863.

[31] P. A. Basore, Large-Area Deposition for Crystalline Silicon on Glass Modules, in: Conference Record 3rd World Conference on Photovoltaic Energy Conversion Osaka 935–938 (2003).

[32] P. A. Basore, Simplified Processing and Improved Efficiency of Crystalline Silicon on Glass Modules, in: Conference Record 19th European Photovoltaic Solar Energy Conference Paris (2004).

[33] D. C. Reynolds, G. Leies, L. L. Antes, R. E. Marburger, Phys. Rev. **96 (**1954**)** 533.

[34] K. W. Boer, J. D. Meakin (editor), in: Proceedings of International NSF workshopon CdS solar cells and other Abrupt heterojunctions, Univ. Delaware Newark (1975).

[35] G. Stanley, Appl. Solid state science. **5** (1975) 251.

[36] Rothwarf, A. M. Barnett, IEEE trans. Electron Devices ED-24, (1977) 381.

[37] M. Barnett, Final report: to the Energy Research and Development Administration E (49-18)-2538 FR77 Univ. of Delaware Newark (1977).

[38] D. Redfield, R. H. Bube, Phil. Mag. B **74** (1996) 309.

[39] R. H. Bube, K. W Mitchell, J. Electron. Mat. **22** (1993) 17.

[40] K. Zanio, Cadmium Telluride Vol. 13, Semiconductors and semimetals Academic press New York (1978).

[41] P. D. Mosokowitz, V. M. Fthenakis, Solar Cells **29** (1990) 63.

[42] http://www.firstsolar.com.

[43] K. Zweibel, A. M. Barnett, Polycrystalline thin film Photovoltaics, in: Renewable Energy Edited by T. B. Johansson, H. Kelly, A. K. N Reddy, R. H Williams, Island press, Washington D.C 437 (1993).

[44] http://rzblx1.uniregensburg.de/ezeit/warpto.phtml?colors=7&jour%5Fid=37775.

[45] P. C. F. Crowson, Minerals handbook 2000-01 statistics & analyses of the world's minerals industry Endenbridge: Mining journal books 2001.

[46] K. Jimbo, R. Kimura, T. Kamimura, S. Yamada, W. S. Maw, H. Araki, K. Oishi, H. Katagiri, Thin Solid Films **515** (2007) 5997.

[47] K. Ito, T. Nakazawa, Jpn. J. Appl. Phys. **27** (1988) 2094.

[48] T. M. Friedlmeier, N. Wieser, T. Walter, H. Dittrich, H. W. Schock, in: Proceedings of the 14th European PVSEC Barcelona 1242 (1997).

[49] H. Katagiri, N. Ishigaki, T. Ishida, K. Saito, Jpn. J. Appl. Phys. **40** (2001) 500.

[50] H. Katagiri, N. Sasaguchi, S. Hando, S. Hoshino, J. Ohashi, T. Yokota, Sol. Energy Mater. Sol. Cells **49** (1997) 407.

[51] B. Shin, O. Gunawan, Yu Zhu, N. A. Bojarczuk, S. J. Chey, S. Guha, Short communication: Prog. Photovolt: Res. Appl. DOI: 10.1002/ pip.1174 (2011).

[52] M. Grätzel, Journal of Photochemistry and Photobiology C: Photochemistry Reviews **4** (2003) 145-153.

[53] R. D. McConnell, V. K. Kapur, in: proceedings of the international symposium Photovoltaics for the 21st II: By Electrochemical Society Energy Technology Division, Electrochemical Society Meeting, Washington DC (2001).

[54] J. Kaneshiro, N. Gaillard, R. Rocheleau, E. Miller, Solar Energy Materials and Solar Cells **94 (**2010) 12-16.

[55] J. J. Loferski, J. Appl. Phys. **27** 777 (1956).

[56] K. T. R. Reddy, N. K. Reddy, R. W. Miles, in: Proceedings of 14th Int. Photovoltaic Science and Engineering Conference *Bangkok Thailand* 627 (2004).

[57] R. Herzenberg, Rev. Miner. **4** (1932) 33.

[58] K. R. Baldwin, C. J. E. Smith, Plating and Surface Finishing **84** (1997) 23-28.

[59] W. Holfmann, Z Kristanllogr **91** (1935) 161.

[60] A. Okazaki , L. Veda, Journal of physics society Japan **11** (1956) 497.

[61] A. Okazaki , L. Veda, Journal of physics society Japan **11** (1956) 470.

[62] S. A. Kissin, D. R. Owens, Canadian Mineralogist **17** (1979) 125-135.

[63] W. Albers, C. Hass, H. J. Vink, J. D. Wasscher, J. Appl. Phys. **32** (1961) 2220.

[64] S. K. Arora, D. H. Patel, M. K. Agarwal, Journal of Crystal growth **131** (1993) 268.

[65] E. P. Trifonova, I. Y. Yanchev, V. B. Stoyanova, S. Mandalidis, K. Kambas, A. N. Anagonostopoulos, Material Research Bulletin **31** (1996) 919.

[66] J. George, C. K. ValsalaKumari, K. S. Joseph, Journal of applied physics **54** (1983) 5347.

[67] M. J. Powel, Journal of Physics C: Solid state Physics **10** (1977) 2967.

[68] C. Hass, M. M. G. Corbey, J. phys. Chem. Solids **20** (1961) 197-203.

[69] R. S. Ram, P. C. Mishra, K. N. Upadhya, Spectroscopy letters **6** (1973) 541-546.

[70] H. R. Chandrasekhar, R. G. Humphreys, U. Zwick, M. Cardona, Physical Review B **15 (**1977) 2177.

[71] J. M. Chamerlain, M. Merdan, J. Phys. C : Solid state Phys. **10 (**1977).

[72] J. M. Chamerlain, P. M. Nikolic, M. Merdan, P. Mihailovic, J. Phys. C: Solid state Phys. **9** (1976) L571.

[73] P. M. Nikolic, L. J. Miljkovic, P. Mihajlvic, La Avrencic, J. of Physics C, : Solid state Physics, **10 (**1977) L289.

[74] A. J. Smith, P. E. Meek, W. Y. Liang, J. Physics C : Solid State Physics **10 (**1977) 1321.

[75] H. R. Chandrasekhar, D. G. Mead, Physical Review B, **19** (1979) 932.

[76] H. Katahama, S. Nakashima, A. Mitsuishi, M. Ishigame, H. Arashi, J. Phys. Chem. Solids **44** (1983) 1081.

[77] P. M. Nikolic, D. M. Todorovic, J. Physics C: Solid state Physics **20** (1987) 39-46.

[78] Parenteau, Martin, Carlone, Cosmo, Physical Review B **41** (1990) 5227-5234.

[79] A. M. Elkorashy, Semicond. Sci. and Technology **4** (1989) 382-387.

[80] A. R. H. F. Ettema, R. A. de Groot, C. Haas, Physical Review B **46 (**1992) 7363-7373.

[81] M. M. Nassary, Journal of Alloys and Compounds **398** (2005) 21-25.

[82] L. Price, I. P. Parkin, A. M. E. Hardy, R. J. H. Clark, Chem. Mater. **11** (1999) 1792.

[83] W. G. Pu, Z. Z. Lin, Z. W. Ming, G. X. Hong, C. W. Quin, in: Proceedings of the first world conference on Photovoltaic Energy Conversion Hawaii 365 (1994).

[84] S. Cheng, Y. Chen, C. Huang, G. Chen, Thin Solid Films **500** (2006) 96.

[85] Z. Zainal, M. H. Sussein, A. Kassim, A. Ghazali, Sol. Energy Mater. Sol. Cells **40** (1996) 347.

[86] L. S. Price, I. P. Parkin, T. G. Hillbert, K. C. Molloy, Chem. Vapor. Depos. **4** (1998) 222.

[87] A. S. Juarez, A. Ortiz, Semicond. Sci. Technol. **17** (2002) 931.

[88] Subramanian, C. Sanjeeveiraja, M. Jayachandran Sol. Energy Mater. Sol. Cells **79** (2003) 57.

[89] C. R. Sehhar, K. K. Malay, D. D. Gupta, Thin Solid Films **350** (1999) 72.

[90] P. Pramanik, P. K. Basu, S. Biswas, Thin Solid Films 150 (1987) 269.

[91] H. Ben Haj Salah, H. Bouzouita, B. Rezig Thin Solid Films **480–481** (2005) 439.

[92] M. M. El-Nahass, H. M. Zeyada, M. S. Aziz, N. A. El-Ghamaz, Optical materials **20** (2002) 159-170.

[93] N. Devika, N. K. Reddy, K. Ramesh, H. R. Sumana, K. R. Gunasekhar, E. S. R. Gopal, K. T. R. Reddy, Semiconductor Science and Technology **21** (2006) 195-1501.

[94] M. Devika, K. T. R. Reddy, N. K. Reddy, K. Ramesh, R. Ganesan, E. S. R. Gopal, K. R. Gunasekhar, Journal of Applied Physics **100** (2006) 023518/1-023518/7.

[95] M. Devika, N. K. Reddy, K. Ramesh, K. R. Gunasekhar, E. S. R. Gopal, K. T. R. Reddy, Semicond science and technology **21** (2006)1125-1131.

[96] N. K. Reddy, K. Ramesh, R. Ganesan, K. T. R. Reddy, K. R. Gunasekhar, E. S. R. Gopal, Appl. Phys. A **83** (2006) 133-138.

[97] R. W. Miles, O. E. Ogah, G. Zoppi, I. Forbes, Thin Solid Films **517** (2009) 4702-4705.

[98] B. Ghosh; R. Bhattacharje; P. Banerjee, S. Das, Applied Surface Science **257** (2011) 3670-3676.

[99] K. T R. Reddy, P. P. Reddy, Materials Letters **56** (2002) 108-111.

[100] G. Gordillo, M. Botero, J. S. Oyola, MicroelectronicsJournal **39** (2008) 1351-353.

[101] S. Lai, S. Cheng, Shao-Peng Peng,, Dian zi Yuan jian Yu Cai liao **28** (2009) 65-68.

[102] Y. J. Kim, S. M. George, High and Low Concentrator Systems for Solar Electric Applications, in: Proceedings of SPIE , 7769 (2010).

[103] P. Pramanik, P. K Basu, S. Biswas, Thin Solid Films **150** (1987) 269-276.

[104] M. Ristov, G. Sinadinovski, I. Grozdanov, M. Mitreski, Thin Sold films **173** (1989) 53-58.

[105] C. D. Lokhande, Materials chemistry and Physics **27** (1991) 1-43.

[106] M. T. S. Nair, P. K. Nair, Semiconductor Science and Technology **6** (1991) 132-134.

[107] P. K. Nair, M. T. S. Nair, J. Physics D: Applied Physics **24 (**1991) 83-87.

[108] Tian-min Lei, Yong-hong Hu, Hong-sheng Li, Liu-chen Li, Xian-feng Feng, Shou-zhi Liu, Journal of Synthetic Crystals **34** (2005) 484-486.

[109] A. Akkari, N. T. Ben, N. Kamoun, Fundamental and Applied Spectroscopy, in: AIP Conference Proceedings 935 37-42 (2007).

[110] P. P. Hankare, A. V. Jadhav, P. A. Chate, K. C. Rathod, P. A. Chavan, S. A. Ingole,, **463** (2008) 581-584.

[111] A. Akkari, C. Guasch, N. Kamoun-Turki, Journal of Alloys and Compounds **490** (2010) 180-183.

[112] E. Guneri, F. Gode, C. Ulutas, F. Kirmizigul, G. Altindemir, C. Gumus, Chalcogenide Letters **7** (2010) 685-694.

[113] E. Guneri, C. Ulutas, F. Kirmizigul, G. Altindemir, F. Gode, C. Gumus, Applied Surface Science **257** (2010) 1189-1195.

[114] A. Kassim, Ho Soon Min, A. Shariff, Md Jelas Haron, Research Journal of Chemistry and Environment **15** (2011) 45-48.

[115] Yanuar, George El-Haj Moussa, F. Guastavino, Llinares, IEEE (2001) 0-7803-7117-8.

[116] B. Thangaraju, P, Kaliannan, J. Physics D: Applied Physics **33** (2000) 1054-1059.

[117] N. K. Reddy, K. T. R. Reddy, Physica B **368** (2005) 25-31.

[118] N. K. Reddy, K. T. R. Reddy, Materials chemistry and physics **102** (2007) 13-18.

[119] M. C. Rodriguez, H. Martinez, A.S. Juarez, J. C. Alvarez, A. T. Silver, M. E. Calixto, Thin Solid Films **517** (2009) 2497-2499.

[120] L. S. Price, I. P. Parkin, A. M. E. Hardy, R. J. H. Clark, T. H. Hibbert, K. C. Molloy, Chem. Mater **11** (1999) 1972-1799.

[121] G. Barone, T. G. Hibbert, M. H. Mahon, K. C. Molloy, L. S. Price, I. P. Parkin, A. M. E. Hardy, M. N. Field, Journal of Materials Chemistry **19** (2000) 5003-5008.

[122] A. S. Juarez, A. Ortiz, Semiconductor Science and Technology **17** (2002) 931-937.

[123] B. P. Bade, S. S. Garje, Y. S. Niwate, M. Afzaal, P. O'Brien, Chemical Vapor Deposition **14** (2008) 292-295.

[124] N. Sato, M. Ichimura, E. Arai, Y. Yamazaki, in: Proceedings of 3rd World conference on photovoltaic energy conversion Osaka, Japan (2003).

[125] L. K. Khel, S. Khan, M. I. Zaman, Journal of the Chemical Society of Pakistan **27** (2005) 24-28.

[126] Z. Zainal, S. Nagalingam, T. M. Hua, Journal of Materials Science: Materials in Electronics **16** (2005) 281-285.

[127] K. Y. Jain, H. Sharma, K. N. Sood, Rashmi, S. T. Lakshmikumar, in: Conference Record of the IEEE Photovoltaic Specialists Conference Florida 468 (2005).

[128] Yan-qing Chen, Shu-ying Cheng, Gongneng Cailiao Yu Qijian Xuebao **12** (2006) 27-30.

[129] S. Cheng, Y. Chen, Y. He, G. Chen, Materials Letters, **61** (2007) 1408-1412.

[130] G. H. Yue, W. Wang, L. S. Wang, X. Wang, P. X. Yan, Y. Chen, D. L. Peng, Journal of Alloys and Compounds, **474** (2009) 445-449.

[131] H. B. M. Anaya, I. Z. Torres, N. R. Mathews, Pulse electrodeposited tin sulfide films for photovoltaic applications, in: Proceedings of SPIE 7409 (2009).

[132] G. H. Yue, D. L. Peng, P. X. Yan, L. S. Wang, W. Wang, X. H. Luo, Journal of Alloys and Compounds **468** (2009) 254-257.

[133] S. Mondal, P. Mitra, Material Science Research India **5** (2008) 67-74.

[134] C. Gao, Hong-lie Shen, Lei Sun, Hai-Bin Huang, Lin-Feng Lu, H. Cai, Materials Letters **64** (2010) 2177-2179.

[135] W. Guang-Pu, Z. Zhi Lin, Z. Wei-Ming, G. Xiang-Hong, Chen Wei-Qun, in: Procedings of First world photovoltaic energy conversion Hawaii (1994).

[136] Qing Li, Yi Ding, Hao Wu, Xianming Liu, Yitai Qian, Materials Research Bulletin **37** (2002) 925-932.

[137] C. Cifuentes, M. Botero, E. Romero, C. Calderon, G. Gordillo, Brazilian Journal of Physics **36** (2006) 1046-1049.

[138] B. G. Jayaprakash, A. Amalarani, K. Kesavan, S. Mohan, Chalcogenide Letters **6** (2009) 455-461.

[139] Z. Xu, Y. Chen, Energy Procedia **10** (2011) 238-242.

[140] I. Lefebvre, M. Lannoo, J. Olivier-Fourcade, J. C. Jumas Physical Review B **44** (1991) 1004-1011.

[141] P. K. Nair, M. T. S. Nair, Ralph, A. Zingaro, E. A. Meyers, Thin Solid Films **239** (1994) 85-92.

[142] T. Jiang, G. A. Ozin, A. Verma, R. L. Bedard, J. Mater. Chem**. 8**, (1998) 1649-1656

[143] T. Jiang, G. A. Ozin, J. matter. Chem. **7** (1997) 2213.

[144] I. Sokolov, T. Jiang, G. A. Ozin, Adv. Mater. **10** (1998) 942.

[145] H. safak, M. Merdan, O. F. Yuksel, Turk. J. Physics **26** (2002) 341-347I.

[146] M. Cruz, J. Morales, J. P. Espinos, J. Sanz, Journal of Solid state chemistry **175** (2003) 359-365.

[147] G. Sharma, M. Sharma, M. C. Mishra, K. B. Joshi, R. K. Kothari, B. K. Sharma, Phys. Status Solidi B **246** (2009) 2263–2269.

[148] B. Ghosh, M. Das, P. Banerjee, S. Das, Solid State Sciences **11** (2009) 461-466.

[149] I. Gaied, A. Akkari, N. Yacoubi, N. Kamoun, Journal of Physics: Conference Series **214** (2010).

[150] N. R. Mathews, Semiconductor Science and Technology, **25**, (2010) 105010 /1-105010/6.

[151] Yu-ying Guo, Wei-min Shi, Guang-pu Wei, Yong-hua Qiu, Yi-ben Xia, Gongneng Cailiao Yu Qijian Xuebao **13** (2007) 651-654.

[152] Yu-ying Guo, Wei-min Shi, Yu Zhang, L. Wang, Guangpu Wei, in:Proceedings of SPIE - Sixth International Conference on Thin Film Physics and Applications 6984 (2008).

[153] D. M. Unuchak, K. Bente, G. Kloess, W. Schmitz, V. F. Gremenok, V. A. Ivanov,V. Ukhov, Physica Status Solidi C: Current Topics in Solid State Physics **6** (2009) 1191-1194.

[154] Y. Yang, S. Cheng, S. Lai, Advanced Materials Research: Micro and Nano Technology **60-61** (2009) 105-109.

[155] Hong-Jie Jia, Shu-Ying Cheng, Xin-Kun Wu, Yong-Li Yang, Natural Science **2** (2010) 197-200.

[156] S. Zhang, S. Cheng, Micro & Nano Letters **6** (2011) 559-562.

[157] A. P. Alivisators, Science **271** (1996) 933.

[158] C. An, K. Tang, Y. Jin, Q. Liu, X. Chen, Y. Qian, Journal of Crystal growth **252** (2003)581-586.

[159] Y. Li, J. P. Tu, X. H. Huang, H. M. Wu, Y. F. Yuan, Electrochemistry Communications **9** (2007) 49-53.

[160] Yu Wang; Y. B. K. Reddy, H. Gong, Journal of the Electrochemical Society **156** (2009) H157-H160.

[161] Y. S. Niwate, S. S. Garje, in: Proceedings of AIP International Conference on Advanced Nanomaterials and Nanotechnology 1276 56-61 (2010).

[162] K. Bente, V. V. Lazenka, D. M. Unuchak, G. Wagner, V. F. Gremenok, Crystal Research and Technology **45** (2010) 643-646.

[163] M. Ristov, G. Sinadinovski, M. Mitreski, M. Ristova, Solar Energy Materials and Solar cells **69** (2001) 17-24.

[164] M. Sharon, K. Basavaswaran, Solar cells **25** **(**1988) 97-107.

[165] H. Noguchi, A. Setiyadi, H. Tanamura, T. Nagatomo, O. Omoto, Solar Energy Materials and Solar Cells **35** (1994) 325-331.

[166] D. Avellaneda, G. Delgado, M. T. S. Nair, P. K. Nair, Thin Solid Films **515** (2007) 5771-5776.

[167] M. Gunasekaran, M. Ichimura, Solar energy materials and Solar cells **91** (2007) 774-778.

[168] M. Ichimura, M. Gunasekaran, T. Sueyoshi, in Proceedings of AIP Conference on Nanoscience and Nanotechnology 1136 138-145 (2009).

[169] N. R. Mathews, D. Avellaneda, H. B. M. Anaya, J. Campos, M. T. S. Nair, P. K. Nair, in: Proceedings of Materials Research Society Symposium on Thin-Film Compound Semiconductor Photovoltaics 1165 1165-M08-35 (2009).

[170] Wu, Li, Faming Zhuanli Shenqing Patent CN 101894877 A 20101124 (2010).

[171] H. A. M. Abdel, M. Ichimura, Japanese Journal of Applied Physics **48** (2009) 035506/1-035506/6.

[172] T. Miyawaki, M. Ichimura, Materials Letters **61** (2007) 4683-4686.

[173] B. Li, C. Shi, L. Li, Y. Wang, Hefei Gongye Daxue Xuebao, Ziran Kexueban **32** (2009) 826-828.

[174] D. Avellaneda, M. T. S. Nair, P. K. Nair, Thin Solid Films **517** (2009) 2500-2502.

[175] B. Ghosh, M. Das, P. Banerjee, S. Das, Semiconductor Science and Technology **24** (2009) 025024/1-025024/7.

[176] B. Ghosh, R. Roy, S. Chowdhury, P. Banerjee, S. Das, Applied Surface Science **256** (2010) 4328-4333.

[177] Li Wu, Wei-min Shi, Zhao-chun Zhang, Juan Qin, Lin-jun Wang, Guang-pu Wei, Yi-ben Xia, Shanghai Daxue Xuebao, Ziran Kexueban **16** (2010) 436-440.

[178] M. Ichimura, K. Akita, Physica Status Solidi C: Current Topics in Solid State Physics **7** (2010) 929-932.

[179] Z. Hu, W. Yang, S. Liu, K. Tang, L. Wang, W. Shi, Advanced Materials Research: Advanced Materials and Structures **335-336** (2011) 1402-1405.

[180] M. Sugiyama , K. T. R. Reddy, N. Revathi, Y. Shimamoto, Y. Murata, Thin Solid Films **519** (2010) 7133.

[181] K. T. R. Reddy, K. Ramya, G. Sreedevi, T. Shimizu, Y. Murata, M. Sugiyama, Energy Procedia **10** (2011) 172-176.

[182] M. Sugiyama, Y. Murata, T. Shimizu, K. Ramya, C. Venkataiah, T. Sato, K. T. R. Reddy, Japanese Journal of Applied Physics **50** (2011) 05FH03/1-05FH03/3.

.....ಶಂಭಾ....

Chapter 2

EXPERIMENTAL TECHNIQUES AND CHARACTERIZATION TOOLS

Contents

2.1 Deposition techniques

After choosing material for the present work, the next important task was to select an appropriate deposition technique. This technique should be viable, cost effective, simple and should be suitable to scale to larger areas. There are different techniques which have been employed by earlier workers to deposit tin-chalcogenides which include both physical and chemical routes. Some of them are vacuum evaporation [1], radio frequency sputtering [2], electrochemical deposition [3,4], atmospheric pressure chemical vapor deposition [5], plasma enhanced chemical vapor deposition [6], brush plating [7], dip deposition [8], chemical bath deposition [9] , and chemical spray pyrolysis (CSP) [10]. Among these, CSP deposited films exhibited better device performance [11]. It is a very effective technique suitable for the preparation of thin films, especially for large area deposition [12]. Easiness of doping and tailoring stoichiometry makes the technique highly suitable for the fabrication of photovoltaic devices and hence we have chosen this technique to deposit thin films in the present study. The following section describes briefly about the

technique. We have indigenously automated the spray coating unit in our lab and a brief description on the instrumentation used for the automation of the unit is also presented here.

2.1.1 Chemical spray Pyrolysis

CSP is a potential deposition technique being considered in research and industry to prepare thin and thick films of ceramic materials and powders. Unlike many other film deposition techniques, this technique is a very simple and cost-effective processing method (especially with regard to equipment and energy requirement) for depositing thin films over very large area. It offers an extremely easy way for preparing films of desired composition and stoichiometry. CSP does not require high-quality substrates or chemicals. The method has been employed for the deposition of dense films, porous films, and for powder production. Even multilayered films can be easily prepared using this versatile technique. Spray pyrolysis has been used for several decades in the glass industry [13] and in solar cell production [14].

Typical spray pyrolysis equipment consists of an atomizer, precursor solution, substrate heater, spray rate controller and temperature controller. A schematic of a typical CSP set-up is given in Figure 2.1. The following atomizers are usually used in spray pyrolysis technique: air blast (the liquid is exposed to a stream of air) [15], ultrasonic (ultrasonic frequencies produce the short wavelengths necessary for fine atomization) [16] and electrostatic (the liquid is exposed to a high electric field) [17].

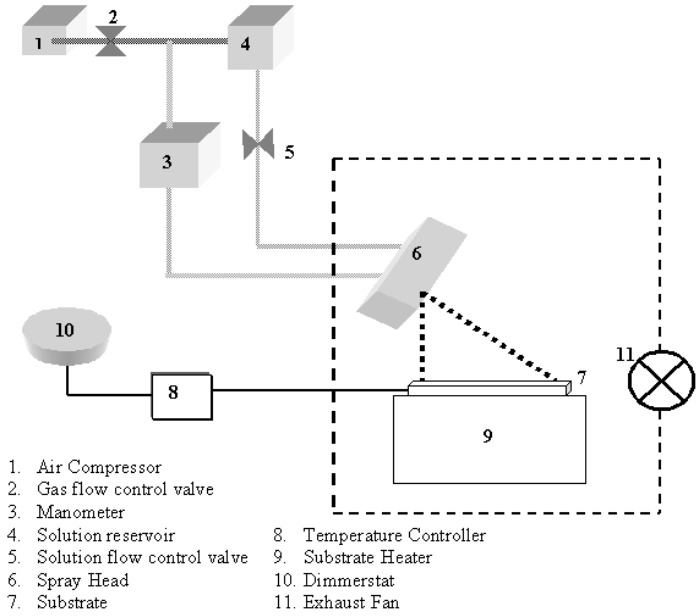

Figure 2.1: Schematic of Spray pyrolysis set-up.

2.1.1.1 A brief review on CSP technique

Film deposition using spray pyrolysis will be discussed in this review with due importance to the effect of deposition temperature and precursor solution on film structure and properties. This will be illustrated with some examples wherever necessary.

Various reviews concerning spray pyrolysis techniques have been published. Mooney and Radding reviewed the spray pyrolysis method, properties of the deposited films in relation to the conditions, specific films (particularly CdS), and device application [18]. Tomar and Garcia discussed preparation and properties of sprayed films as well as their application in solar cells, anti-reflection coatings, and gas sensors [19]. Albin and Risbud presented a review of the equipment, processing parameters, and optoelectronic materials deposited using CSP technique [20]. Pamplin published another review on the use of spraying for

preparing solar cells as well as a bibliography of references on the spray pyrolysis technique [21]. Recently, deposition of thin metal oxide and chalcogenide films using spray pyrolysis and different other atomization techniques were reviewed by Patil [22]. Bohac and Gauckler discussed the mechanism of chemical spray deposition and presented some examples of sprayed Yttria-stabilized zirconia (YSZ) films [23].

Thin film deposition, using the spray pyrolysis technique, involves spraying metal salt solution(s) onto a heated substrate (Figure 2.1). Droplets impact on the substrate surface, spread into a disk shaped structure and undergo thermal decomposition. Shape and size of the disk depends on the momentum and volume of the droplet, as well as the substrate temperature. Consequently, the film is usually composed of overlapping disks of metal salt whose film is required on the heated substrate.

The deposition parameters are very critical in deciding the material properties of the films deposited using this technique. The following paragraphs will give an overview of the significance of various deposition parameters in view of the reports already published by earlier workers.

Spray pyrolysis involves many processes occurring either simultaneously or sequentially. The most important of these are aerosol generation and transport, solvent evaporation, droplet impact with consecutive spreading, and precursor decomposition. Deposition temperature is involved in all mentioned processes, except in the aerosol generation. Consequently, the substrate surface temperature is the main parameter that determines the film morphology and properties. By increasing the temperature, the film morphology can change from a cracked to a porous microstructure. In

many studies, the deposition temperature was reported as the most important one in spray pyrolysis. Properties of deposited films can be varied and/or controlled by changing the deposition temperature. For instance, it influences optical and electrical properties of ZnO films [24]. Films with the lowest electrical resistivity and improved crystallinity were deposited using an aqueous solution of zinc acetate at 490˚C, while films prepared at 420˚C and 490˚C showed high transmission (90–95%) in the visible range. This was attributed to the decrease of the film thickness and an increase in the structural homogeneity. Physical properties of fluorine-doped indium oxide films were investigated with respect to deposition temperature, dopant concentration, air flow rate, and film thickness [25]. It was found that the deposition temperature had remarkable influence on the structure of the films. The extent of preferential (4 0 0) orientation increases with increasing film thickness. Terbia-doped yttria-stabilized thin films were deposited using electrostatic spray deposition [26]. Surface morphology was controlled by changing the deposition parameters and solution compositions. By increasing the deposition temperature, the morphology of the film was shifted from a dense to a highly porous structure.

The precursor solution is probably the second important one in deciding the film properties prepared using CSP technique. Solvent, type of salt, concentration of salt, and additives influence physical and chemical properties of the precursor solution. Therefore, structure and properties of a deposited film can be changed / tailored by changing any one of the above parameters of precursor solution. Chen *et al.* showed that morphology of thin films can be changed considerably by adding additives to the precursor solutions [27]. Structure of deposited TiO_2 film

was changing from a cracked to a 'crack-free reticular' after the introduction of acetic acid into the precursor solution. Change of morphology was attributed to the modification of precursor solution chemistry. Transparent SnO_2 electrodes were deposited through spray pyrolysis using tetra-*n*-butyltin (IV) as precursor [28]. Deposition efficiency and crystallinity of the films deposited at 340˚C were improved by adding H_2O_2 to the alcoholic precursor solution. The authors proposed two explanations for this effect. One was that H_2O_2 decomposes easily on a substrate to produce an oxygen atmosphere, which promotes the oxidation of tetra-*n*-butyltin and reduces residuals within the film. The second explanation was that H_2O_2 and tetra-*n*-butyltin form tin peroxide complexes with direct atomic bonding between Sn and O in the precursor solution. This kind of structure is desirable for formation of SnO_2. Of these, the second explanation is more reasonable, because in the spray pyrolysis process usually there is enough oxygen in air for the oxidation of salts. Porous SnO_2 and SnO_2-Mn_2O_3 films have been prepared using the electrostatic spray deposition technique [29]. These films were used in 'Taguchi type' hydrogen sensors. Grain size of the porous films ranged from 1 to 10 µm. It was observed that the grain size increased with a higher concentration of the precursor in the ethanol solvent.

Caillaud *et al.* investigated the influence of pH of the solution on the thin film deposition and found that the growth rate depended on the pH [30]. The rate was only significant if $3.5 \leq pH \leq 4.3$. In this pH range the vaporized precursors were the zinc acetate complexes. Formation of basic salts, adsorption compounds, or precipitates slowed down the growth at higher pH. At low pH, both the amount of zinc acetate and the growth rate decrease until no more deposition occurs. Thin SnO_2 films for gas sensing

applications have been prepared also by spray pyrolysis using inorganic as well as organic precursor solution [31]. Smooth but not very uniform films were obtained using a solution of $(NH_4)_2.SnCl_6$ in water. On the other hand, very uniform but relatively rough films were deposited using a solution of $(CH_3COO)_2SnCl_2$ in ethylacetate. Suitable electric properties were obtained for films deposited using organic solution. Sensitivity and rise time were depending on the deposition temperature and the type of precursor solution used. The best results were achieved by spraying an organic precursor solution onto a substrate at ~300˚C. In reference [32] the effect of glycerol in aqueous nitrate solutions on the growth of $YBa_2Cu_3O_7$ (YBCO) films was reported. Superconductor films on YSZ substrates, prepared from precursor solutions with glycerol, showed a sharp superconducting transition, (T_c) as for bulk material (above 90 *K*), and a strong *c*-axis oriented texture. On the other hand, surface of the film, prepared from the aqueous precursor solution, was irregular and had a lower T_c than the bulk material. Authors suggested that glycerol improves production of fine droplets, which improved the surface morphology of the deposited film. It was observed that the growth rate of SnO_2 films prepared from $SnCl_4.5H_2O$ was higher while the resistance was lower in comparison with those prepared from anhydrous $SnCl_4$ [33]. The authors suggested that, under identical conditions, the droplets containing $SnCl_4.5H_2O$ require more thermal energy to form SnO_2 than those containing $SnCl_4$. Thus the water molecules seemed to influence the reaction kinetics, particularly the growth rate of the films. The influence of process parameters on the sensitivity to humidity of SnO_2-Fe_2O_3 films was investigated [34]. Nature of the iron salt influenced the sensitivity to humidity of the samples. The films deposited from an alcohol solution

containing $Fe_2(C_2O_4)_3$ exhibited higher sensitivity than those from a solution containing $Fe(NH_4)(SO_4)_2$. This fact was explained by the higher porosity of the structure obtained from iron oxalate, because during the oxalate pyrolysis a lot more gaseous decomposition products are released compared to the sulphate precursors. Kim *et al.* studied the influence of additives on the properties of MgO films deposited using electrostatic spray deposition [35]. A large number of separated particles were observed on the surface of MgO films when pure tetrahydrofuran (THF) was used as a solvent. However, smooth and particle free MgO films were obtained when 1-butyl alcohol or 1-octyl alcohol was added to THF. The authors suggested that the alcohols effectively restrain MgO nucleation resulting from the vaporization of droplets.

Spray rate, angle of spray, height of the spray head from the heater / substrate, carrier gas used for the spray, molarity and ratio of the constituent precursor solutions, pressure of the carrier gas, etc are some of the other major deposition parameters as far the coating technique is concerned [36].

Indeed it is very difficult to control all these deposition parameters in manual spray technique. Therefore, the technique has been automated indigenously in our lab with the help of a company M/s. Hollmark, Kalamassery, India.

2.1.1.2 Indigenously developed Automated Spray coating unit

A circular S.S plate having thickness 6 mm and 15 cm diameter has been used as the hot plate after machining it finely. A single heater coil having 1.5 kW, embedded in a ceramic grove is then attached to this base plate to facilitate resistive heating. This heater assembly is capable of providing a

uniform temperature of 500˚C (with a maximum variation of ±5˚C over the surface of the hot plate) over the S.S hot plate. A proper insulation was then given to this set-up using thermal bricks and rock wool. A K-type thermocouple attached in a grove located near the top surface of the base plate detected temperature on the substrate surface. During the spray, substrate temperature was kept constant with an accuracy of ±5˚C using a temperature controller equipped with 10 A on/off relay circuit.

The designing of the dispensing unit for controlling the spray rate is based on the principle of screw gauge and syringe action. By varying the speed of the micro processor controlled stepper motor attached to the piston of the container, dispensing rate was controlled. The motor shaft is connected to a lead screw through a gear and the piston is attached to this lead screw. Using this setup, the spray rate can be precisely controlled in the range 1 ml/min to 20 ml/min. The container and the connecting tubes are made of Teflon, a corrosion free material.

The spray head (Figure 2.2) consisted of an air nozzle placed at right angle to the needle through which the solution is dispensed from the container.

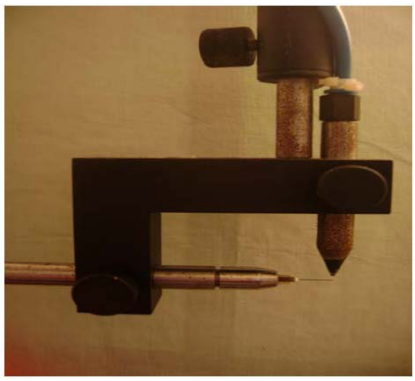

Figure 2.2: Photograph of the air blast type spray nozzle used for the work.

The spray head, heater and the substrate were kept inside a chamber provided with an exhaust fan for removing the gaseous byproducts and the solvent vapor.

Uniform coverage of large area was achieved by moving the spray head over the substrate surface by employing a mechanism having two stepper motors. The spray head could scan an area of 15 cm x 15 cm. There is also a provision to control the speed of the 'X and Y scan'. X movement can be varied from 50 mm/sec to 400 mm/sec. Usually we prefer slow Y-movement. Typically a scan speed of 50 mm/sec was fixed for the Y direction movement.

The atomization technique adopted for the system is air blast. Filtered air is used as the carrier gas. Required pressure is achieved using a 0.5 HP compressor and it is controlled and air is fed to the nozzle with the help of a mechanical pressure gauge.

Picture of the automated spray coating unit used for the present work is given in Figure 2.3.

Figure 2.3: The Indigenously developed Automated CSP unit used for the work.

2.1.2 Vacuum evaporation

For purposeful and controlled diffusion of metal atoms in to the SnS matrix, we employed thermal evaporation technique. This technique was employed to enhance / modify the material properties of the spray deposited films. This deposition technique also has been used for coating electrodes for the trial devices fabricated in the present work.

In this technique, molecules (of the evaporant material) coming out from the heated material will spread out in all directions. But their velocity distribution will depend on the nature of the source [37]. If a source can be approximated to a tiny sphere compared to its distance from the receiving substrate, then the emitted vapor stream will have the same velocity distribution in all directions and hence resembling the emission from a point source. Usually source is assumed to be a "point source". For the present study we have adopted "resistive heating" method to supply heat of vaporization of materials. There are several types of practical heating sources made from refractory metals such as tungsten, molybdenum, tantalum etc. We used a 200 A molybdenum source in the form of a boat supplied by HHV pvt. Ltd, India. Material to be evaporated is placed in the boat and is converted in to vapor form by means of resistive heating. The vapor atoms thus created are transported through vacuum of 2×10^{-5} Torr to get deposited on the substrate. At a steady state of evaporation these vapor atoms or molecules will have an equilibrium vapor pressure (p), which is given by the relation [37,38].

$$p = \frac{NkT}{V} \quad \text{---------- (2.1)}$$

Where N is the total number of vapor atoms or molecules V is the volume of the enclosed chamber T is the absolute temperature of the gaseous species and k is Boltzmann's constant. These atoms or molecules in the gaseous state will however collide with one another after a certain mean free time (τ) and the average distance of travel before suffering a collision with another can be expressed by the relations.

$$l=\left(\frac{N}{V}\pi x\sigma^2\sqrt{2}\right)^{-1} \quad \text{----------} \quad (2.2)$$

where, *l* is the mean free path (mfp) in cm of the vapor species and σ is the conductivity of the film. From the above relations, it is seen that the lower the equilibrium vapor pressure the more will be l and when p is very low vapor atoms or molecules will travel a long distance without encountering any collision i.e. these will be moving in a straight path relatively unhindered. The above equation for air at room temperature can be written as

$$l = \frac{5}{p} \quad \text{----------} \quad (2.3)$$

where, p is expressed in micron pressure. Thus in an evacuated system if the residual air pressure at steady state is, say, 10^{-4} torr, then corresponding *l* will be 50 cm and with lower p, mfp will still be larger. Thus in a highly evacuated system, evaporated atoms or molecules from a heated source will have high *l* and if *l* is greater than the length of the enclosed chamber then there will not be any collision of the atoms or the molecules and these will move unhindered.

2.2 Characterization techniques

2.2.1 Thickness measurement- Stylus profilometer

Thickness is one of the most important parameter of a thin film to be characterized since it plays an important role in the film properties unlike in bulk material. Microelectronic applications generally require the maintenance of precise and reproducible film metrology (i.e., thickness as well as lateral dimensions). Various techniques are available to characterize the film thickness which are basically divided into optical and mechanical methods, and are usually nondestructive; but sometimes it can be destructive in nature. Film thickness may be measured either by in-situ monitoring of the rate of deposition or after the film deposition.

Stylus profilometer is an advanced tool for thickness measurement of both thin and thick films. It is capable of measuring steps even below 100 Å. This instrument can also be used to profile surface topography and waviness, as well as measuring surface roughness in the sub nanometer range [39]. The stylus profiler takes measurements electromechanically by moving the sample beneath a diamond tipped stylus. The high precision stage moves the sample according to a user defined scan length, speed and stylus force. The stylus is mechanically coupled to the core of a linear variable differential transformer (LVDT). The stylus moves over the sample surface. Surface variations cause the stylus to be translated vertically. Electrical signals corresponding to the stylus movement are produced as the core position of the LVDT changes. The LVDT scales an ac reference signal proportional to the position change, which in turn is conditioned and converted to a digital format through a high precision, integrating, analog-to-digital converter. The film whose thickness has to be measured is deposited with a region masked. This creates a step on the

sample surface. Then the thickness of the sample can be measured accurately by measuring the vertical motion of the stylus over the step. Thicknesses of the films prepared for the work presented in this thesis were measured using a Dektak 6M stylus profiler.

2.2.2 Structural characterization

2.2.2.1 Raman Spectroscopy

Raman spectroscopy is a vibrational spectroscopic technique that can detect both organic and inorganic species and measure the crystallinity of the solids. It is free from charging effects that can influence electron and ion beam techniques [40].

Raman spectroscopy is based on Raman Effect, first reported by Raman in 1928 [41]. If the incident photon imparts part of its energy to the lattice in the form of a phonon (phonon emission) it emerges as a lower energy photon. The down-converted frequency shift is known as Stokes-shifted scattering. Anti stokes-shifted scattering results when the photon absorbs a phonon and emerges with a higher energy. The anti-stokes mode is much weaker than the Stokes mode and it is Stokes-mode scattering that is usually monitored.

During Raman spectroscopic measurements a laser beam, referred to as the pump, is incident on the sample. The weak scattered light or the signal is passed through a double monochromator to reject the Raleigh scattered light; the Raman shifted wavelengths are detected by a photo detector. In the Raman microprobe, a laser illuminates the sample through a commercial microscope. Laser power is usually held below 5mW to reduce sample heating and specimen decomposition. In order to separate the signal from the pump it is necessary that the pump should be a bright,

monochromatic source. Detection is made difficult by the weak signals against the intense background of scattered pump radiation. The signal-to-noise ratio is enhanced if the Raman radiation can be observed at right angles to the pump beam. A major limitation in Raman spectroscopy is the interference caused by the fluorescence, either of impurities or of sample itself. This fluorescent background problem is eliminated by combining Raman spectroscopy with Fourier Transform Infrared Spectroscopy (FTIR).

Raman is very sensitive to crystal structure. For example, various crystal orientations give slightly different Raman shifts. The frequencies are shifted due to the stress and strain in the thin film also.

In the present work, Raman analysis was performed in the back scattering mode at room temperature using micro Raman system from Jobin Yvon Horibra LABRAM-HR visible (400 -1100 nm) with a spectral resolution of $1cm^{-1}$. Argon ion laser of wavelength 488nm was used as the excitation source.

2.2.2.2 X-ray diffraction technique

The most common technique for analyzing thin films as thin as 100 Å is to use a 'grazing incidence angle' arrangement. Samples can be analyzed using this technique in a non-destructive way. Glancing angle XRD is used when the information needed lies within a thin top layer of the material. We employed the 'Seemann-Bohlin geometry' [42] for the present study. Incident x-ray is impinging on the fixed specimen at a small angle, γ (typically <1˚ to 3˚) and the diffracted x-rays are detected by a detector that moves along the focusing circle. This method provides good sensitivity for thin films, due to para-focusing and the large diffracting

volume, which results from γ being small and x-ray path length in the film being large (proportional to 1/sin γ). By increasing the path length of the incident x-ray beam through the film, intensity from the film can be increased, while at the same time, the diffracted intensity from the substrate can be reduced. Overall, there is a dramatic increase in the film signal to background ratio. During the collection of the diffracted spectrum, only the detector rotates through the angular range, keeping the incident angle, the beam path length and the irradiated area constant.

XRD gives whole range of information about crystal structure, orientation, crystallite size, composition defects and stresses in thin films [43]. Experimentally determined data is compared with JCPDS file for standards. The inter-planar spacing (d) can be calculated from the Bragg's formula,

$$2d \sin\theta = n\lambda \quad \text{----------} \quad (2.4)$$

where, θ is the Bragg angle, n is the order of the spectrum; λ is the wavelength of x-rays which is equal to 1.5405 Å for CuK_α radiation used for the present study. Using d values, the plane (h k l) can be identified and lattice parameters are calculated with the help of following relations: For the orthorhombic systems,

$$\frac{1}{d_{hkl}} = \sqrt{\frac{h^2}{a^2} + \frac{k^2}{b^2} + \frac{l^2}{c^2}} \quad \text{----------} \quad (2.5)$$

where a, b and c are lattice parameters. The grain size 'L' can be calculated from the Debye-Scherrer formula,

$$L = k\lambda / (\beta . \cos\theta) \quad \text{----------} \quad (2.6)$$

Where, k is a constant equal to 0.9 and β is the full width at half maximum (FWHM) measured in radians. In the present study XRD measurements was performed employing Rigaku (D.Max.C) x-ray diffractometer having CuK_α (λ=1.5405 Å) radiation and Ni filter operated at 30 kV and 20 mA. All samples were scanned in the range 10˚ to 60˚ with a scan speed of 5˚/min.

2.2.2.3 Scanning electron microscopy (SEM)

In SEM, a source of electrons is focused in vacuum into a fine probe that is rastered over surface of the specimen. The electron beam passes through scan coils and objective lens that deflects the beam horizontally and vertically so that the beam scans the surface of the sample. As electrons penetrate the surface, a number of interactions occur that can result in the emission of electrons or photons from or through the surface. A reasonable fraction of the electrons emitted can be collected by appropriate detectors, and the output can be used to modulate the brightness of a cathode ray tube (CRT) whose x and y inputs are driven in synchronism with the x-y voltage rastering the electron beam. In this way an image is produced on the CRT; every point that the beam strikes on the sample is mapped directly on to a corresponding point on the screen. Linear magnification obtained can be calculated from the simple expression [40]

$$M = L/I \quad \text{----------} \quad (2.7)$$

where, L is the raster's length of the CRT monitor and I *is* the raster length on the surface of the sample. SEM works on a voltage between 2 to 5 kV and the beam diameter that scans the specimen in 5 nm to 2 μm. The principle image produced in SEM is of three types: secondary electron images, backscattered electron images and elemental x-ay maps.

Secondary and backscattered electrons are conventionally selected and separated according to their energies. When the energy of the emitted electron is less than about 50 eV, it is referred to as a secondary electron and backscattered electrons are considered to be the electrons that exit the specimen with energy greater than 50 eV. Detectors of each type of electrons are placed in the microscope in proper positions to collect them.

The SEM instrument JEOL, JSM-840 was employed to characterize films in this work. Operating voltage of SEM measurements was 20 kV and the surface morphology of the samples was compared at 25,000X magnification. Compositional variation of the samples was analyzed using energy dispersive x-ray **(**EDAX) analysis (operated at 20 kV), which is attached with the SEM.

2.2.2.4 Atomic force microscopy (AFM)

AFM has the advantage of imaging almost any type of surface (conducting, semiconducting, insulator). Binning, Quate, and Gober invented the AFM in 1985 [44]. Their original AFM consisted of a diamond tip attached to a strip of gold foil. The diamond tip contacted the surface directly, with the interatomic van der Waals force providing the interaction mechanism. Detection of the cantilever's vertical movement was done with a second tip.

Today, most AFMs use a laser beam deflection system, introduced by Mayer and Amer, where a laser is reflected from the back of the reflective AFM lever and on to a position sensitive detector. AFM tips and cantilevers are micro fabricated from Si or Si_3N_4. Typical tip radius is from a few nm to few tens of nm [45].

The "Nanoscope AFM", which has been used to characterize films in the present work, employs an optical detection system in which the tip is attached to the underside of a reflective cantilever. A diode laser is focused onto the back of a reflective cantilever. As the tip scans the surface of the sample, moving up and down with the contour of the surface, the laser beam is deflected off the attached cantilever into a dual element photodiode.

The photo detector measures the difference in light intensities between the upper and lower photo detectors, and then converts to voltage. Feedback from the photodiode difference signal, through software control from the computer, enables the tip to maintain either a constant force or constant height above the sample. In the constant force mode the piezo-electric transducer monitors real time height deviation. In the constant height mode, the deflection force on the sample is recorded. The latter mode of operation requires calibration parameters of the scanning tip to be inserted in the AFM head during force calibration of the microscope. In 'non contact' mode, the AFM derives topographic images from measurements of attractive forces; the tip does not touch the sample. AFMs can achieve a resolution of 10 pm. In the present work, AFM-Nanoscope-E, Digital Instruments, USA was used in contact mode for the measurements.

2.2.3 Electrical characterization

Conductivity of a semiconductor crystal is considerably affected by lattice vibrations, impurities, strain, displaced atoms in the lattice, grain boundaries etc. Conductivity can be expressed in terms of material dimensions through resistivity or resistance (ρ or R). If L and B are the

length and breadth of a rectangular shaped specimen and d is the thickness [46] then,

$$\rho = \frac{RBd}{L} \quad \text{---------- (2.8)}$$

where ρ is the resistivity and its unit is Ω.cm

$$\sigma = \frac{1}{\rho} \quad \text{---------- (2.9)}$$

ρ and σ are constant for any particular bulk material at a fixed temperature. However, for films, since these are dependent on thickness and grain size unlike the bulk material.

$$\frac{\rho}{d} = \frac{RB}{L} = R_s \quad \text{---------- (2.10)}$$

where R_s is known as the 'sheet resistance' which is expressed in ohm per square.

If we assume L=B, then

$$\frac{\rho}{d} = R = R_s \quad \text{---------- (2.11)}$$

Which means that the resistance of one square of a film is its sheet resistance R_S and it is independent of the size of the square; but this depends only on resistivity and film thickness. If the film thickness is known, then resistivity is given by,

$$\rho = d.\ R_s \quad \text{---------- (2.12)}$$

2.2.3.1 Two-point probe method

Two probe method is a very easy technique to implement because here only two probes are needed to be manipulated and also the resistivity

range of the films under study is appropriate for this technique. This is especially suitable to characterize low resistive materials. Each probe in the two probe configuration serves as a current and voltage probe. Theoretically the total resistance R_T between the two probes is given by [40],

$$R_T = V/I = 2.R_P + 2.R_C + 2.R_{SP} + R_S \quad \text{----------} \quad (2.13)$$

where, R_P is the probe resistance, R_C is the contact resistance at each metal probe / semiconductor contact, R_{SP} is the spreading resistance under each probe, and R_S is the semiconductor resistance. We assume R_C and R_{SP} to be identical and by choosing suitable probes we make its contribution very negligible.

Silver electrodes were painted on the surface of the film on a fixed area which serves as electrodes for the two probe measurements. Width and length of these line electrodes were 0.5 mm and 5 mm respectively with uniform thickness (~1.5 µm), keeping a distance of 5 mm in between the electrodes.

2.2.3.2 Four Probe method

This is the most common method for measuring resistivity of compound semiconducting thin films and is especially suitable for measurements in the low resisivity regime. It is an absolute measurement without recourse to calibrated standards. The idea of four point probe was first proposed by Wenner [47] in 1916 to measure the earth's resistivity and in 1954 Valdes [48] adopted this technique for the resistivity measurements of semiconductors.

Figure 2.4 is an illustration of a collinear four probe setup. Two probes carry the current and other two probes sense the voltage. Use of four probes has an important advantage over two probes. Although the current carrying probes still have contact and spreading resistance (as given in the above section) associated with them, that is not true for the voltage probes because the voltage is measured either with a potentiometer, which draws no current at all, or with a high impedance voltmeter, which draws little current.

$$R = 2\pi s\,(V/I) \quad \text{---------- (2.14)}$$

where s is the distance between the probes,

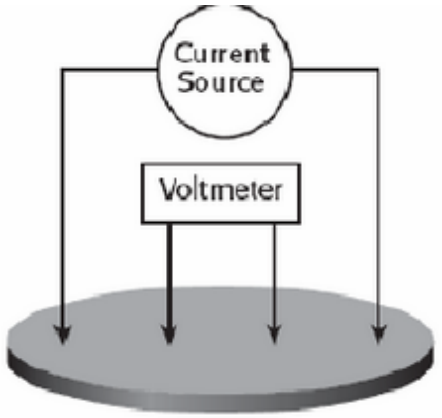

Fig 2.4: Schematic diagram of four probe set-up.

2.2.3.3 Photosensitivity measurement

Photosensitivity is an indirect measure of the minority carriers in a semiconductor produced on illumination with light. In the present work, it is calculated as

$$\varphi = (I_L - I_D)/I_D \quad \text{---------- (2.15)}$$

where, I_L is the current under illuminated condition and I_D is the current under dark conditions. In this work, samples are illuminated using a tungsten halogen lamp to measure photosensitivity.

In the present work, Keithley-236 source measure unit (SMU) was employed for electrical characterization and photosensitivity measurements by applying an electric field of 1000 V/m to the films. For photosensitivity measurements, the samples were illuminated through the glass substrate with a tungsten halogen lamp (white light) capable of giving intensity of 60 mW/cm^2 over the sample surface. IR filter and a water column were kept in between the light source and sample to avoid heating of the sample.

2.2.3.4 Hot probe Technique

This technique is otherwise known as 'thermoelectric probe' method. In this method the conductivity type is determined by the sign of thermal EMF or Seebeck voltage generated by a temperature gradient. Two probes contact the sample surface: one is hot, the other is cold as shown in Figure 2.5.

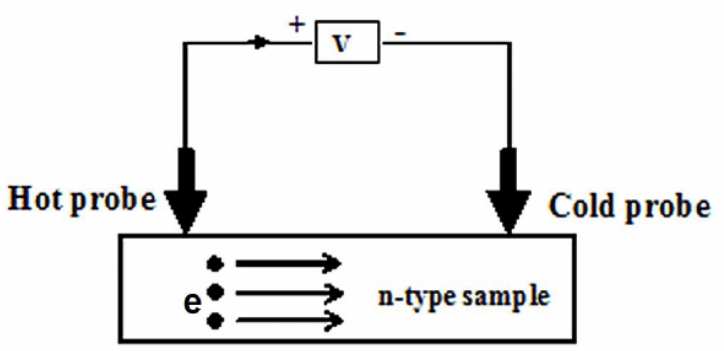

Figure 2.5: The hot probe set-up.

Thermal gradients produce currents in a semiconductor; the majority carrier currents for n and p-type materials are [40]

$$J_n = -qn\mu_n P_n \frac{dT}{dx} \quad \text{---------- (2.16)}$$

$$J_p = -qn\mu_p P_p \frac{dT}{dx} \quad \text{---------- (2.17)}$$

where q is the charge, n and p are the number of electrons and holes, μ is the mobility of the charge carriers, $\frac{dT}{d\chi}$ is the temperature gradient, $P_n<0$ and $P_p>0$ are the differential thermoelectric power.

In Figure 2.5, $\frac{dT}{d\chi} > 0$, and the electron current in an n-type sample flows from left to right. A part of the current flows through the voltmeter causing the hot probe to develop positive potential with respect to the cold probe [40]. Electrons diffuse from the hot to the cold region setting up an electric field that opposes diffusion. The electric field produces a potential detected by the voltmeter with the hot probe positive with respect to the cold probe. Analogous reasoning leads to the opposite potential for p-type samples.

Hot probes are usually effective in resistivity range of 10^{-3} to 10^{3} Ω.cm. The voltmeter tends to indicate n-type for high resistivity material even if the sample is weakly p-type, because this method actually determines the $n.\mu_n$ or the $p.\mu_p$ product. With $\mu_n > \mu_p$, intrinsic or high resistivity material is measured as n-type if $n \approx p$.

2.2.3.5 Hall effect

The Hall Effect measurement technique is widely applied in the characterization of semiconductor materials as it gives resistivity, carrier density, type of carriers and mobility of carriers.

When a magnetic field is applied to a conductor perpendicular to the current flow direction, an electric field will be developed perpendicular to the direction of magnetic field and the current. This phenomenon is known as Hall Effect and the developed voltage is called "Hall voltage". The force acting on a charge (q) moving with a velocity v in the presence of an electric (E) and magnetic (B) fields is given by the vector expression,

$$F = q\,(E + (v \times B)) \quad \text{---------- (2.18)}$$

For n-type and p-type samples, the electrons and holes respectively deflect to the same side of the sample for the same current direction because electrons flow in the opposite direction to holes and have opposite charge. The Hall coefficient R_H is defined as

$$R_H = \frac{V_H d}{BI} \quad \text{---------- (2.19)}$$

where, d is the sample dimension in the direction of magnetic field B, V_H is the Hall voltage and I is the current through the sample [40] .

For semiconducting films on insulating substrates, the mobility is frequently observed to decrease towards the substrate. Surface depletion forces the current to flow in the low-mobility portion of the film, giving apparent mobility lower than true mobility. Hall Effect measurements are simple to interpret for uniformly doped samples. Non-uniformly doped layer measurements are more difficult to interpret. If the doping density varies with film thickness, then its resistivity and mobility also vary with

thickness. It is to be noted that Hall Effect measurement gives average resistivity, carrier density, and mobility.

Electrical resistivity and Hall coefficients of the films described in this thesis were measured using four probe van der Pauw configuration with AC modulation of magnetic field at room temperature using Ecopia model No HMS-3000 (magnetic field = 0.57 T and capable of current measurement in the range 1–25 mA).

2.2.4 Compositional analysis

2.2.4.1 Energy dispersive x-ray analysis (EDAX)

EDAX stands for energy dispersive x-ray analysis. This technique, sometimes referred to also as EDS or EDX analysis, is used for identifying the elemental composition of the specimen, on an area of interest. The EDAX works as an integrated feature of a SEM and cannot be operated its own without the latter [49].

During EDAX, the specimen is bombarded with an electron beam inside the scanning electron microscope. The bombarding electrons collide with the specimen atom's own electrons, knocking some of them off in the process. A position vacated by an ejected inner shell electron is eventually occupied by a higher-energy electron from an outer shell. To be able to do so, however, the transferring outer electron must give up some of its energy by emitting an x-ray. The amount of energy released by the transferring electron depends on which shell it is transferring from, as well as which shell it is transferring to. Furthermore, the atom of every element releases x-ray photons with unique amounts of energy during the transferring process. Thus, by measuring the energy of the x-ray photons emitted by a specimen during electron beam bombardment, identity of the

atom from which the x-ray was emitted can be established. The output of an EDAX analysis is an EDAX spectrum, which is a plot of how frequently x-ray is received for each energy level.

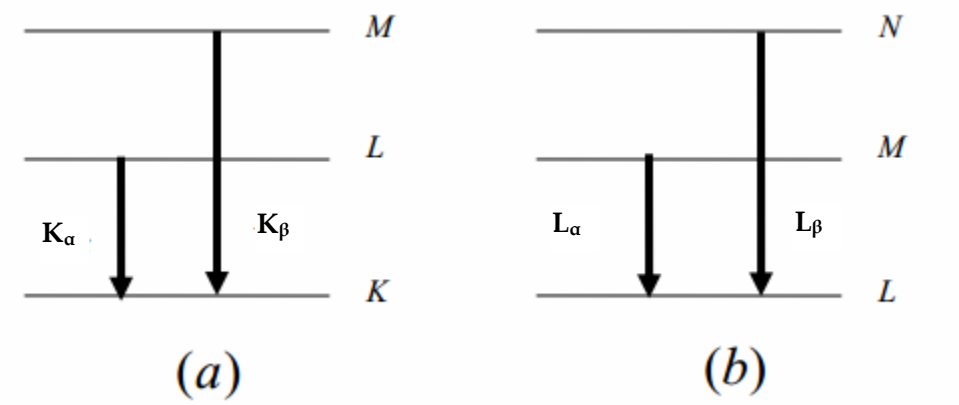

Figure 2.6 : Schematic of electron transitions responsible for the production of (a) K_α , K_β (b) L_α and L_β x-rays.

EDAX spectrum normally displays peaks corresponding to the energy levels for which the most x-rays had been received. Each of these peaks is unique to an atom, and therefore corresponds to a single element. The higher a peak in a spectrum, the more concentrated the element is in the specimen. An EDAX spectrum plot not only identifies the element corresponding to each of its peaks, but the type of x-ray to which it corresponds as well. For example, a peak corresponding to the amount of energy possessed by x-rays emitted by an electron in the L-shell going down to the K-shell is identified as a K_α peak. The peak corresponding to x-rays emitted by electrons transition from upper levels to the K-shell is identified as a K_α, K_β, K_γ etc as shown in Fgure 2.6.

In this work, the compositional analysis and surface morphology were studied using the SEM instrument model JEOL JSM-5600.

2.2.4.2 X-ray Photoelectron spectroscopy

Detection and energy analysis of photoelectrons produced by radiation whose energy exceeds their binding energy (BE) is the subject of an extensively used technique known as photoelectron spectroscopy. X ray photo electron spectroscopy (XPS) employs x-rays to produce photoelectrons [51].

Figure 2.7 shows the schematic of process involved in the emission of a photo- or Auger electron. XPS involves the removal of a single core electron while Auger electron spectroscopy (AES) is a two electron process subsequent to the removal of the core electron. Auger electrons are produced in XPS along with photoelectrons.

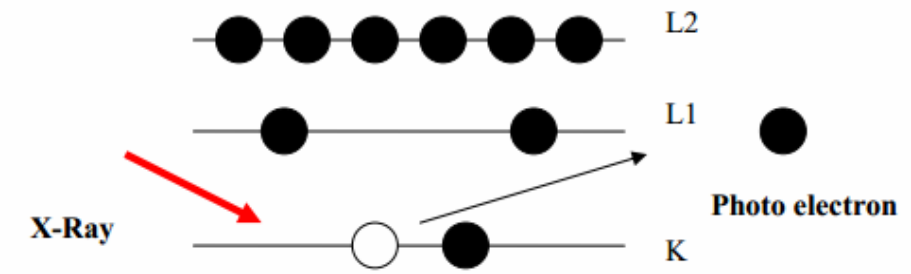

Figure.2.7: Process involved in photoelectron emission

In XPS the samples are irradiated with x-rays of known energy, hν and electrons of BE E_b are ejected, where E_b<hν. These electrons have a kinetic energy (KE) E_k which can be measured in the spectrometer and is given by,

$$E_k = h\nu - E_b - \Phi_\phi \quad \text{---------- (2.20)}$$

where, Φ_ϕ is the spectrometer work function, and is the combination of sample wok function, Φ_s and the work function induced by the analyzer. Since we can compensate for the work function term electronically, it can be eliminated, leaving

$E_k = h\nu - E_b$ ---------- (2.21)

OR

$E_b = h\nu - E_k$ ---------- (2.22)

Thus by measuring the KE of the photo electrons we can determine the BE of the electrons. The BEs is the characteristics of each element and is a direct representation of the atomic orbital energies.

The exact BE of an electron depends not only upon the level from which photoemission is occurring, but also upon the formal oxidation state of the atom and the local chemical and physical environment. Changes in either of the above will give rise to small shifts in the peak position in the XPS spectrum- so called the 'Chemical shifts'. Such shift is readily observable and interpretable in XP spectra because, the technique is of high intrinsic resolution (as core levels are discrete and generally of a well defined energy) and is a one electron process. Atoms of higher possible oxidation state exhibits a higher BE due to extra columbic interaction between the photo-emitted electron and the core ion. This ability to discriminate between different oxidation states and chemical environment is one of the major strengths of the XPS technique.

XPS is a very much surface sensitive technique and surface sensitivity of XPS is due to the low inelastic mean free path, (λ_m) of the electrons within the sample. For XPS the main region of interest relates to electron energies from 100 – 1200 eV, which gives rise to a λ_m value of 0.5 to 2 nm. However, the actual escape depth of the photoelectron, λ depends on the direction in which they are travelling with in the same sample, such that

$\lambda = \lambda_m \cos\theta$ ———————————————————— (2.23)

where θ is the angle of emission to the surface normal. Thus electrons emitted perpendicular to the surface (θ = 0˚) will arise from maximum escape length, where as electrons emitted nearly parallel to the surface (θ = 90˚) will be purely from the outermost surface layers.

The basic requirements for photoemission due to x-rays are:

1) A source of fixed-energy radiation (an x-ray source).

2) An electron energy analyzer (which can disperse the emitted electrons according to their kinetic energy, and thereby measure the flux of emitted electrons of a particular energy).

3) A high vacuum environment (to enable the emitted photoelectrons to be analyzed without interference from gas phase collisions).

The schematic of an XPS set-up is given in Figure 2.8.

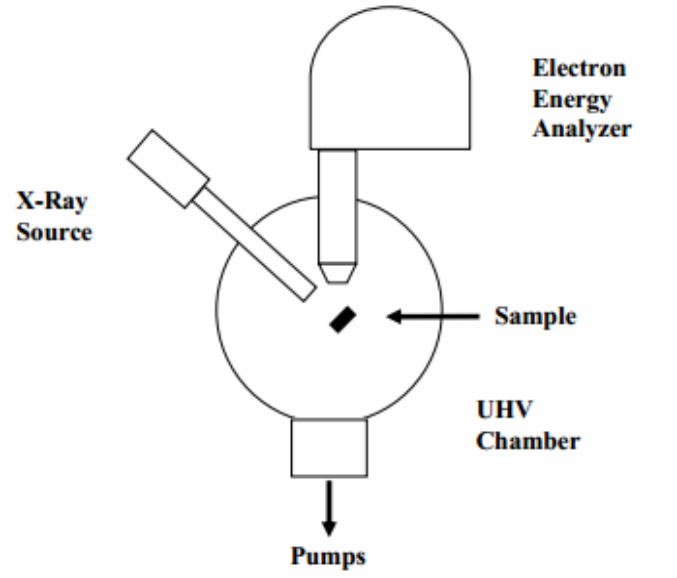

Figure 2.8: Schematic of XPS system.

For the present study, X-ray Photo electron spectra were recorded using ULVAC-PHI Unit (model: ESCA- 5600CIM). To obtain the depth-wise information, outer layers of the samples were sputtered using 200 keV Ar ions and XPS spectra was recorded.

2.2.5 Optical properties

2.2.5.1 Optical absorption studies

Most of the semiconductors absorb strongly in the visible region of the spectrum, having absorption coefficients of the order of 10^4 cm^{-1}. The characteristic feature of semiconductors in the pure state is that at a certain wavelength, generally in the near or in the infra-red region, absorption co-efficient drops rapidly and the material becomes fairly transparent at longer wavelengths. This marked drop in the absorption is called 'fundamental absorption edge' or 'lattice absorption edge'. Absorption of light by different materials can induce various types of transitions such as band to band, between sub-bands, between impurity levels and bands, interactions with free carriers within a band and resonance due to vibrational state of lattice and impurities. These lead to the appearance of absorption peaks in the absorption spectra. Hence the spectral positions of bands determine the types of transitions occurring during the process. In the absence of any thermal energy (about 0˚K), the only possible absorption that can take place is the one from valence band to conduction band when the incident radiation is of sufficient energy.

Electronic transition between valence and conduction bands can be direct or indirect. In both cases, it can be allowed as permitted by the transition probability (p) or forbidden where no such probability exists. Transition probability follows the relation, which relates the energy band

gap of the films and the absorption coefficient, (*a*) as a function of photon energy, *hv*,[37,51,52]

$$(\alpha h\nu)^p = A\,(h\nu - E_g) \quad \text{---------- (2.24)}$$

where A is a constant and E_g is the optical energy band gap. Nature of transition can be determined by plotting $(\alpha h\nu)^p$ against photon energy. For a suitable value of *p*, straight line behavior of the plot can be obtained and extrapolation of which on to the energy axis gives the value of the energy band gap of the material. The value of $p = 2$ and 3 represents the direct allowed and direct forbidden transitions respectively. Further, the value of $p=1/2$ and $1/3$ represents the indirect allowed and indirect forbidden transitions respectively.

In the present work, band gap of films was measured using optical absorbance and transmittance of the films. Spectrum was recorded using UV-VIS-NIR Spectrophotometer (JASCO V 570 model).

2.2.5.2 Photoluminescence

Photoluminescence (PL) spectroscopy is a contactless, nondestructive method of probing the electronic structure of materials. Luminescence in solids is the phenomenon in which (valence) electrons in solids are excited by optical energy from an external source and the excited electrons de-excite releasing the energy as light. These excited charge carriers return to ground state through radiative or non-radiative transitions, by emitting photons or by emitting heat via phonon interaction respectively. Phenomenon of de-excitation of charge via photon emission is called PL [53]. There are mainly two types of PL viz., intrinsic and extrinsic PL, depending on the nature of electronic transition producing it.

(i) Intrinsic luminescence

Intrinsic luminescence is again classified into three: band-to-band, exciton and cross-luminescence.

a) Band–to–band luminescence: Luminescence owing to the band-to-band transition, (i.e., through recombination of an electron in the conduction band with a hole in the valance band), can be seen in pure crystal at relatively high temperature. This has been observed in Si, Ge and III_b-V_b compounds such as GaAs.

b) Exciton luminescence: An exciton is a composite particle of an excited electron and a hole, interacting with one another. It moves in a crystal conveying energy and produces luminescence owing to the recombination of the electron and the hole. There are two kinds of excitons: Wannier exciton and Frenkel exciton. The Wannier exciton model describes an exciton composed of an electron in the conduction band and a hole in the valence band bound together by coulomb interaction. Wave function of the electron and hole in Wannier exciton is much larger than the lattice constant. Excitons in IIIb-Vb and IIb-VIb compounds are examples for Wannier exciton. Frenkel exciton model is used in cases where electron and hole wave functions are smaller than lattice constant. The excitons in organic molecular crystals are examples of Frenkel exciton.

c) Cross luminescence: Cross luminescence is produced by the recombination of an electron in the valance band with a hole created in the outer most core band. This is observed in number of alkali and alkaline-earth halides and double halides. This takes place only when the energy difference between the

top of valance band and that of conduction band is smaller than the band gap energy. This type of luminescence was first observed in BaF_2.

(ii) Extrinsic luminescence

Luminescence caused by intentionally incorporated impurities, mostly metallic impurities or defects, is classified as extrinsic luminescence. Most of the observed type of luminescence of practical application belongs to this category. Intentionally incorporated impurities are 'activators' and materials made luminescent in this way are called 'phosphors'. Extrinsic luminescence in ionic crystals and semiconductors is classified into two types: unlocalized and localized. In the former type, electrons and holes of the host lattice participate in the luminescence process, while in localized type luminescence excitation and emission process are confined in a localized luminescence centre.

a) ***Unlocalized type:*** In semiconductors donors and accepters act as luminescence activators. There are two types of luminescence transitions i.e. the transition of a free carrier to a bound carrier and the transition of a bound electron at a donor to a bound hole at an acceptor. These kinds of luminescence lines and bands are usually observed in compound semiconductors.

b) ***Localized type:*** Various kinds of metallic impurities intentionally incorporated in ionic crystals and semiconductors create efficient localized luminescence centres.

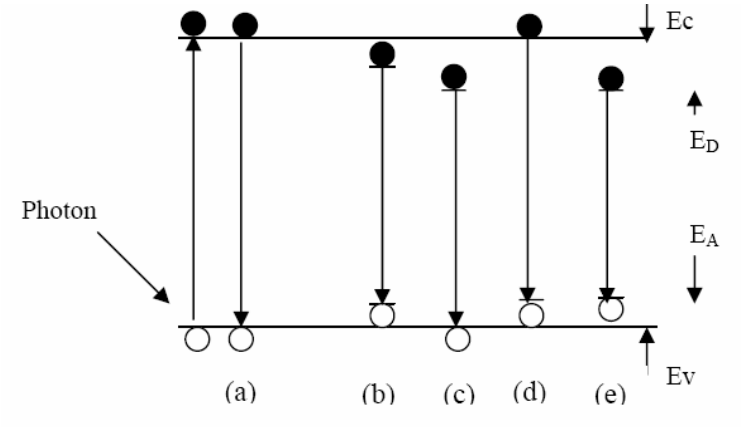

Figure 2.9: Transitions occurring in PL spectra

Five kinds of transitions mostly occurring in the PL measurement are shown in Figure.2.9. Band to band recombination (a), excitonic recombination (b), bound excitonic recombination (c & d) and donor-acceptor recombination (e).

The photon energy in a direct band gap semiconductor is [54]

$$h\nu = E_g - E_x \quad \ldots\ldots\ldots\ldots\ldots\ldots\ldots\ldots\ldots\ldots\ldots\ldots\ldots\ldots(2.25)$$

where, E_x is the excitonic binding energy. In the case of donor-acceptor recombination, the emission line has an energy modified by the Coulombic interaction between donors and acceptors

$$h\nu = E_g - (E_A+E_D) + e^2/\varepsilon_r \quad \ldots\ldots\ldots\ldots\ldots\ldots\ldots\ldots\ldots\ldots\ldots..(2.26)$$

where r is distance between donor and acceptor. The full width at half maximum (FWHM) for bound exciton transitions is typically ≤ kT/2 and resemble slightly broadened delta functions.

Intensity and spectral content of PL emission is a direct measure of various important material properties. In the present study PL is used to determine the defect levels in the samples. It is particularly suited for the

detection of shallow level impurities, but can be applied to certain deep level impurities provided their recombination is radiative. In general, non-radiative processes are associated with localized defect levels, whose presence is detrimental to material quality and subsequent device performance. Thus, material quality can be measured by quantifying the amount of radiative recombination.

The main components of PL set-up are monochromatic light source, normally a laser with energy higher than the band gap of the material, a detector to detect the emitted luminescence from the sample and lenses for focusing.

For low temperature PL measurements, the sample is placed inside a cryostat and cooled to temperatures near liquid Helium. Low temperature measurements are necessary to obtain the full spectroscopic information by minimizing thermally activated non-radiative recombination processes and thermal line broadening. Thermal distribution of carriers excited into a band contributes a width of approximately kT/2 to an emission line originating from that band. This makes it necessary to cool the sample to reduce the width. The thermal energy kT/2 is only 1.8meV at T=4.2 K.

Using a scanned photon beam or moving the sample one can do 'PL mapping' of the sample surface. The sample is excited with an optical source (typically a laser with energy $h\nu > E_g$), generating electron-hole pairs which recombine by one of several mechanisms described earlier. Photons are emitted due to radiative recombination. Photons are not emitted for the non-radiative recombination in the bulk or at the surface. For good PL output, majority of the recombination process should be radiative.

In the present work, PL measurements were carried out in the temperature range 12 to 300˚K with a closed cycle liquid Helium cryostat (Janis Research Inc.). Temperature was maintained with an accuracy of ±1 K using a temperature controller (Lake Shore Model 321). The 632.8 nm line of a He-Ne laser (5 mW, Melles Griot) was used as the excitation source. The laser beam was focused onto the samples with a beam diameter of 1mm. Emission spectra were analyzed using spectrophotometer (Ocean optics NIR 512) having a InGaAs linear array detector. Geometry of the experimental arrangement for low temperature PL measurements used in the work is given in Figure 2.10.

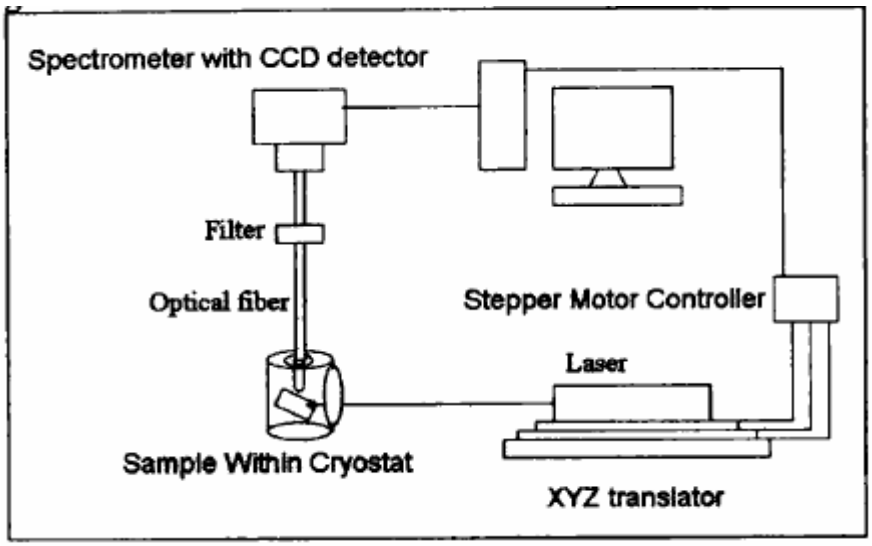

Figure 2.10: Schematic of the low temperature PL scanning system.

2.2.5.3 Photo thermal deflection spectroscopy:

Transport properties of semiconductors play a crucial role in determining the capability of the material when used for fabricating device. The knowledge of transport properties like minority carrier lifetime (τ_r), surface recombination velocity (V_{sr}) and thermal diffusivity

(D_{th}) are necessary for optimizing the entire device fabrication process. Photo thermal deflection (PTD) technique offers a relatively simple non-contact and non-destructive approach for measurement of V_{sr}, τ_r and D_{th}. This technique deals with indirect detection of heat generated by the sample, due to non-radiative de-excitation processes, following the absorption of light [55]. When the thin films are excited using the intensity-modulated beam, there arises a deflection of probe beam path, which is detected using a bi-cell PSD (photosensitive detector). A graph is plotted indicating the variation of the generated deflection signal amplitude with respect to the modulation frequency. A plot of log (signal amplitude) versus (chopping frequency)$^{1/2}$ shows the dependence of the signal on frequency. Nature of variation of signal amplitude with chopping frequency depends on changes in the composition and surface morphology of the film. Thus we can analyze the graphs and study the origin of non-radiative process in the film. The detailed explanation regarding the theory and modeling used have been reported elsewhere [56]. The schematic sketch of the PTD set-up used in the present study is given in Figure 2.11.

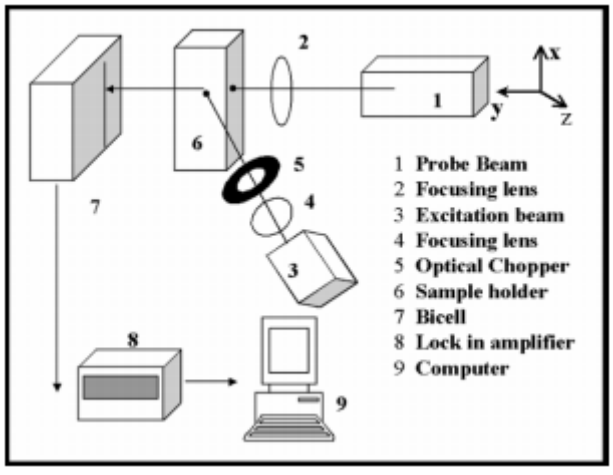

Figure 2.11: Schematic sketch of the PTD set-up.

2.2.6 Kelvin probe- Estimation of the work function

Kelvin probe force microscopy (KPFM) is carried out to map the surface potential of the thin film with a spatial and voltage resolution [57]. KPFM allows us to quantify surface potential, which in turn, can be used to estimate the work function of the sample. The measured local surface potential difference $\Delta SP = (\varphi_{tip} - \varphi_s)/e$, where φ_{tip} is the work function of the conductive tip and φ_s is the work function of the measured sample and 'e' the electronic charge.

KPFM measurement was carried out on a system (Asylum Research MF3PD AFM) using platinum-coated Si cantilever (Olympus AC240 TM, resonant frequency ~ 70 KHz, spring constant of 2 N/m, tip height 14 μm and tip radius ~ 30 nm). Topographic noncontact imaging was performed in frequency modulation mode, while KPFM data was recorded simultaneously in amplitude modulation mode. KPFM images of the sample were acquired with the tip biased at 1 V with a scan rate of 0.2 Hz on a typical scan area of 1 μm × 1 μm.

Reference

[1] L. Price, I. P. Parkin, A. M. E. Hardy, R. J. H. Clark, Chem. Mater. **11** (1999) 1792.

[2] W. G. Pu, Z. Z. Lin, Z. W. Ming, G. X. Hong, C. W. Quin, in: Proceedings of the first world conference on Photovoltaic Energy Conversion Hawaii 365-368 (1994).

[3] S. Cheng, Y. Chen, C. Huang, G. Chen, Thin Solid Films **500** (2006) 96.

[4] Z. Zainal, M. H. Sussein, A. Kassim, A. Ghazali, Sol. Energy Mater. Sol. Cells **40** (1996) 347.

[5] L. S. Price, I. P. Parkin, T. G. Hillbert, K. C. Molloy, Chem. Vapor. Depos. **4** (1998) 222.

[6] A. S. Juarez, A. Ortiz, Semicond. Sci. Technol. **17** (2002) 931.

[7] B. Subramanian, C. Sanjeeveiraja, M. Jayachandran, Sol. Energy Mater. Sol. Cells **79** (2003) 57.

[8] C. R. Sehhar, K. K. Malay, D. D. Gupta, Thin Solid Films **350** (1999) 72.

[9] P. Pramanik, P. K. Basu, S. Biswas, Thin Solid Films **150** (1987) 269.

[10] H. Ben Haj Salah, H. Bouzouita, B. Rezig, Thin Solid Films **480-481** (2005) 439.

[11] K. T. R. Reddy, N. K. Reddy, R. W. Miles, Sol. Energy Mater. Sol. Cells **90** (2006) 3041.

[12] T. V. Vimalkumar, Highly conductive and transparent ZnO thin film using chemical spray Pyrolysis technique: Effect of doping and deposition parameters Ph.D thesis Cochin University of Science and technology (2011).

[13] J. M. Mochel, US Patent 2,564,707 (1951).

[14] J. E. Hill, R. R. Chamberlin, US Patent 3,148,084 (1964).

[15] A. R. Balkenende, A. Bogaerts, J. J. Scholtz, R. R. M. Tijburg, H. X. Willems Philips Journal of Research **50** (1996) 365.

[16] S. P. S. Arya, H. E. Hintermann, Thin Solid Films **193** (1990) 841.

[17] C. H. Chen, E. M. Kelder, P. J. J. M. van der Put, J. Schoonman, J. Mater. Chem. **6** (1996) 765.

[18] J. B. Mooney, S. B. Radding, Annu. Rev. Mater. Sci. **12** (1982) 81.

[19] M. S. Tomar, F. J. Garcia, Progress in Crystal Growth and Characterization of Materials **4** (1981) 221.

[20] D. S. Albin, S. H. Risbud, Advanced Ceramic Materials **2** (1987) 243.

[21] B. R. Pamplin, Progress in Crystal Growth and Characterization of Materials **1** (1979) 395.

[22] P. S. Patil, Mater. Chem. Phys. **59** (1999) 185.

[23] P. Bohac, L. J. Gauckler, Oxygen Ion and Mixed Conductors and their Technological Applications Edited by H. L. Tuller, J. Schoonman, I. Riess, Kluwer Academic Publishers Dordrecht 271 (2000).

[24] H. H. Afify, S. A. Nasser, S. E. Demian, J. Mater. Sci.: Materials in Electronics **2** (1991) 152.

[25] S. Mirzapour, S. M. Rozati, M. G. Takwale, B. R. Marathe, V. G. Bhide, J. Mater. Sci. **29** (1994) 700.

[26] N. H. J. Stelzer, J. Schoonman, J. Materials Synthesis and Processing **4** (1996) 429.

[27] C. H. Chen, E. M. Kelder, J. Schoonman, J. Eur. Ceram. Soc. **18** (1998) 1439.

[28] M. Okuya, S. Kaneko, K. Hiroshima, I. Yagi, K. Murakami, J. Eur. Ceram. Soc. **21** (2001) 2099.

[29] H. Gourari, M. Lumbreras, R. Van Landschoot, J. Schoonman, Sensors and Actuators B, **47** (1998) 189.

[30] H. Gourari, M. Lumbreras, R. Van Landschoot, and J. Schoonman, Sensors and Actuators *B* **58** 365 (1999).

[31] F. Caillaud, A. Smith, J. F. Baumard, J. Amer. Ceram. Soc. **76** (1993) 998.

[32] H. Pink, L. Treitinger, L. Vite, Jpn. J. Appl. Phys. **19** (1980) 513.

[33] S. P. S. Arya, H. E. Hintermann, Thin Solid Films **193** (1990) 841.

[34] V. Vasu, A. Subrahmanyam, Thin Solid Films **193** (1990) 973.

[35] T. M. Racheva, I. D. Stambolova, T. Donchev, J. Mater. Sci. **29** (1994) 281.

[36] S.G. Kim, K.H. Choi, J.H. Eun, H.J. Kim, C.S. Hwang, Thin Solid Films **377** (2000) 694.

[37] A. .Goswami, Thin Film fundamentals, New age international Pvt. Ltd. New Delhi, India, (1996).

[38] K.L. Chopra, Thin film phenomena, Mc Graw-Hill, 1969.

[39] L. I. Maissel, R. Glang, Handbook of thin film technology McGraw-Hill, India (1970).

[40] D. K. Schroder, Semiconductor Materials and Device Characterisation, John Wiley and Sons New York (1998).

[41] C. V. Raman, K. S. Krishna, Nature **121** (1928) 501-502.

[42] D. Milathianaki, J. Hawreliak, J. M. McNaney, B. S. El-Dasher, M. D. Saculla, D. C. Swift, H. E. Lorenzana, T. Ditmire, Rev. Sci. Instrum. **80** (2009) 093904.

[43] B. E. Warren, X-ray Diffraction, General Publishing Company Toronto (1969).

[44] G. Binnig, C. F. Quate, Ch. Gerber, Phys. Rev. Lett. **56** (1986).

[45] E. Meyer, Progress in Surface Science **41** 3-49.

[46] K. L. Chopra, I. Kaur, Thin film device applications Plenum Press New York (1983).

[47] F. Wenner, Bur. Stand. (U.S.) Bull. **12** (1915) 469–478.

[48] L. B. Valdes, Proc. Inst. Rad. Engrs. **42** (1954) 420.

[49] P. E. J. Flewitt, R. K. Wild, Physical methods for materials characterization IOP Publishing Ltd London (2003).

[50] D. J. O'Connor, B. A. Sexton, R. S. C. Smart, Surface Analysis Methods in Materials Science Springer Germany (1992).

[51] O. S. Heavans, Optical properties of thin solid films Dover Publications New York (1991).

[52] R. H. Bube, Photoelectronic properties of semiconductors Cambridge university press India (1992).

[53] D. R. Vij, Luminescence of solids Plenum Press New York (1998).

[54] R. Jayakrishnan, Defect analysis of semiconductor thin films for photovoltaic applications using photo-luminescence and photo-conductivity Ph.D thesis (2008).

[55] J. A. Sell, Photothermal Investigations of Solids and Fluids Academic Press San Diego (1989).

[56] A. R. Warrier, Photothermal beam deflection for non-destructive evaluation of semiconductor thin films Cochin University of Science and Technology India (2010).

[57] A. Liscio, V. Palermo, P. Samori, ACS Nano **43** (2010) 541.

.....ജോ....

Chapter 3

OPTIMIZATION OF DEPOSITION PARAMETERS OF SnS THIN FILMS

Contents

3.1 Introduction

As the research work aims at the fabrication of cost-effective, eco-friendly thin film solar cells using readily available materials and easily adaptable techniques, Sn chalcogenide based window and absorber layers, deposited using Chemical spray pyrolysis (CSP) technique, were selected considering the aspects mentioned in previous chapters. CSP is one of the simplest and cost effective means of thin film deposition, especially when large area deposition is required. Moreover, ease of doping and flexibility of tailoring the stoichiometry make this technique more popular in the field and it adapt well to our requirements of photovoltaic device fabrication [1]. However, the deposition conditions are very critical for this particular deposition technique. There are 'n - number' of parameters to be optimized for depositing uniform, single phase thin films using CSP technique. Once these parameters are optimized one can obtain very uniform thin films over large area with good repeatability.

There are very few works available in the literature on spray deposited tin chalcogenide thin films. Thankaraju *et al.* deposited n-type SnS films using CSP technique, from $SnCl_2$ and thio-urea (TU) on glass substrates at 350˚C. But these films were highly resistive and amorphous [2]. Deposition of Sn_2S_3 mixed valency compound films was reported by Salah *et al.* using $SnCl_2$ and TU as the components of the precursor solution and they investigated effect of substrate temperature on the material properties [3]. Reddy *et al.* reported spray pyrolytic deposition of Sn_xS_y films on antimony doped tin oxide (Sb-SnO_2) coated glass substrates [4]. They deposited Sn_xS_y films at different substrate temperatures and investigated physical properties. Resistivity of these films was 30 Ω.cm, while the band gap and carrier concentration were 1.32 eV and $2x10^{15}$ cm^{-1} respectively [4]. In another report the same group (Reddy *et al.*) presented the effect of variation of concentration of precursor solution on sprayed SnS thin films. Films obtained from solution of molarity in the region 0.09-0.13 M were nearly stoichiometric and had resistivity of 32 Ω.cm [5].

The aim of the present study is to prepare SnS films using CSP technique and make it suitable for fabricating p-n junctions for thin film solar cells. Knowledge of variation of structural, compositional and optoelectronic properties of the material with deposition conditions are very much essential for getting films optimized for photovoltaic device applications. Therefore we deposited SnS films by varying the parameters of CSP technique extensively. It is to be specifically noted that in CSP technique, it is comparatively easy to tailor stoichiometry of the material [6]. A detailed study on variations in structural, compositional, optical and electrical and transport properties of Sn_xS_y films due to changes in various

deposition parameters were done as we could not find such an extensive study on this important material from earlier publications.

Following sections of this chapter describe in detail, the process of optimization of various deposition parameters of CSP technique so as to deposit uniform SnS thin films. We used the indigenously developed automated spray machine for the deposition of the samples throughout this work and this was to ensure the film quality and repeatability. A detailed description on the instrumentation and automation part of the automated spray coating machine developed completely in-home can be found in the previous chapter.

Major parameters affecting structural and optoelectronic properties of thin films deposited using this technique are precursor solutions used, spray rate, precursor concentration, substrate temperature, precursor ratio and post annealing time. For studying the effect of spray parameters on the properties of films, depositions were carried out by varying only one sparameter at a time, keeping all other conditions the same. Structural, optical and electrical characterizations of these films were carried out. In some cases, studies on transport properties were also included. Results of these studies are discussed in the following sections.

3.2 Preparation of Precursor solutions

Precursors used for spraying is very important and it affects the film properties seriously. The solvent, type of salt, concentration, etc can critically influence the physical properties of the films. Different solvents had been used by various workers and were chosen with care. Generally de-ionized water is ideal as the solvent. A few others had tried alcohol as the solvent. Interesting results were obtained when

different precursor solutions were used for the deposition. For example, transparency of the as deposited ZnO films increased when ethanol was used instead of water as the solvent for zinc acetate [7] and this work was carried out in our own lab. Chen *et al.* [8] observed that surface morphology of the films changed from cracked to crack free reticular after introduction of acetic acid in to the precursor solution. The change in morphology was attributed to chemical modification of the precursor solution.

Usually metal halides are used as the inorganic cationic precursor solution. The type of precursor used for spraying can also affect the film properties. For example, when In_2S_3 films were deposited using chloride based and nitrate based precursors, properties of the samples differed drastically. Films from chloride based precursors were crystalline and highly photosensitive compared to those formed from nitrate based precursors which are amorphous [9]. Also few reports are available, where the workers have purposefully used organo metallic compounds as the precursor solution [10,11].

Under this section, we will discuss the preparation of cationic and anionic precursor solution for depositing Sn_xS_y thin films.

3.2.1 Cationic Precursor solution

Dihydrated Stannous Chloride ($SnCl_2.2H_2O$) was selected as the cationic precursor solution. The usage of $SnCl_2$ instead of $SnCl_4$ reduces material cost as well as deposition temperature required for the deposition substantially [12]. This is very vital as far as the possible device level application of the material is concerned. $SnCl_2.2H_2O$ (Qualigens, assay = 98% , M.W = 225.25 g) does not readily dissolve in water to give clear

aqueous cationic precursor solution as it precipitates due to hydroxide formation. To dissolve the salt we had tried different methods. The solution was stirred for 5-6 hours using a magnetic stirrer and also varied the temperature in the range 40˚C-70˚C. However, the results were negative and all these procedures did not yield a clear aqueous solution. After a few trials it was found that clear aqueous solution of $SnCl_2.2H_2O$ can be prepared by completely dissolving $SnCl_2.2H_2O$ powder in few milliliters of high pure concentrated (35% assay) HCl and then make up the solution using de-ionized water so as to have the required molarity. A stock solution of $SnCl_2.2H_2O$ (molarity 0.5 M) was thus prepared by dissolving 11.282 g of $SnCl_2.2H_2O$ in 20 ml HCl and then made-up the solution to 100 ml by using de-ionized water.

3.2.2 Anionic Precursor Solution

Thiourea ($CS(NH_2)_2$; (Nice, M.W = 76.2 g, assay = 99%) was used as the precursor solution for Sulfur in the present study. Stock solution of TU (Molarity = 1M) was prepared by dissolving 7.62 g of TU salt in 100 ml of de-ionized water.

Using stock solution, we can prepare precursor solution of desired molarity by making use of the equation

$$m_1 v_1 = m_2 v_2 \quad \text{.....(1)}$$

where, m_2 and v_2 is the desired molarity and volume of the precursor solution, and m_1 is the molarity of the stock solution. Substituting all these in Eq. (1), one can find out the required volume v_2 of the stock solution to be taken. For example, to prepare 15 ml of 0.1 M, $SnCl_2$ precursor solution, one has to take 3 ml of the 0.5 M respective stock solution and then make up it to 15 ml using de-ionized water.

The complex compound formed in the solution while mixing metal chloride and TU will be of the form [13].

$$\begin{aligned} &SnCl_2 : TU \;\; : : 1:2 \;\; \rightarrow \;\; [Sn(TU)_2]Cl_2.H_2O \\ &SnCl_2 : TU \;\; : : 1:3 \;\; \rightarrow \;\; [Sn_2(TU)_6]Cl_2.2H_2O \text{ or } Sn(TU)_3Cl \end{aligned} \quad \text{.....(2)}$$

where, 1:2 and 1:3 stands for the ratio of the cationic precursor to anionic precursor solution. On the substrate, pyrolytic reduction of these complexes will takes place resulting in the formation of Sn_xS_y thin films.

3.3 Optimization of the deposition parameters

3.3.1 Effect of Spray Rate

Rate of spray is an important parameter as it is directly related to the growth/deposition rate and thereby the morphology of the thin films deposited using CSP technique. Higher spray rate results in formation of rough films. It has already been reported that films deposited at lower spray rates are thinner due to higher re-evaporation rate [14]. Also there are reports saying that properties like crystallinity, surface morphology, resistivity and even thickness are affected by changes in spray rate. It is generally observed that lower spray rate favors formation of better crystalline films [14].

So far no groups have ever reported the effect of spray rate variation in the deposition of Sn_xS_y films to the best of our knowledge. Therefore, initially it was vital to optimize the rate of spray required for depositing uniform Sn_xS_y thin films. From our experience with manual spray deposition, we could understand that uniform, pin hole free Sn_xS_y films have been started obtaining from substrate temperature (T_S) 250˚C onwards. So we maintained the substrate temperature at 250˚C for the spray rate

optimization studies. The Sn/S ratio in the solution was fixed at 1 by taking 0.2 M of $SnCl_2$ and TU . For this, equal volumes (15 ml) of solutions of $SnCl_2$ and TU were mixed so that the total spray volume is 30 ml. The spray rate of the deposited films was then varied as 1 ml/min, 2 ml/min, 4 ml/min and 6 ml/min. These samples were named as SR1, SR2, SR4 and SR6 respectively, where 1, 2, 4 and 6 represent the values of 'spray rate'.

3.3.1.1 Optical characterization

The $(\alpha h\nu)^2$ versus $h\nu$ plot for different spray rates is given in Figure 3.1. Linearity of the plot confirmed direct band gap of the material. It can be seen from the plot that the band gap of the material remains unaltered irrespective to the variation of spray rate. The band gap value obtained was 1.03 eV. Small magnitude of band gap obtained may be due to the possible presence of mixed valency compound like Sn_2S_3 at the present (low) T_S. Higher thickness of the film can also be a reason for lower magnitude of optical band gap.

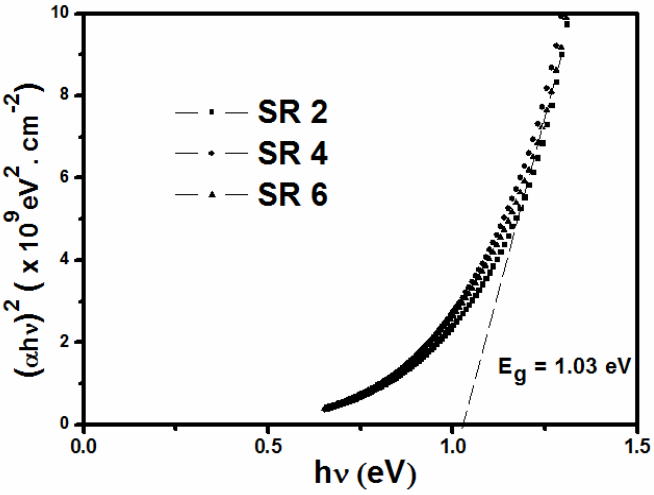

Figure 3.1: $(\alpha h\nu)^2$ vs $h\nu$ plot for samples deposited at different spray rates.

3.3.1.2 Structural characterization

X-ray diffraction (XRD) pattern of the samples SR1, SR2, SR4 and SR6 are shown in Figure 3.2. All these samples had a prominent orientation along (0 4 0) plane (2θ = 31.9^0, d= 2.797 Å) crystallized in Herzenbergate orthorhombic structure of SnS. Adjacent to it at 2θ = 30.53˚, a clear X-ray reflection peak was obtained corresponding to (1 1 1) plane of SnS for all the samples. Peaks corresponding to the mixed valency compound Sn_2S_3 phase were also present in all the films. This may be due to the lower T_S used for film preparation [15].

Grain size of the films was then calculated from the peak at 2θ=31.9° using the Debye–Scherer formula, D=0.9λ/(β cos θ), where D is the diameter of the crystallites forming the film, λ is the wavelength of CuK_α line, β is the full width at half maximum in radians and θ is the Bragg angle. The grain size was found to be better for the sample SR2 (Figure 3.3). Detailed observations from the XRD pattern are tabulated in Table 3.1.

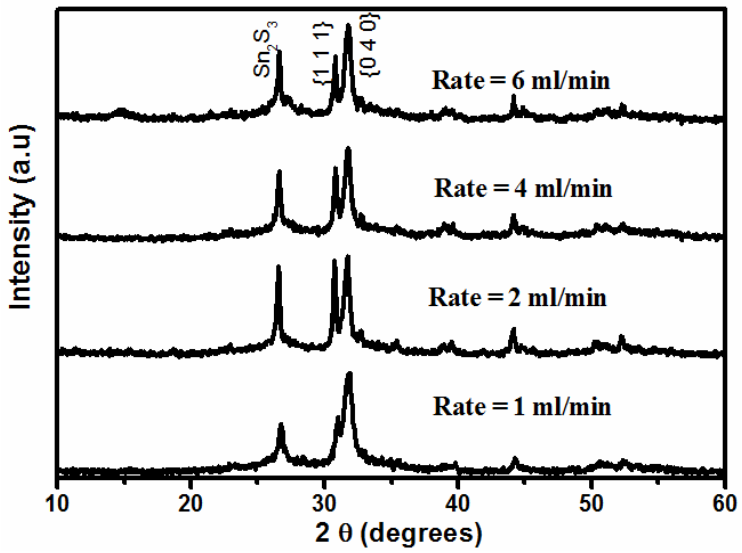

Figure 3.2: XRD pattern of samples SR1, SR2, SR4 and SR6.

Table 3.1 : Parameters obtained from the XRD pattern of the samples with varied spray rate.

Sample name	2θ (degree)	D spacing (in Å)	Phase	Plane	Grain size (nm)
SR1	31.5	2.835	SnS	(1 1 1)	
	31.9	2.797	SnS	(0 4 0)	15.9
	26.6	3.35	Sn_2S_3	(1 1 1)	
SR2	31.5	2.835	SnS	(1 1 1)	
	31.9	2.797	SnS	(0 4 0)	27.0
	26.6	3.35	Sn_2S_3	(1 1 1)	
SR4	31.5	2.835	SnS	(1 1 1)	
	31.9	2.797	SnS	(0 4 0)	20.0
	26.6	3.35	Sn_2S_3	(1 1 1)	
SR6	31.5	2.835	SnS	(1 1 1)	
	31.9	2.797	SnS	(0 4 0)	18.2
	26.6	3.35	Sn_2S_3	(1 1 1)	

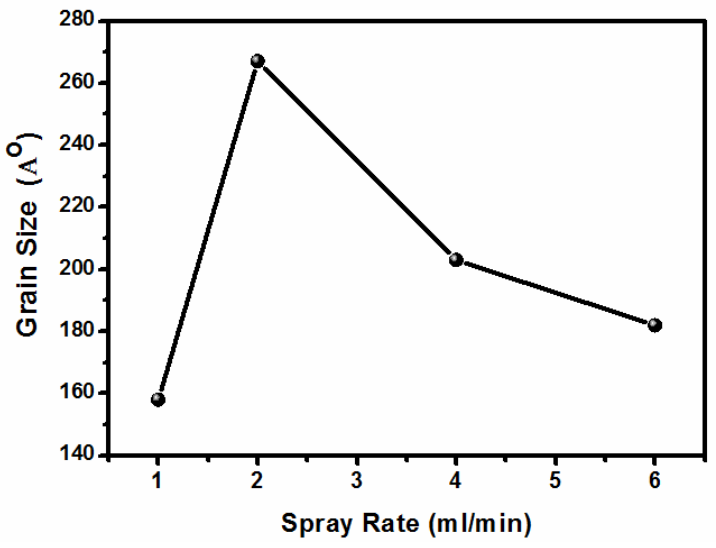

Figure 3.3: Variation in grain size with spray rate.

Therefore from the crystalline point of view, samples deposited at low spray rate were preferred. However, smaller spray rate requires higher deposition time for obtaining films of same thickness prepared at higher spray rate and therefore not recommended for the device fabrication process. Surface temperature of the substrate may deviate to a lower value at higher spray rate. These two factors may contribute to the higher crystallinity at small spray rates. Decrease in crystallinity usually results in increased resistivity of the films. Therefore, for further studies we selected the spray rate as 2ml/min. This observation is also in agreement with the findings of Tina *et al.* [14] that the lower spray rate favors the formation of films with superior properties.

3.3.1.3 Photothermal analysis

Photothermal deflection (PTD) analysis was employed to analyze the transport properties and surface uniformity of the samples, prepared at different spray rates.

Figure 3.4 depicts the photo thermal beam deflection signal plot of Log (signal amplitude) versus (chopping frequency)$^{1/2}$ for the SnS samples SR1, SR2 and SR6. Table 3.2 depicts values of thermal diffusivity (D_s), mobility (μ), surface recombination velocity (V_{sr}), and relaxation time (τ_r) of SR1, SR2, SR4 and SR6 samples.

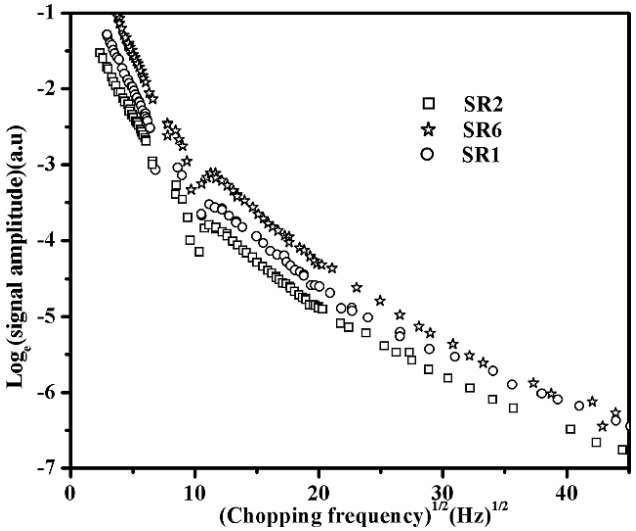

Figure 3.4: Photo thermal response of SnS samples SR1, SR2 and SR6.

Table 3.2: Transport properties of samples coded SR1, SR2, SR4 and SR6.

Sample code	D_s ($x10^{-4}$ cm^2/s)	μ (cm^2/Vs)	V_{Sr} (cm/s)	τ_r (μs)
SR1	7	0.93	$4x10^2$	0.9
SR2	9	1.10	$1x10^4$	3.5
SR4	9	0.75	$1.8\ x10^4$	3.3
SR6	9	0.36	$3x10^4$	3.0

When spray rate was 2 ml/min, values of V_{Sr} ($1x10^4$ cm/s) and τ_r (3.5 μs) were comparatively high. In addition to this, Figure 3.4 also makes it clear that the non-radiative loss was least in this sample. Therefore in sample SR2, despite having V_{sr} values higher than SR1 samples, density of non-radiative recombination centre was the least. But it showed highest mobility value (1.1 cm^2/Vs). Hence the spray rate of 2 ml/min was chosen

for further studies, as it yielded films with least non-radiative states, high lifetime and high mobility.

Figure 3.5 shows the photo thermal image of sample prepared at rate of 2 ml/min. The surface uniformity of this film was also better compared to films prepared at higher spray rate.

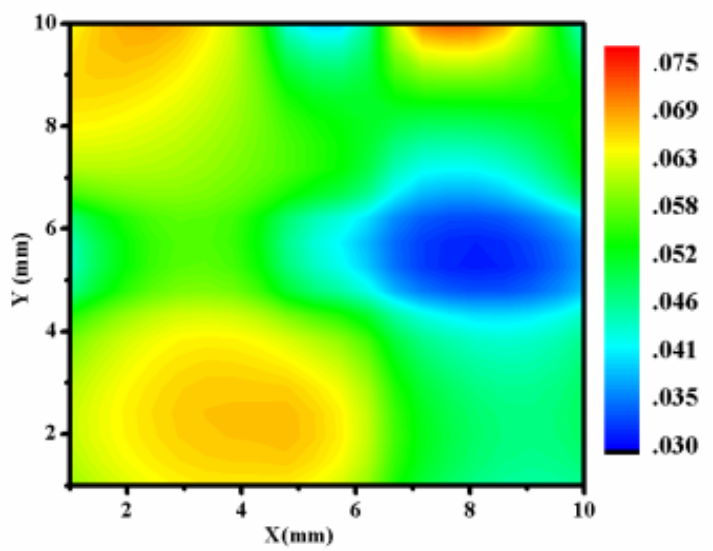

Figure 3.5: 2-D Photo thermal image of SnS thin film (SR2).

3.3.1.4 Morphology and composition of sample SR2:

The SEM image of the sample SR2 is shown in Figure 3.6. It is evident from figure that, the film was devoid of any pinholes or cracks. Surface of the sample was seems to be a bit rough which may be due to the small T_S which had been used for the film deposition.

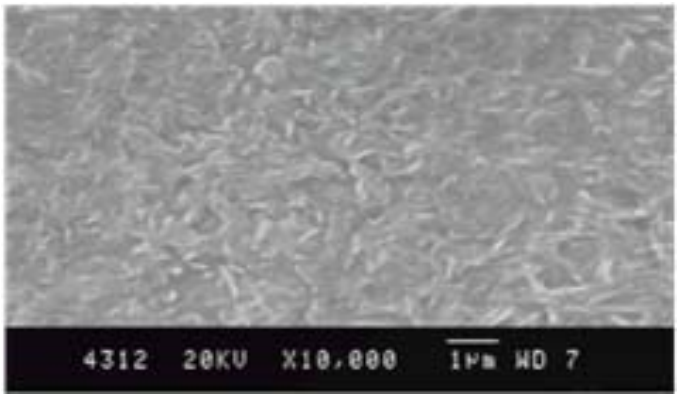

Figure 3.6 : SEM image of the sample SR2.

EDAX analysis of SR2 (Figure 3.7) gave the atomic percentage of Sn, S and Cl as 54.62%, 44.03%, and 1.36% respectively. Presence of Cl could be due to usage of chloride-based cationic precursor and low value of T_S.

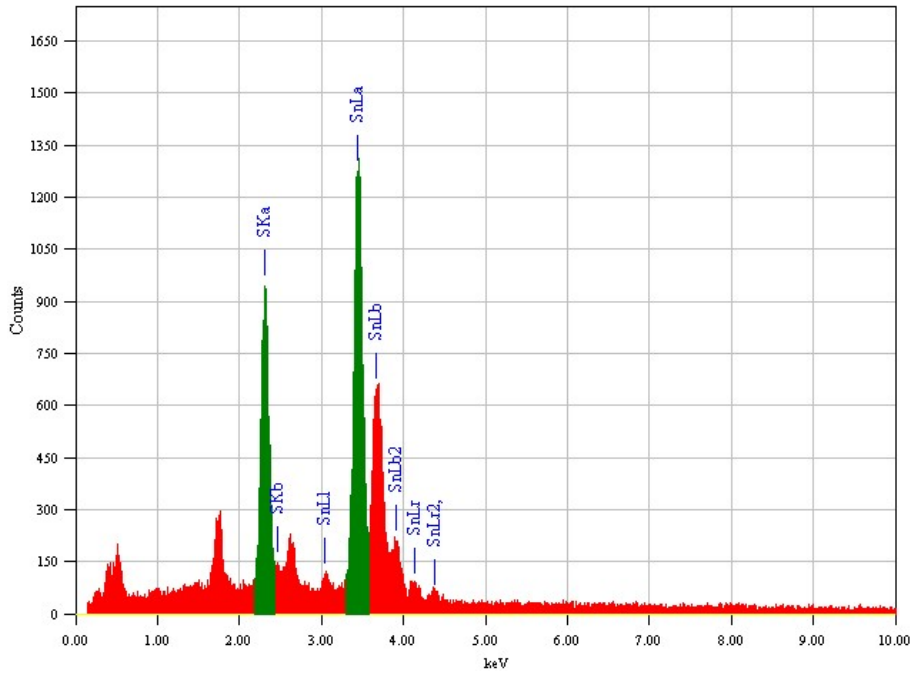

Figure 3.7: EDAX spectrum of sample SR2.

3.3.2 Effect of molarity of precursor solution

It is apparent that the molarity of precursor solutions used for spraying has a significant role in determining the properties of thin films because it directly affects reaction cross section of the precursors.

If the molarity of the precursors is very low, there will not be any film formation. It was also seen that smooth films of columnar grains are obtained with low concentration and low spray rate. On the other hand, if the molarity is higher than a critical value, the solution will immediately get precipitated so that it is no longer useful for spraying. Therefore, there will be an optimum molarity for the precursors which will result in the formation of the films with desired properties.

This section deals with the optimization of molarity of the precursor solution. For this, we fixed the rate of spray at 2 ml/min as it was found to be optimum value from our previous study. All other parameters were kept the same as described in the earlier section. Now the molarity of the precursor solution was varied from 0.05M to 0.3M. Still higher molarities resulted in the precipitation of the precursors. The samples were named as SM0, SM1, SM2, SM3, SM4, and SM5 corresponding to the precursor molarities, 0.05M, 0.075M, 0.10M, 0.15M, 0.20M, and 0.30M respectively.

3.3.2.1 Thickness Measurements

As expected, thickness of the films increased with increase in the molarity of the precursor solution. Table 3.3 shows the thickness of the samples (measured using stylus thickness profiler) prepared with different molarity of precursors.

Table 3.3: Table showing the nomenclature and thickness of samples deposited at different precursor molarity.

Sample Name	Molarity	Thickness (μm)
SM0	0.05 M	0.21
SM1	0.075 M	0.5
SM2	0.10 M	0.75
SM3	0.15 M	0.9
SM4	0.2 0 M	1.1
SM5	0.30 M	1.5

3.3.2.2 Structural Characterization:

XRD pattern of the samples prepared at different molarities (SM0 to SM4) is depicted in Figure 3.8. It was interesting to note the change in preferential orientation of grain growth of the samples with variation in the molarity of the precursors. It is clear from the figure that, there is a switching between (1 1 1) plane to (0 4 0) plane with increase in molarity of the precursors. In the figure, magnified XRD pattern in different Y-axis scale is intentionally shown so as to distinguish the changes in the orientation of the planes. Such shifting of the phase has been observed earlier in other compound semiconductors as well [17]. This might be due to the variation in thickness [18]. Intensity of the highest peak also found increase with increase in molarity and this is obviously due to the increased thickness of the samples prepared using higher molarity precursors.

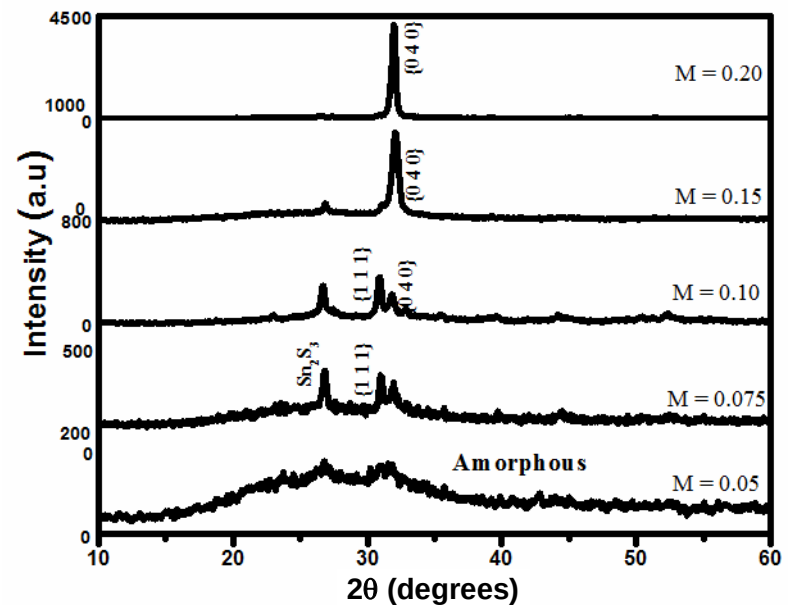

Figure 3.8: XRD pattern of the samples prepared at different precursor molarity.

Table 3.4: The intensity ratio of the (1 1 1) to (0 4 0) plane deduced from the XRD pattern.

Sample name	$I_{(111)}$ (in arb. units)	$I_{(040)}$ (in arb. units)	Ratio : $I_{(111)}/ I_{(040)}$
SM0	……..	……	……
SM1	265	200	1.325
SM2	405	257	1.6
SM3	165	886	0.19
SM4	150	4300	0.03

The (1 1 1) orientation of SnS thin films is generally preferred for the PV applications as the maximum efficiency SnS based solar cell is having SnS with (1 1 1) plane [19]. Table 3.4 Shows the intensity ratio of (1 1 1) plane to (0 4 0) plane. It is clear from the table that the ratio is quite higher for the SM2 sample.

3.3.2.3 Optical Characterization

Figure 3.9 shows variation of optical band gap with respect to molarity of precursor solution. From this figure we could understand that the magnitude of band gap decreased progressively from 1.75 eV to 1.15 eV with increase in molarity. The decrease in band gap may be due to the improvement in crystallinity and thickness of the films. The change in orientation of the planes of the films would also be a reason to alter the band gap [20].

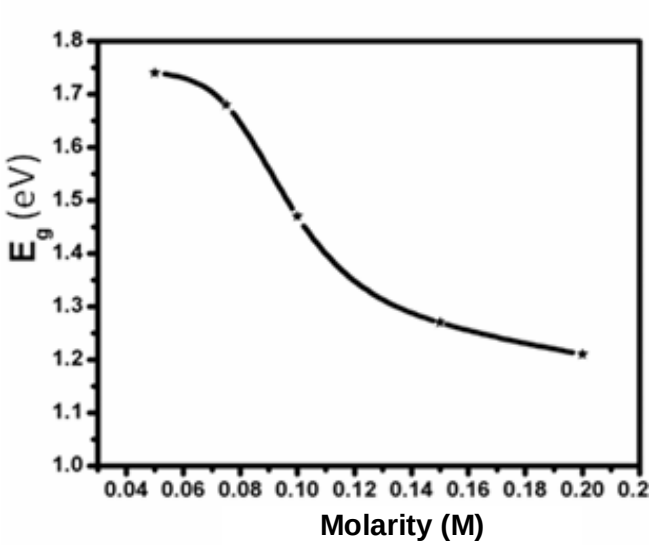

Figure 3.9: Variation of Band gap of the samples with molarity

3.3.2.4 Electrical characterization

Figure 3.10 depicts the change in sheet resistance of the films at different precursor molarities.

Sheet resistance showed rapid decrease with increase in molarity. The reduction in the sheet resistance could be due to the improvement in crystallinity and thickness of the films [21].

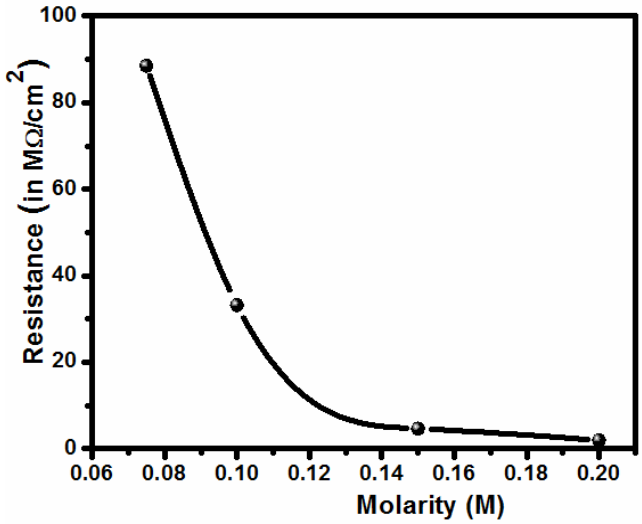

Figure 3.10: Variation in resistance of the film with molarity

3.3.2.5 Morphological analysis:

SEM images of the samples SM0 to SM4 are shown below in Figure 3.11. The two dimensional atomic force microscopy (AFM) image of Sample SM2 is also given. Samples SM4 and SM5 were comparatively rough and had a 'flowery' grain structure.

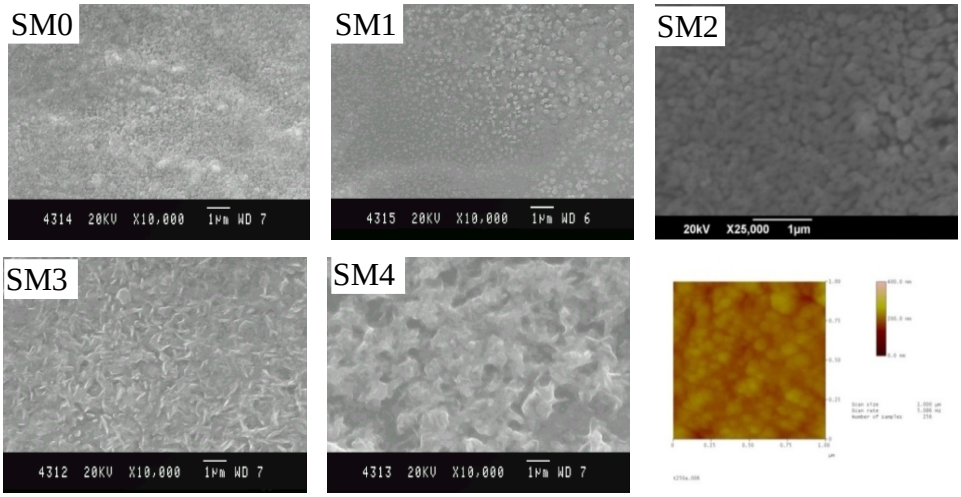

Figure 3.11: (Left) SEM image of the samples SM0, SM1, SM3 and SM4; (Right) SEM &AFM image SM2.

Sample prepared with lower molarity precursor (SM1), seems to be amorphous and the grains were not visible even at higher magnification levels. Sample SM2 had regularly distributed spherical grains.

3.3.2.6 Compositional Analysis:

Chlorine was present in all samples as an involuntary dopant. This may be due to the low temperature employed for deposition. This was observed in the case of other spray deposited compound semiconductor films prepared using chloride based precursors [22]. Atomic percentages of Sn, S and Cl of the samples prepared at different precursor molarity are tabulated in Table 3.5.

Table 3.5: Atomic Percentage of Sn, S and Cl deduced from EDAX analysis

Molarity	Sn	S	Cl	Sn/S
0.2	53.62%	42.53%	3.85%	1.26
0.15	51.04%	42.52%	6.44%	1.2
0.1	58.05%	36.5%	5.36%	1.59
0.075	54.69%	40.02%	5.29%	1.37

3.3.3 Effect of substrate temperature

Substrate temperature plays a major role in determining properties of the films because energy required for the pyrolytic reduction has been supplied by this parameter. It is generally observed that higher T_S results in the formation of films having better crystallinity [23, 24]. Grain size is preliminarily determined by initial nucleation density. Indeed re-crystallization to form larger grains is enhanced at higher temperature [25]. By increasing the T_S, film morphology can be changed from cracked to dense and then to porous [26]. Variation of T_S over different points results in formation

of non-uniform films. Composition and thickness of the films can be affected by changes in T_S which consequently affects the opto-electronic properties of the deposited films. High T_S can also result in the re-evaporation of anionic species as in the case of metal sulfide films [27]. In metal sulfides, re-evaporation of S from film occurs at high T_S, leaving metal rich surface, which may react with oxygen to form oxides. Though T_S is a critical factor, most investigators have not known the actual surface temperature of the substrate. Also, maintenance of T_S at a preset value and its uniformity over large area are challenging. Liquid metal baths offer good contact at the interface and are widely used. But when solid surface are used, the actual area of contact is lesser than 1% of the surface area. Spraying in pulses or bursts also has been used to assure that T_S is reasonably constant.

Optimization of T_S is so critical to obtain uniform film with desired properties. This section is therefore entirely dedicated in optimizing the T_S required for the deposition of uniform single phase SnS thin films. Here we have used the previously optimized values for parameters. The only difference made here was 'molarity of TU' was taken twice as that of $SnCl_2$. We have intentionally chosen the higher value for M_S owing to the higher vapor pressure of S and there by its increased chance of evaporation while undergoing the pyrolytic reduction [28].

Then samples were deposited by varying T_S from 100°C to 500°C with an accuracy of ±5°C. These films were characterized using stylus thickness profiler, XRD, UV-Vis Spectrophotometer, X-ray photoelectron spectroscopy (XPS), SEM and AFM analysis to understand the effect of substrate temperature on the properties of the Sn_xS_y thin films. Results of these measurements are discussed below

All the films deposited with T_S > 200˚C were uniform and free of pinholes and/or cracks. For T_S <200°C, white spots were observed all over the film surface, which indicated presence of unreacted precursors, as T_S was lower than the "pyrolytic temperature". When T_S was in the range 300˚C to 400˚C, the films were having brownish grey color while, for T_S > 450°C the films were yellowish in color. This may be due to possible presence of SnS_2 phase at elevated T_S.

3.3.3.1 Thickness

Thickness of the films decreased from 1.4 μm to 0.55 μm with the increase in T_S (Figure 3.12). This might be due to re-evaporation of the compounds at elevated temperatures. Such a decrease in thickness with increase in T_S for films fabricated using CSP had been reported earlier [29].

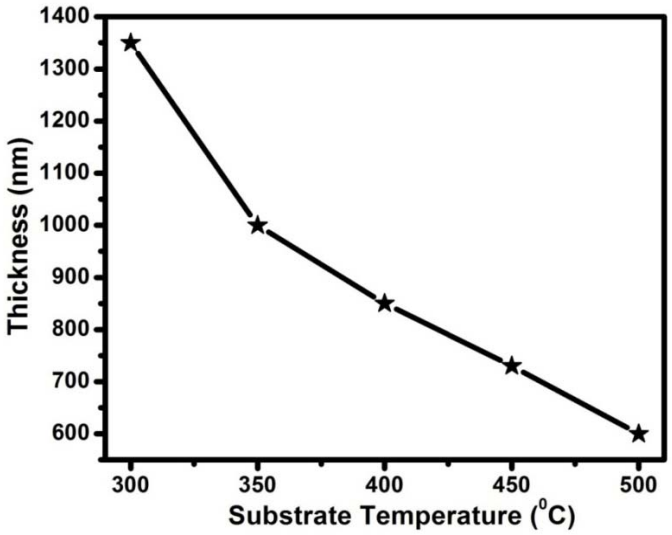

Figure 3.12: Plot showing variation of film thickness with substrate temperature.

3.3.3.2 Structural analysis

A) XRD:

Figure 3.13 shows XRD pattern of films deposited at different T_S (250˚C – 500˚C). Films deposited in the range 300˚C < T_S <450˚C, had predominantly SnS phase, crystallized in 'Herzenbergate' orthorhombic structure, as observed from the XRD pattern with SnS phase orientated along (1 1 1) plane having lattice parameters a=4.329 Å, b= 11.19 Å, c=3.983Å, at 2θ =31.53° (JCPDS data card 39-0354). The XRD pattern clearly indicated prominent peaks of Sn_2S_3 phase at lower T_S (< 300˚C) and SnS_2 phase at higher T_S (> 400˚C). These impurity phases almost vanished for 350˚C < T_S < 400˚C, and at 375˚C, the films were having better crystallinity with nearly single phase SnS (Figure 3.14).

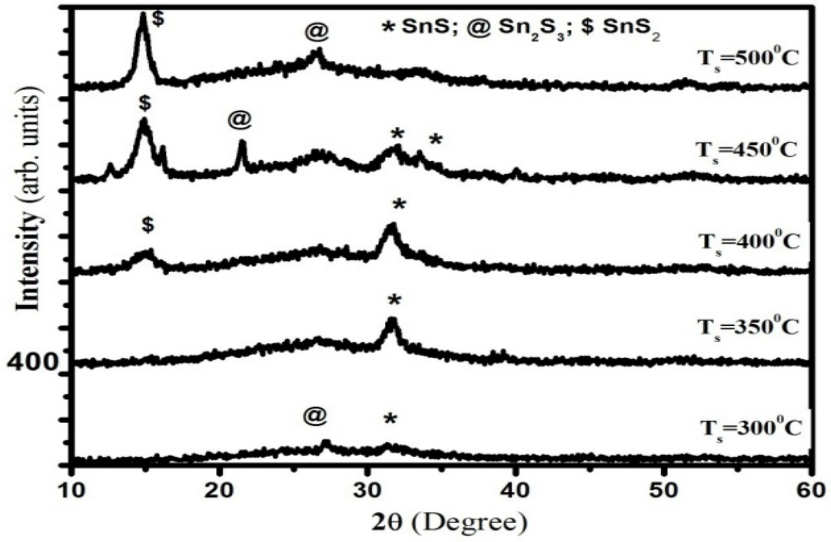

Figure 3.13 : XRD pattern of the samples deposited at different substrate temperature.

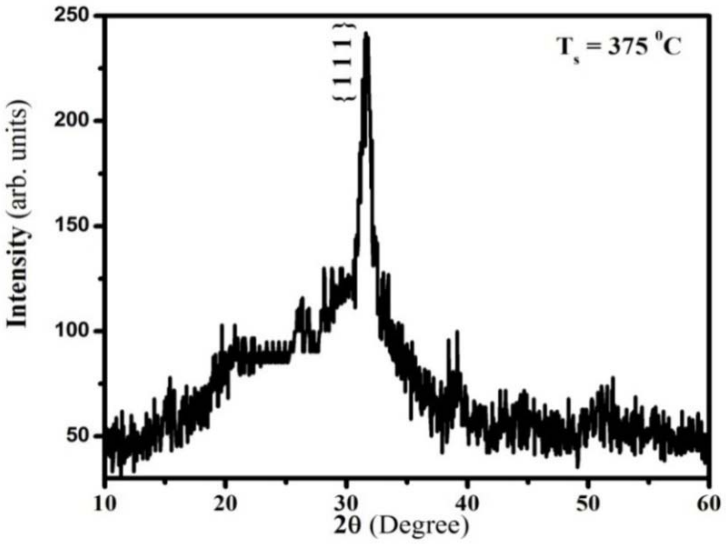

Figure 3.14 : XRD pattern of the sample deposited at T_S = 375°C.

Grain size of the films (calculated from the peak at 2θ = 31.53° using the Debye-Scherer formula) decreased slightly (from 12 to 9 nm) as T_S increased from 300°C to 400°C and that of the films prepared at T_S = 375°C was 10 nm.

B) Raman analysis:

XRD analysis clearly indicated the formation of Sn_2S_3 at 250°C, SnS at 375°C and SnS_2 at 450°C. SnS films thus obtained have band gap of 1.33 eV while that of the SnS_2 films was 2.42 eV. Raman analysis was also performed on the samples as it is more sensitive to the structural and compositional changes of the material [30].

We know that, among the IV-VI compounds GeS, SnS, SnSe have orthorhombic structure with eight atoms per unit cell forming double layer planes normal to the longest axis. For orthorhombic structure, the 24 vibrational

modes are represented by the following irreducible representations at the centre of Brillouin zone as:

$$\Gamma = 4Ag + 2B1g + 4B2g + 2B3g + 2Au + 4B1u + 2B2u + 4B3u \quad .....(3)$$

SnS has 21 optical phonons of which 12 are Raman active modes (4Ag, 2B1g, 4B2g and 2B3g), seven are infrared active modes (3B1u, 1B2u and 3B3u) and two are inactive (2Au) [31].

Figure 3.15 shows room temperature Raman spectrum of Sn_xS_y films deposited at different T_S. Raman spectrum has distinct peaks for each binary sulfides of Sn (SnS, Sn_2S_3, SnS_2). For the sample prepared at T_S =375˚C, Raman mode was observed at 224 cm^{-1}. Based on the previous report on Raman spectra of SnS single crystal, the observed Raman modes were assigned to Ag mode [31]. In accordance with Raman spectra of GeS also, the Raman mode at 224cm^{-1} was assigned to Ag mode [32].

For the sample prepared at T_S = 250˚C, Raman mode at 304 cm^{-1} was also present in addition to the peak at 224 cm^{-1}. This mode observed at 304 cm^{-1} was in agreement with Raman peak for Sn_2S_3 phase [33].

Raman spectrum of the sample deposited at T_S = 450˚C consisted of three distinct Raman peaks. The one obtained at 335 cm^{-1} was due to the SnS_2 phase (A_{2u} mode) [34]. The other modes obtained for this sample were due to Ag modes of SnS (at 224 cm^{-1}) and Sn_2S_3 (at 304 cm^{-1}).

Therefore, both Raman and XRD results were complimentary to each other. Both the analyses confirmed that deposition temperature to obtain single phase SnS thin films is 375˚C.

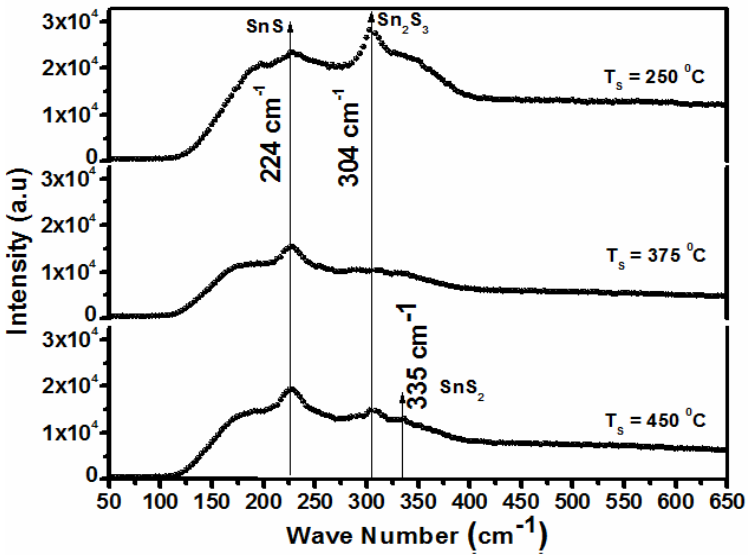

Figure 3.15: Raman spectra of the sample deposited at Ts =250˚C, 375˚C and 450˚C.

The large background noise observed in the Raman spectra while comparing to that of single crystal is due to the small grain size of the samples. Also the Raman modes of SnS thin films show broadening and are shifted towards lower wave number side as compared to the Raman modes of single crystal counterpart. This is due to 'phonon confinement' effect. Liu *et al.et al.* [35] observed 2Ag modes at 223 cm^{-1} for SnS nano-wires and Gou *et al.* [36] observed only 2Ag modes at 189 and 220cm^{-1} for SnS nano particles. Similar observations were observed by other workers also [37].

3.3.3.3 Morphological Analysis:

Surface morphology of the samples showed noticeable changes when T_S was enhanced from 300˚C to 375˚C. It is evident from SEM image (Figure 3.16(b) that the samples prepared at T_S = 375˚C had needle like polycrystalline growth, while Figure 3.16(a) depicts that, for samples prepared at T_S =300˚C, the surface was smooth with regular spherical grains. Figures 3.17(a) and 3.17(b) show AFM images of the samples prepared at T_S=300˚C and T_S=375˚C respectively. These images agreed well with the SEM images (Figure 3.16(a) & (b)) and confirmed that, due to the increase in temperature from 300˚C to 375˚C, the film surface changed from regular spherical grain structure to needle like structures. Huilan Su *et al.* claimed 'rod-like' morphology for SnS films deposited through ethanol thermal reactions between $SnCl_2$ and Thioacetamide [38].

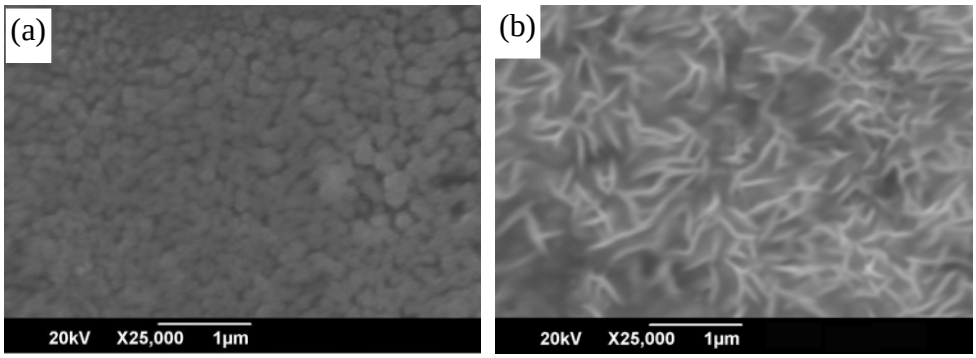

Figure 3.16 : SEM image of the sample deposited at (a) 300 ^{0}C (b) 375 ^{0}C.

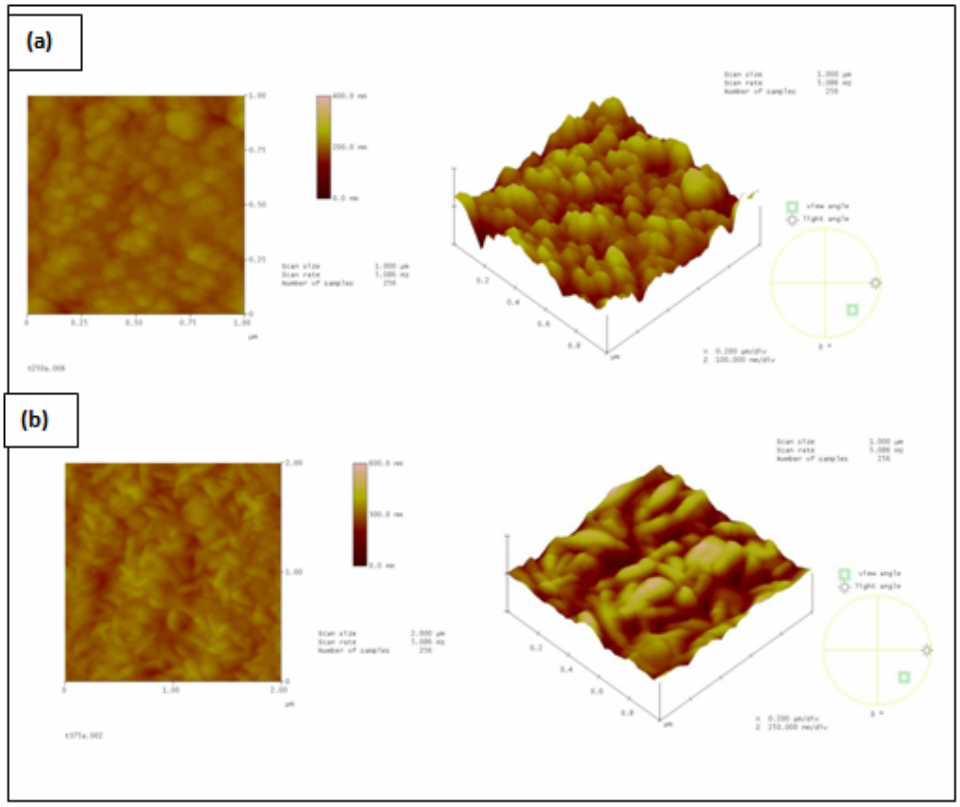

Figure 3.17: 2D and 3D AFM image of the sample deposited at (a) 300°C (b) 375°C.

3.3.3.4 Optical characterization:

Optical band gap of the films was determined from the '$(\alpha h\nu)^2$ versus $h\nu$' plot (Figure 3.18). All the samples had very high absorption coefficient (> 10^5 cm^{-1}). Linearity of the graphs confirmed that all the Sn_xS_y thin films had direct band gap. Band gap of SnS films prepared at T_S=375°C was 1.33 eV which is almost same as that for single-phase SnS films. For SnS films deposited in the range T_S = 350°C to T_S = 400°C, band gap was found to vary. That means we can easily tune the band gap (between 1.33 -1.5 eV) of the SnS films slightly by varying the T_S alone in this range. There was no significant variation in the grain size with T_S in

this temperature range which can affect the band gap. Figure 3.19 depicts the variation of band gap for the entire range of T_S. This indicated the dependence of band gap on composition. High value of band gap at lower and higher temperature was probably due to the formation of Sn_2S_3 and SnS_2 phases respectively [4, 39].

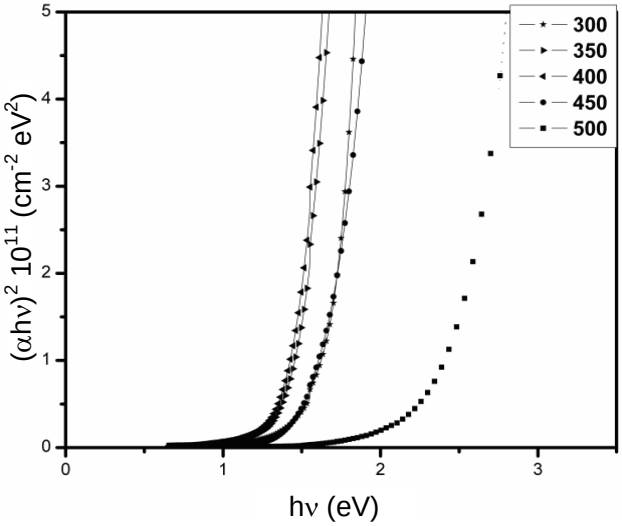

Figure 3.18: $(\alpha h\nu)^2$ versus $h\nu$ plot of samples deposited at different T_S.

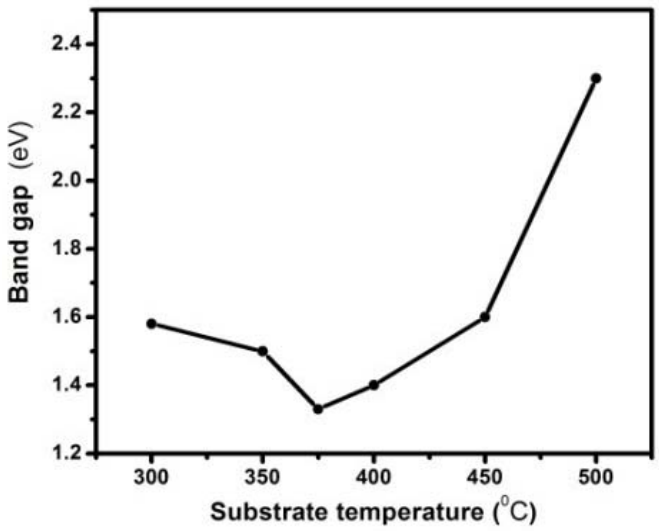

Figure 3.19: Variation in optical band gap with T_S.

Figure 3.20 shows transmittance spectra of samples prepared at T_S=250˚C, 375˚C and 450˚C. The transmittance (T%) of the films increased with T_S. We observe that T% was considerably low at T_S= 375˚C indicating high absorbance for these films in the region λ < 850 nm.

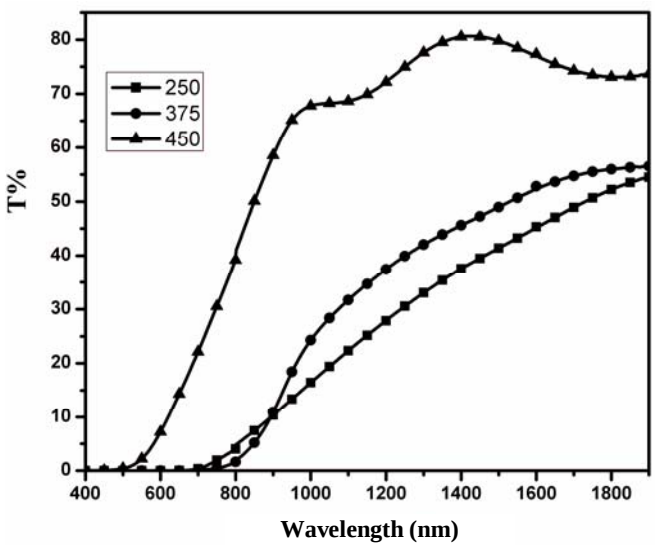

Figure 3.20: T% Vs Wavelength for samples prepared at different T_S.

3.3.3.5 Compositional analysis

A) ***EDAX Results:***

Atomic ratios of Sn and S in the films were examined using EDAX. Variation of Sn/S ratio in the films with respect to T_S has been depicted in Figure 3.21. It was observed that, as T_S was increased, the S incorporation in the film also increased, and at T_S=375˚C, we obtained nearly stoichiometric SnS films (Figure 3.22). But at still higher T_S (> 400˚C) the S content in the film started decreasing, probably due to re-evaporation of S owing to its high vapor pressure [28]. Earlier from the XRD pattern (Figure 3.13) and Raman spectra (Figure 3.15) we found that, different binary sulfides of Sn have been obtained at different in T_S. The variation in

Sn:S ratio in the film with respect to change in T_S is therefore, obviously due to the variation in stoichiometry in these compounds.

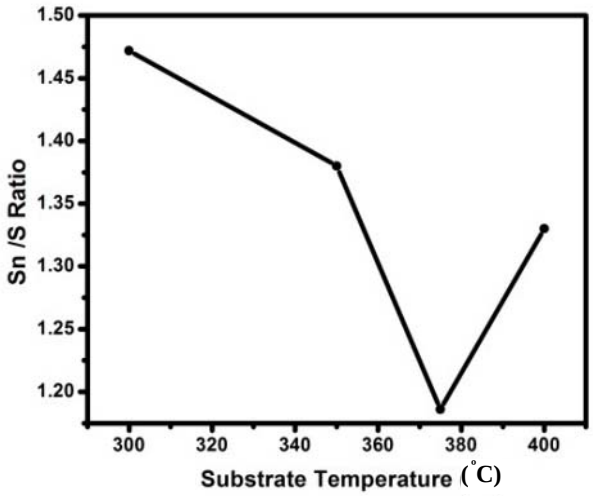

Figure 3.21: Plot showing Sn/S ratio variation with substrate temperature.

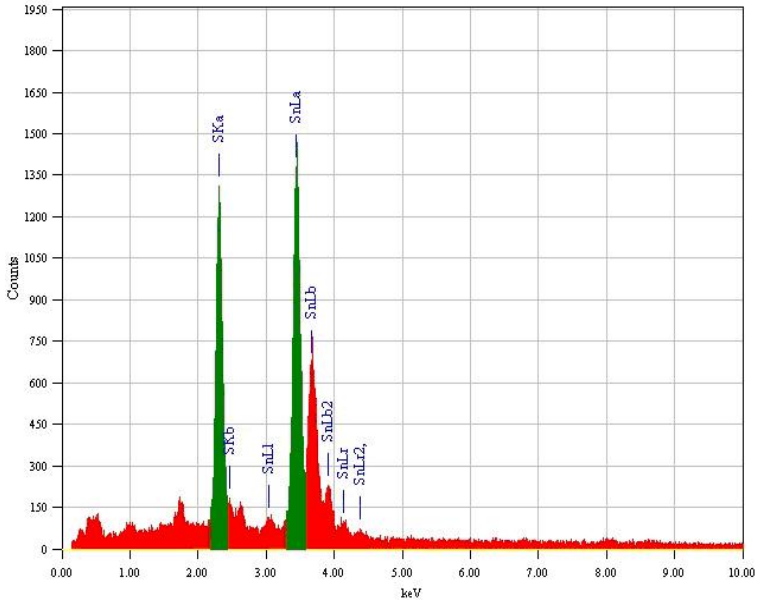

Figure 3.22: EDAX spectrum of sample deposited at T_S = 375°C.

B) ***XPS analysis:***

XPS analysis were performed on samples deposited at T_S=250˚C, T_S= 375˚C and T_S = 450˚C to estimate chemical states and composition. The XPS spectrum thus obtained for samples deposited at T_S=250˚C, T_S= 375˚C and T_S = 450˚C are shown in Figure 3.23. As XPS is a very powerful surface sensitive tool (XPS interrogates the surface ~ 10 atomic layers), the XPS spectrum did show some O and C contamination on the surface of all the samples apart from the constituent elements Sn and S. Incorporation of O in the films could have occurred during their deposition and come from residual gases in the system. Oxygen and carbon were predominantly surface bound; a situation which may also probably as a result of handling and storage of the films in air. Hence before taking the XPS spectrum a few surface layers were etched out. Presence of the elements Sn, S and O were checked by doing detailed high resolution scan. Binding energies (BEs) were calibrated with that of C contaminant present on the sample surface (BE of C 1S is 285 eV).

BE observed for S occurred at 161.5 eV is characteristic of S in a metal sulfide. Sulfur has a large range of binding energy from 161.7 eV (for compounds with oxidation state of S is 2) to 171 eV (for compounds with oxidation state of S is 4). Binding energies of S at 161.5 eV obtained for sample deposited at T_S = 375˚C corresponds to that of S(II) and indicates the formation of SnS. This is also in agreement with the reported statement; "BE of Sulfur in the nano crystalline SnS was among the lowest recorded for sulfur" [38]. For films deposited at T_S = 250˚C and T_S = 450˚C, the BE of S shifted to higher energy end corresponding to the formation of Sn_2S_3 and SnS_2 as the BE of Sn(IV) in nano crystalline SnS_2 or Sn_2S_3 was 0.9 eV greater than that of e Sn(II) in nano crystalline SnS. These results agreed

with the fact that there is a variation of 0.8 - 1.0 eV between the Sn(IV) compound and the Sn(II) analogue found in other studies of tin halides and organo-metallic compounds [38, 40].

For Sn environment shift in BE corresponding to the formation of Sn_2S_3 at 250˚C, SnS at T_S = 375˚C, and SnS_2 at T_S = 450˚C were obtained. The sample deposited at T_S=375˚C had Sn 3*d* 5/2 (B.E at 485.2 eV) which agreed well with the Sn 3*d* 5/2 peak reported for SnS of 485.6 eV [38, 40]. Sample deposited at T_S = 450˚C had Sn 3*d* 5/2 peak at 486.1 eV corresponding to the formation of SnS_2 phase. These values were consistant with those for SnS_2 [40, 42]. B.E obtained for Sn 3 d5/2 for sample deposited at T_S = 250˚C was almost in accordance with that of Sn_2S_3. Notably BEs of the product Sn_2S_3 was corresponding to those of Sn in the oxidation state $^{+}4$ and $^{+}2$. Hence it can be probably considered that Sn_2S_3 was a solid solution of SnS_2 and SnS [42].

Oxygen observed in the bulk of the material had binding energy of 533.4 eV which was not due to a metal oxide for which the characteristic BEs are in the region 529 - 532 eV (for tin(IV) oxide BE is 530.6 eV). Other molecular oxygen species also have binding energies in this vicinity. It suggests that the O arises during the reaction, possibly adsorbed from the ambience. The BE of Sn 3 d5/2 in Tin (II)) oxide is 486.9 eV and in Tin(IV) oxide is 486.6 eV; both these peaks were absent in the samples [38].

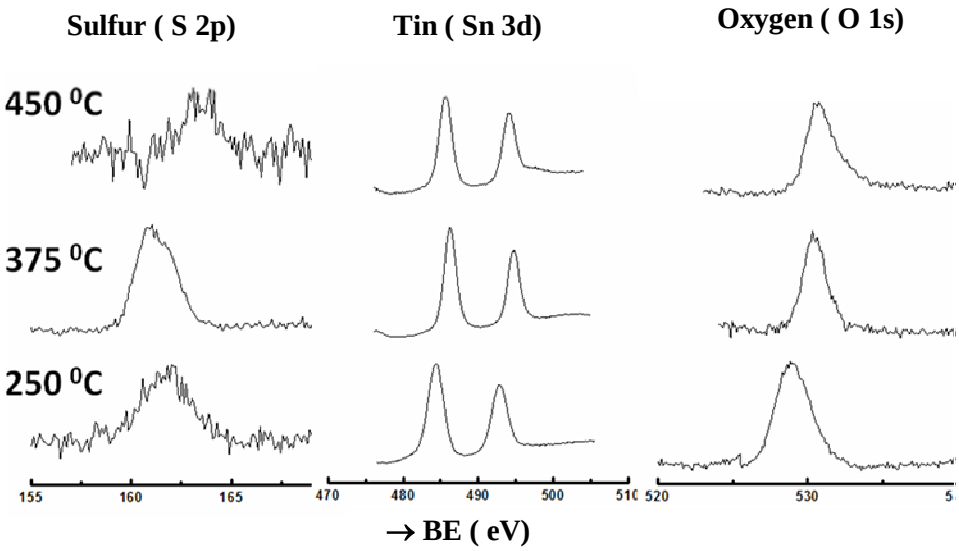

Figure 3.23 : XPS spectra of the sample deposited at TS = 450°C, 375°C and 250°C showing the BEs of S, Sn and O.

For the sample deposited at T_S = 375°C, which gave almost single phase SnS film, the composition of elements Sn, S and O was checked along the sample thickness. In order to get this information, first XPS analysis was done on surface of the sample. After this the sample was etched using Ar-Ion etching (sputtering) and the analysis was repeated. As in the above case here also the spectra were calibrated against shifts due to machine errors, using the C 1s line of the hydrocarbon contamination on the films as the standard (Binding energy of C 1s is 284.5 eV). Employing Ar-ion sputtering, the depth profiles showing variation in concentration and binding energies of S, Sn, O along the sample thickness were obtained. At the end of sputtering, the glass substrate was exposed. The depth profile XPS spectrum of Sn and S is shown in Figure 3.24. It is evident from the figure that, although the surface was heavily contaminated with carbon and oxygen, the bulk composition showed less oxygen and almost no carbon.

The B.E at 25 eV is corresponding to the elemental Sn present in the film. This peak could be a result of preferential sputtering of S during etching leaving some exposed Sn metal. This effect has been observed in an XPS study of tin nitride films where preferential sputtering caused all the N to be removed, leaving Sn metal [25].

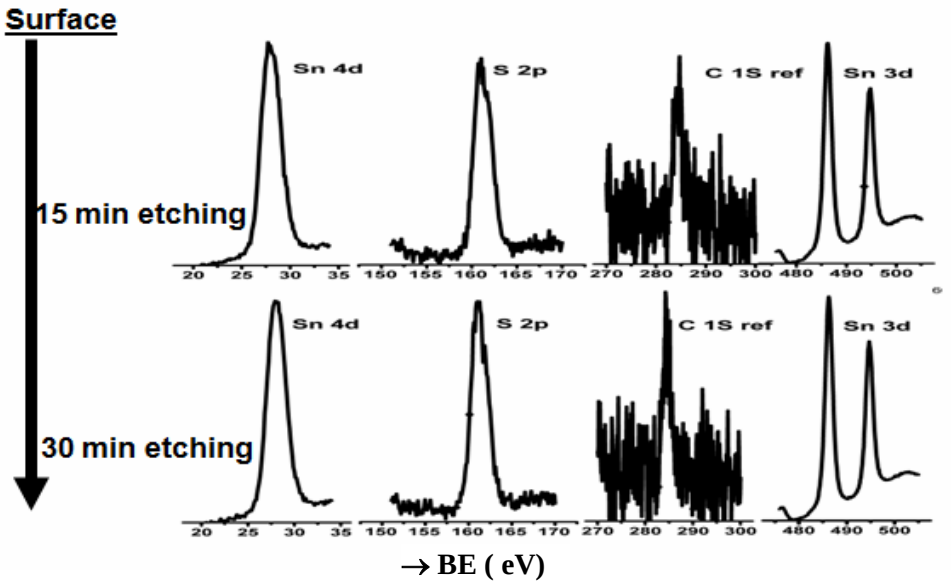

Figure 3.24: XPS depth profile of the sample prepared at Ts= 375^{0}C.

3.3.3.6 Electrical characterization

Resistivity of the films decreased from 5 x 10^3 Ω.cm to 5 Ω.cm with the increase in T_S. High value of resistivity of the films prepared below 300˚C must be due to presence of highly resistive mixed valency compound Sn_2S_3 [43]. Sheet resistance for the samples deposited at various T_S is depicted in Figure 3.25. Hot probe analysis was carried out on the samples to determine the conductivity type. This measurement indicated that the films prepared in the range T_S = 300˚C – 400˚C were p-type and those prepared at T_S > 450˚C, (where the SnS_2 phase was dominating) were n-type. The films prepared at

T_S < 300˚C showed fluctuating nature in hot probe analysis, which could be due to the very high resistivity of these films [44].

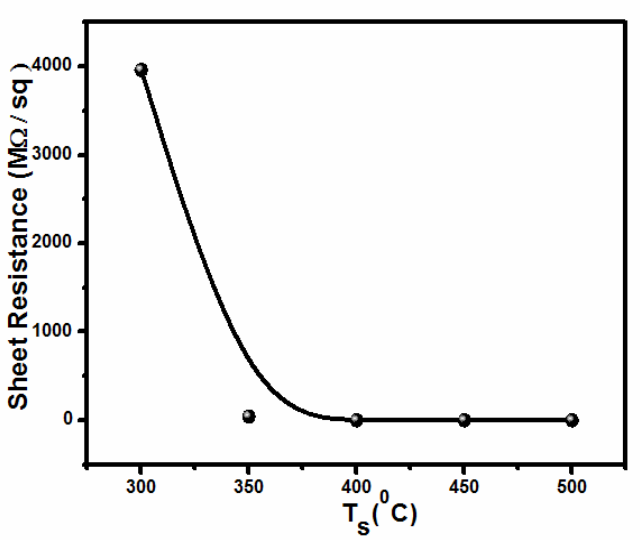

Figure 3.25: Variation of Sheet Resistance of the samples with T_S.

3.3.4 Effect of variation of anionic precursor concentration

Ratio of anionic to cationic precursors in spray solution plays a significant role in compound formation as well as in determining optoelectronic properties of the films [45]. This section deals with the study of the effect of variation of anionic to cationic precursor ratio in the properties of the films. Samples were deposited by varying 'molarity of TU (M_S) alone from 0.1 M to 0.4 M, keeping molarity of $SnCl_2$ (M_{Sn}) fixed at 0.1 M, in order to optimize the composition ratio required for deposition of p-type SnS thin films. Analyzing these films deposited by varying M_S, we could optimize M_S required for obtaining single-phase SnS at 375°C.

3.3.4.1 XRD analysis

XRD analysis was performed to probe the variation in crystallinity, orientation and phase of the films with variation in concentration of the

anionic precursor solution. Figure 3.26 shows XRD pattern of the samples with different S concentration. When M_S was 0.2 M in the precursor solution of S, resulted in the formation of films with SnS phase only. But for M_S > 0.2 M, SnS_2 phase was dominating and films with M_S < 0.2 M showed presence of the 'mixed valency' compound Sn_2S_3, as observed from the XRD pattern (Figure 3.26).

From these results it appears that, for a given ratio of precursors, there will be an optimum pyrolytic temperature, which favors formation of a particular compound; when we select 0.2 M as the value of M_S, 375°C is found to be optimum T_S for depositing SnS films.

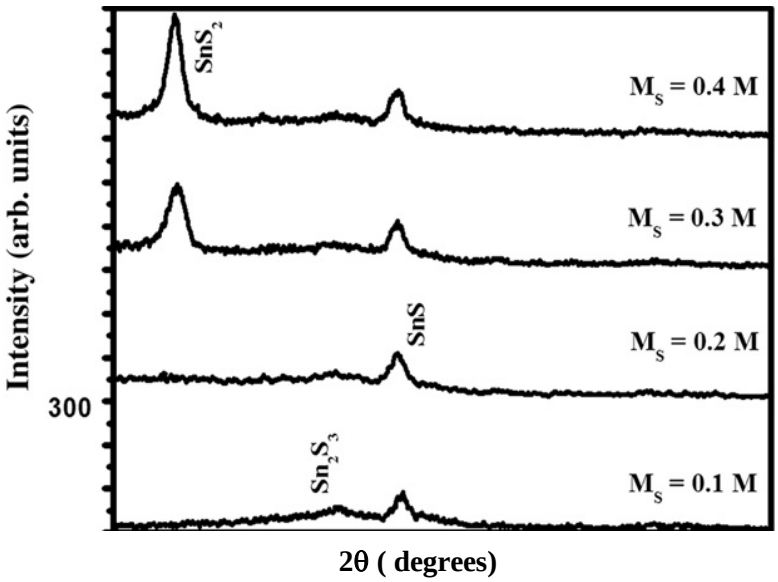

Figure 3.26: XRD pattern of SnS samples deposited at different M_S.

3.3.4.2 Optical characterization

$(\alpha h\nu)^2$ vs $h\nu$ plots of the samples of different M_S are shown in Figure 3.27. Variation of band gap with M_S is depicted in Figure 3.28. Optical band gap of the samples deposited at M_S = 0.2 M was 1.33 eV. From the

XRD pattern, this was the optimum value of M_S to obtain single phase SnS films. Slightly higher value of optical band gap for the lower and higher values of M_S might be due to the presence of other binary sulfides of Sn which are having wider band gaps [4].

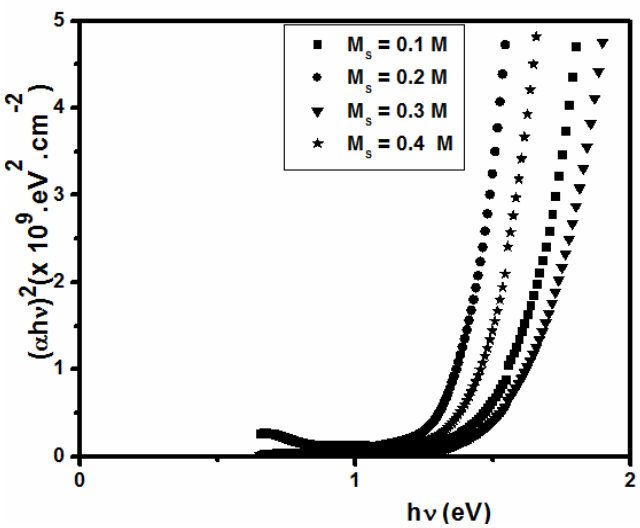

Figure 3.27: $(\alpha h\nu)^2$ vs $h\nu$ plot of the samples deposited at different M_S.

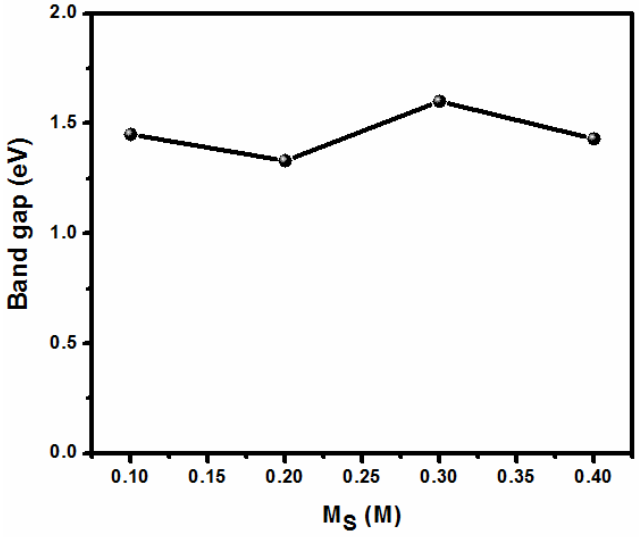

Figure 3.28 : Plot showing variations in band gap of the samples due to the change in anionic concentration in the precursor solution.

3.3.4.3 Electrical characterization

Hot probe analysis indicated that SnS films thus deposited were p-type and resistivity (using 'two probe method') was 60 Ω.cm.

3.3.4.4 Composition analysis

Result of EDAX analysis in Table 3.6 shows atomic percentage of Sn, S and Cl with the respective Sn/S ratio. Even though stoichiometric films were obtained for M_S = 0.3 M, we chose M_S= 0.2 M for the future studies due to the presence of impurity phases observed for Ms > 0.2 M.

Table 3.6: EDAX report of S11, S12, S13 samples.

Ratio	Sn	S	Cl	Sn/S
1/1	58.52	33.94	8.34	1.72
1/2	48.78	46.42	4.79	1.05
1/3	49.01	48.55	2.44	1.009

3.3.5 Effect of variation of concentration of cationic precursor solution: Deposition of n-SnS

Through the studies presented in the earlier sections, we could optimize conditions to obtain uniform, single-phase, p-type SnS thin film. Next aim was to study the possibility of changing conductivity type of the material to get n-type SnS suitable for fabricating homojunction solar cells. It has been reported by earlier workers that inherent Sn vacancies, present in the lattice of the SnS films, make it p- type [46] by birth. There are also reports available stating that the conductivity type of the SnS films is essentially controlled by the concentration of Sn in the compound [47, 48]. In view of these aspects, we prepared samples by varying metal concentration (M_{Sn}). The major aim behind these studies was to deposit Sn-rich SnS films

so that all the possible inherent Sn vacancies are compensated. Samples were prepared by varying M_{Sn} alone from 0.06M to 0.12M, fixing M_S at 0.10M. For the particular study, M_S was purposefully kept low (0.1M), because at higher M_S, probability to grow Sn compounds with large Sn vacancies is high.

For the fabrication of homojunction by sequential deposition employing CSP technique, it would be beneficial to have the same T_S for both n and p-type layers. Therefore, we selected the previously optimized T_S (375°C) for the deposition of n-type films.

The samples exhibited considerable changes in structural, optical and electrical properties with variation in M_{Sn}. These interesting observations are given in the following sections.

3.3.5.1 XRD analysis

Figure 3.29 shows the XRD pattern of the samples prepared by varying M_{Sn}. These samples had 'Herzenbergate orthorhombic' SnS phase with preferential orientation along (1 1 1) plane and crystallinity of the samples increased with the increase in M_{Sn}. Sn_2S_3 impurity phase was present in all the samples irrespective of variation in M_{Sn}.

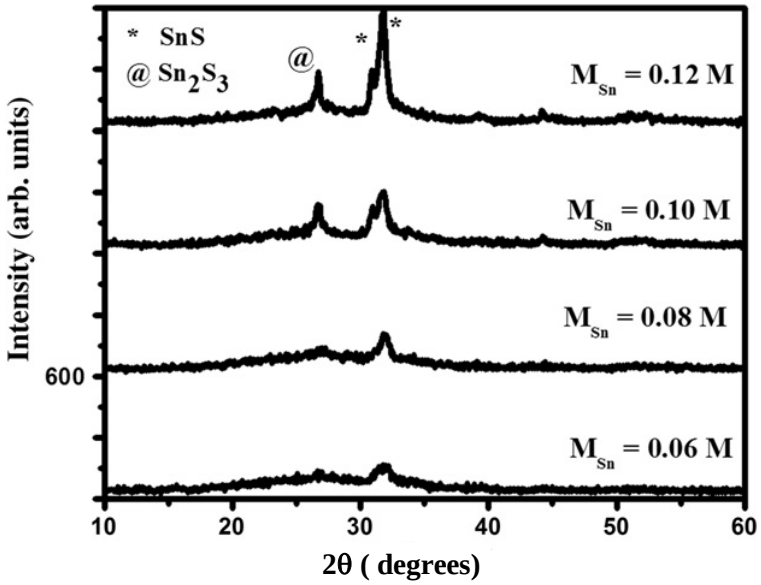

Figure 3.29 : XRD pattern of samples deposited at different M_{Sn}.

3.3.5.2 Optical studies

For higher values of M_{Sn}, the films were metallic gray in color and their optical band gap decreased with increase in M_{Sn}. Variation of optical band gap with Sn concentration in the solution is shown in Figure 3.30.

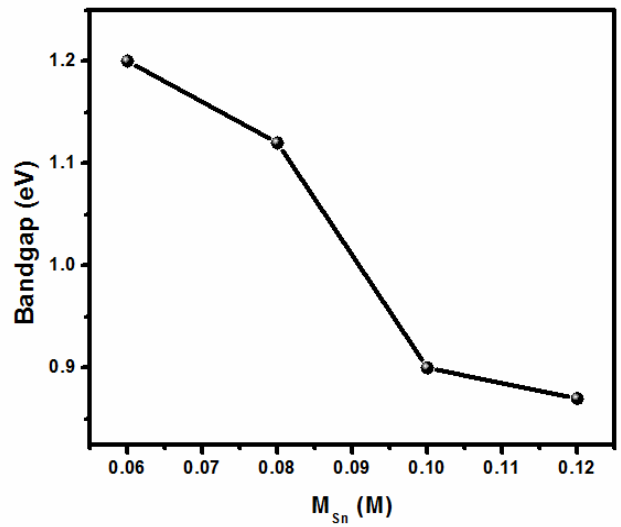

Figure 3.30 : Plot showing variation in optical band gap w.r.t change in the M_{Sn} in the precursor solution.

3.3.5.3 Electrical Studies

Hot probe analysis proved these samples to be n-type, only when M_{Sn} is 0.12 M. Further increase in M_{Sn} resulted in visibly non-uniform films. Figure 3.31 shows variation in resistivity of the samples with M_{Sn}. It was observed that resistivity decreases up to M_{Sn} = 0.1 M and then started increasing slightly with further increase in M_{Sn}. Slight increase in resistivity for M_{Sn}=0.12 M could be due to the type conversion. Photosensitivity was measured using the formula, $G = I_L - I_D / I_D$, where G is the photosensitivity, I_D the dark current and I_L is the illuminated current measured under illumination. All the samples were illuminated for 1 min before recording I_L. Variation in photosensitivity was observed (Figure. 3.32) which followed the same trend as that of the resistivity (Figure 3.31). A high photosensitivity of 2.3 was shown by films prepared with M_{Sn}=0.06 M. We could thus engineer the photosensitivity of SnS films by varying the concentration of Sn in spray solution.

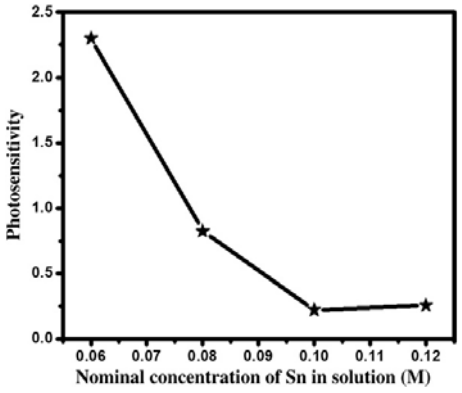

Figure 3.31: Plot showing variation in resistivity w.r.t M_{Sn}.

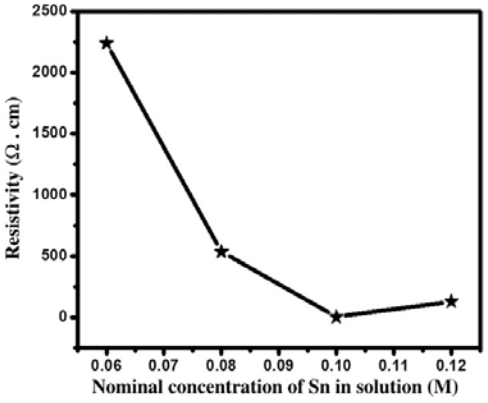

Figure 3.32: Graph showing variation in Photosensitivity w.r.t M_{Sn}.

3.3.6 Effect of post annealing time

Post annealing was given to the sample prepared using CSP technique to assure that pyrolytic reduction has been completed properly. This is very important because, if we place the sample for longer time on the hot plate after the deposition, there are chances for the re-evaporation /reaction with air to form other oxide phases. If the annealing time is very low, pyrolytic reduction will not be complete which critically affects the crystallinity and other material properties of the deposited material. In order to optimize the post annealing time, samples were removed from the hot plate at different times after the deposition.

Five set of samples were prepared to understand the effect of post annealing time on the material properties of SnS thin films. After the deposition, samples were removed from the hot plate at every 15 minutes ie., at 15 min, 30 min, 45 min, 60 min and 75 min and were named as R15, R30, R45, R60 and R75. The results of Structural, Optical and electrical characterization of the samples are given in the following subsections.

3.3.6.1 XRD Analysis

The XRD pattern of the samples removed from the hot plate at different times after deposition is shown in Figure 3.33. It is evident from the figure that very long annealing resulted in the formation of other binary compounds of Sn. This result is consistent with the observation by Nair *et al.* on the conversion of SnS to SnO_2 with air annealing [27]. Grain size of the samples were determined using Debye Scherrer formula and found that films which are given 30 min post annealing time exhibited the maximum grain size (10 nm).

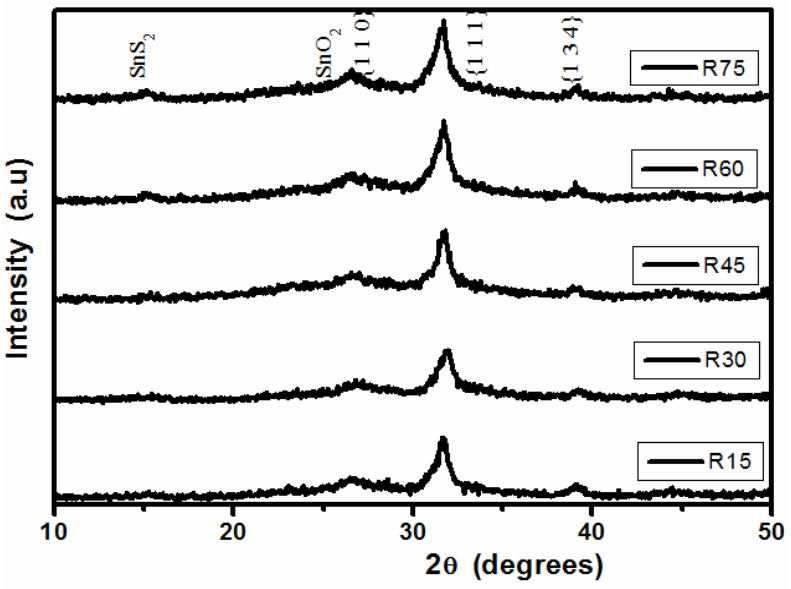

Figure 3.33: XRD pattern of samples R15 to R75.

3.3.6.2 Optical characterizations

$(\alpha h\nu)^2$ vs $h\nu$ plot of the sample with different post annealing time is given in Figure 3.34. Optical band gap of the films increased slightly with increase in annealing time.

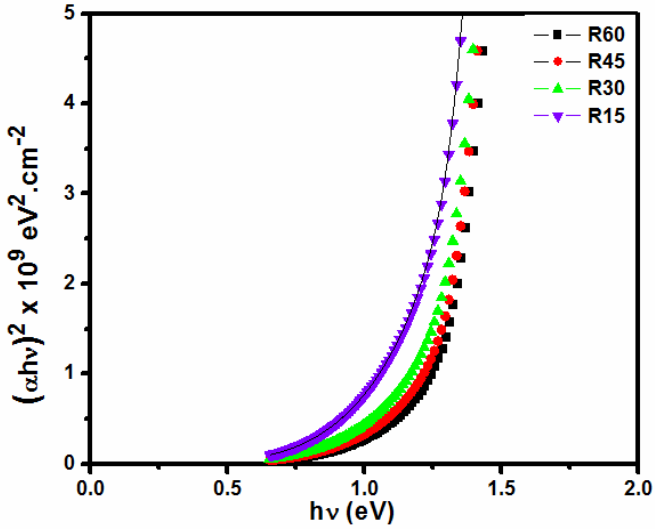

Figure 3.34: $(\alpha h\nu)^2$ vs $h\nu$ plot of the sample with different post annealing time.

3.3.6.3 Electrical characterization:

Figure 3.35 is the plot showing the variation in conductivity of the samples with respect to post annealing time. It can be seen from the figure that the resistivity of the samples decreases with increase in the annealing time.

Even though the resistivity is the least for longer post annealing time, we chose 30 min post annealing for the future studies due to the formation of SnO_2 for still longer annealed samples.

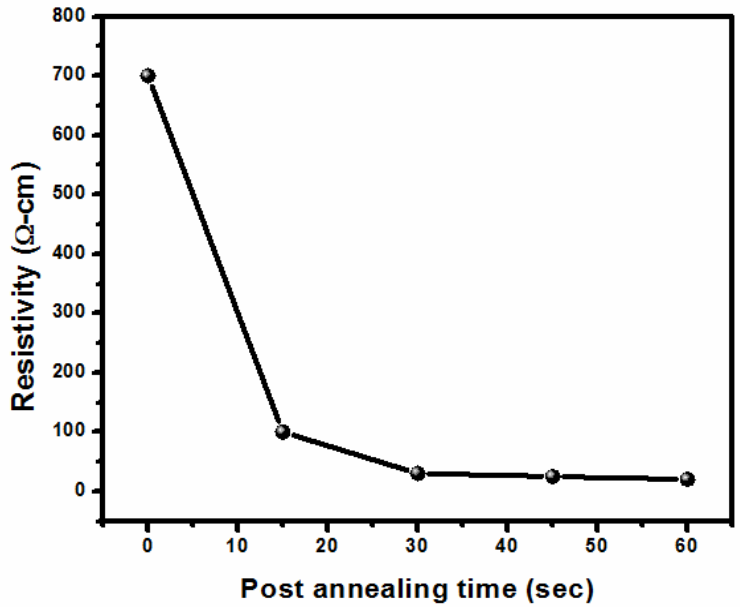

Figure 3.35 : Plot showing Variation in resistivity of the samples w.r.t post annealing.

3.4 Conclusion

Deposition parameters were optimized for stoichiometric SnS films which can be used as p-type, direct band gap absorber layer with very high absorption coefficient suitable for solar cells. Band gap engineering of single-phase SnS thin film was achieved in the temperature regime 300°C –

400°C, which finds application in fabrication of solar cells as here we need both lower and higher band gap layers. n-type SnS films could be obtained when content of metallic precursor is higher than that of the sulfur precursor in spray solution. As the deposition temperature is same for the deposition of both n and p-type SnS films, it is possible to have sequential deposition of n and p-type layers for fabrication of SnS homojunction. Highly photosensitive SnS films which had photocurrent value thrice that of dark current, can also find application as smart material. The optimized deposition conditions for p- type and n-type SnS thin films are tabulated in Table 3.7.

Table 3.7 : The optimized deposition conditions for getting p-type and n-type SnS thin films.

Deposition parameters	For p-type SnS	For n-type SnS
Substrate temperature	375 ^{0}C	375 ^{0}C
Molarity of $SnCl_2$	0.1 M	0.12 M
Molarity of Thiourea	0.2 M	0.1 M
Sn/S ratio in the precursor	1 / 2	1.2 / 1
Spray rate	2 ml / min	2 ml / min

Reference

[1] P. S. Patil, Mater. Chem. Phys. **59 (**1999) 185-198.

[2] B. Thangaraju, P. Kaliannan, J. Phys. D: Appl. Phys. **33** (2000) 1054-1059.

[3] H. B. H. Salah, H. Bouzouita, R. Rezig, Thin Solid films **480-481**(2001) 439-442.

[4] N. K. Reddy, K. T. R. Reddy, Physica B **368** (2005) 25-31.

[5] N. K. Reddy, K. T. R. Reddy, Mater. Chem. Phys. **102** (2007) 13-18.

[6] T. T. John, S. Bini, Y. Kashiwaba, T. Abe, Y. Yasuhiro, C. S. Kartha, K. P. Vijayakumar, Semicond. Sci. Technol. **18** (2003) 491-500.

[7] P. M. Ratheesh Kumar, Spray Pyrolyzed Zinc Oxide Thin Films: Effects of Doping and Beam Irradiation Ph.D Thesis Cochin University of Science and Technology, India (2007).

[8] C. H. Chen, E. M. Kelder, J. Schoonman, J. Eur. Ceram. Soc. **18** (1998) 1439.

[9] T. T. John, Spray Pyrolysed $CuInS_2/In_2S_3$ Solar Cell:Material Charecterization and Device Fabrication Ph.D Thesis Cochin University of Science and Technology India (2005).

[10] C. Natarajan, N. Fukunaga, G. Nogami **,** Thin Solid Films **322 (**1998) 6-8.

[11] P. Bohac, L. Gauckler, Solid State Ionics. **119** (1999) 317-321.

[12] G. Gordillo, L. C. Moreno, W. de. La Cruz, P. Teheran, Thin Solid Films **252** (1994) 61.

[13] P. Bombicz, I. Mutikainen, M. Krunks, T. Leskelä, J. Madarász, L. Niinistö, Inorg.Chim. Acta **357** (2004) 513.

[14] T. Sebastian, R. Jayakrishnan, C. S. Kartha, K. P. Vijayakumar, The Open Surface Science Journal, **1** (2009), 1.

[15] B. Thangaraju, P. Kaliannan, J. Phys. D: Appl. Phys. **33** (2000) 1054.

[16] T. Sebastian, Automation of Chemical Spray Pyrolysis Unit and Fabrication of Sprayed $CuInS_2/In_2S_3$ Solar Cell Ph.D Thesis, Cochin University of Science and Technology, India, (2009).

[17] T. V. Vimalkumar, N. Poornima, C. S. Kartha, K. P. Vijayakumar, , Appl. Surf. Sci. **256** (2010) 6025-6028.

[18] P. Prathap, Y. P. V. Subbaiah, K. T. R. Reddy, Optoelectronic and Advanced Materials, **1** (2007) 252–260.

[19] K. T. R. Reddy, N. K. Reddy, R. W. Miles, Sol. Energy Mater. Sol. Cells **90** (2006) 3041.

[20] P. Thilakan, J. Kumar, Vacuum **48** (1997) 463-466.

[21] H. Tanaka, K. Ihara, T. Miyata, H. Sato, T. Minami, J. Vac. Sci. Technol., A **22** (2004) 1757.

[22] M. Mathew, Engineering the Properties of Indium Sulfide for Thin Film solar Cells by Doping Ph.D Thesis Cochin University of Science and Technology India (2009).

[23] H. H. Affify, S. A. Nasser, S. E. Demian, J. Mater. Sci.: Mater. Electron. **2** (1994) 700.

[24] J. B. Mooney, S. B. Radding, Annu. Rev. Mater. Sci. **12** (1982) 81.

[25] K. L. Chopra, I. Kaur, Thin Film Device Applications Plenum Press New York (1983).

[26] N. H. J. Stelzer, J. Schoonman, J. Materials Synthesis and Proceedings. **4** (1996) 429.

[27] P. K. Nair M. T. S. Nair, J. Campos, A. Sanchez, Adv. Mater. Opt. Electron **1** (1992) 117–121.

[28] M. Devika, K. T. R. Reddy, N. K. Reddy, K. Ramesh, R. Ganesan, E. S. R. Gopal, K. R. Gunasekhar, J. Appl. Phys. **100** (2006) 023518.

[29] T. Sebastian, M. Gopinath, C. S. Kartha, K. P. Vijayakumar , T. Abe, Y. Kashiwaba**,** Solar Energy **83** (2009) 1683-1688.

[30] K. G. Deepa, K. P. Vijayakumar,C. S. Kartha, Mater. Sci. Semicond. Process. Article in press (2011).

[31] P. M. Nikolic, P. Lj Miljkovic, B. Mihajlovic, Lavrencic, J. Phys. C: Solid Status Phys. **10** (1977) L289–L292.

[32] H. R. Chandrasekhar, R. G. Humphreys, U. Zwick, M. Cardona, Phys. Rev. B **16** (1977) 2981–2983.

[33] H. R. Chandrasekhar, D. G. Mead, Phys. Rev. B: Condens. Matter Mater. Phys. **19** (1979) 932.

[34] G. Lucovsky, J. C. Mikkelsen, W. Y. Liang, R. M. White, R. M. Martin, Phys. Rev. B: Condens. Matter Mater. Phys. **14 (**1976) 1663.

[35] Y. Liu, D. Hou, G. Wang, Chem. Phys. Lett. **379** (2003) 67–73.

[36] X. L. Gou, J. Chen, P. W. Shen, Mater. Chem. Phys. **93** (2005) 557–56636.

[37] S. Sohilaa, M. Rajalakshmib, C. Ghoshc, A. K. Arorab, C. Muthamizhchelvana, J. Alloys Compd. **509** (2011) 5843–5847.

[38] H. Su, Yi Xie, Y. Xiong, P. Gao, Y. Qian, J. Solid State Chem. **161** (2001) 190-196.

[39] M. Khadraoui, N. Benramdane, C. Mathieu, A. Bouzidi, R. Miloua, Z. Kebbab, K. Sahraoui, R. Desfeux, Solid State Commun. **150** (2010) 297-300.

[40] C. A. Formstone, E. T. Fitzgerald, P. A. Cox, D. O'Hare, Inorg. Chem. **29** (1990) 3860.

[41] K. Mishra, K. Rajeshwar, A. Weiss, M. Murley, R. D. Engelken, M. Slayton, H. E. McCIoud, J. Electrochem. Soc. **136** (1989) 1915-1923.

[42] C. D. Wagner, W. M. Riggs, L. E. Davis, J. F. Moulder, G. E. Muilenberg, Handbook of X-Ray Photoelectron Spectroscopy, Perkin-Elmer Eden Prairie Minnesota (1979).

[43] A. S. Juarez, A. Ortiz, Semicond. Sci. Technol. **17** (2002) 931.

[44] D. K. Schroder, Semiconductor Materials and DeviceCharacterisation, John Wiley and Sons New York (1998).

[45] M. A. Hernández-Fenollosa, M. C. López, V. Donderis, M. González, B. Marí, J. R. Ramos-Barrado, Thin Solid Films **516** (2008) 1622–1625.

[46] H. Noguchi, A. Setiyadi, H. Tanamura, T. Nagatomoto, O. Omoto, Sol. Energy Mater. Sol. Cells **35** (1994) 325.

[47] N. K. Reddy, K. T. R. Reddy, Mater. Chem. Phys. **102 (**2007) 13.

[48] O. E. Ogah, G. Zoppi, I. Forbes, R. W. Miles, in:Proceedings of 23rd European Photovoltaic Solar Energy Conference, Valencia Spain (2008).

…..ꕥ….

Chapter 4

ENGINEERING THE STRUCTURAL AND OPTO–ELECTRONIC PROPERTIES OF SnS THIN FILMS

Contents

4.1 Introduction

Tin monosulfide (SnS) is one of the Tin chalcogenide (IV-VI group) compounds having layer structure. It has direct band gap of 1.33 eV [1], which is near to the optimum value 1.5 eV required for an ideal absorber for efficient light absorption. Its absorption coefficient is comparatively higher than that of presently existing materials like CdTe [2] and $CuInSe_2$ [3]. The light conversion efficiency of this material (from Loferski diagram) is 25% [4] and its electro-optical properties can be controlled by doping with suitable dopants [5]. In addition, its constituent elements Sn and S are abundant and less toxic in nature compared to GaAs, CdTe, InP, etc [6]. These properties emphasize that SnS could be a good absorber material to absorb major portion of electromagnetic spectrum. In recent years, many groups have come up with quite a few interesting results on SnS thin films [7-12].

In spite of possessing the aforementioned good qualities, conversion efficiency of the photovoltaic devices fabricated with this material is quite low as compared to theoretical predictions [13-15]. The major parameters

that pull back from attaining higher efficiency may be the large resistivity of SnS films and/or due to the presence of impurities / other binary sulfides of Sn such as Sn_2S_3 and SnS_2. Defects and traps present in the SnS film can play crucial role in determining the optoelectronic properties of the material [16]. Another major problem of this class of materials is the control over the stoichiometry; i.e., metal to chalcogen ratio. Because of large difference in the vapor pressures of Sn and S, the stoichiometry is generally controlled by means of sophisticated vapor-monitoring techniques [17]. In contrast to Physical Vapor Deposition (PVD) techniques, in Chemical Spray Pyrolysis (CSP) technique, ratios of the constituents are directly linked to their concentrations in the spray solution. Moreover, this technique is ideally suited for deposition of large area films with controlled dopant profiles [18-20].

By optimizing the deposition parameters as explained in the previous chapter, we could obtain phase-pure, uniform SnS thin films having very high absorption coefficient and optimum band gap for maximum photovoltaic conversion. The study demonstrated the potential and suitability of the technique to deposit stoichiometric SnS thin films which are quite difficult to obtain employing other techniques.

Further reading in this regard revealed that a reduction of lattice mismatch, defect density, electrical resistivity (with an improvement in the grain size) and removal of the impurity phases (if any) of the film are vital and this could significantly improve the performance of the device. Hence we decided to first deposit thin films of pure SnS employing CSP technique and then modify the properties of these films using two entirely different methods viz., (1) ex-situ Sn- diffusion technique and (2) pH variation of the starting precursor solution.

4.2 Ex-situ Sn diffusion process

Structural, optical, and electrical properties of SnS films could be modified by addition of traces of suitable impurities to the material called doping. But in literature, there were only a few reported works on doping of these films. Yang Yongli *et al.* [16] found that the semiconducting properties of the SnS films deposited using 'pulsed electro deposition' technique could be improved by Ag-doping. GE Yan-hui *et al.* [17] reported the doping of SnS films (deposited using chemical bath technique) with In resulted in tuning the band gap of the material. Guo Yuying *et al.* [18] tried doping of vacuum evaporated SnS films with Sb, which enhanced conductivity and photosensitivity of the films.

In compound semiconductors, the excess and deficiency of the constituent elements can itself play a similar role as that of dopants [19]. The inherent Sn vacancies present in the lattice are responsible for the p-type conductivity of SnS thin films. Therefore the variation of concentration of either Sn or its vacancy in the SnS matrix can affect the material properties quite significantly. Reddy *et al.* [20] reported that the films with excess Sn exhibited good conductivity. Main focus of this work is to reduce the resistance of SnS layer without affecting any of its favorable optical and structural properties. It is generally difficult to prepare low resistive SnS films [21-26]. Therefore, we thought of purposefully incorporating excess Sn in to the SnS films and thus modifying the opto-electronic properties of the material, considering the facts mentioned above.

Since our concern was to develop a good absorber layer for photovoltaic applications, we preferred to have the low resistive film extended only to very thin layer (few hundred Å) and existing at the top of

the SnS film and a comparatively high resistive layer towards the junction region. Carrier generation and collection can be promoted by such a structure, which is very useful for photovoltaic applications [27]. For this purpose, we introduced a process known as "ex-situ thermal diffusion." Here one can limit the diffusion to surface layer so that, during junction fabrication for photovoltaic applications, one gets a low resistive p^+ layer near the electrode. This could reduce the series resistance of the cell and also act as an electron reflector, reducing the back surface recombination. This will further result in increased short circuit current. The other aims of the works were to enhance the photosensitivity of the SnS films and to remove the impurity phases from the surface layer formed due to the inevitable contamination by oxygen.

4.2.1 Experimental details

Pristine SnS thin films were deposited on Soda-lime glass substrates using CSP technique. Aqueous spray solution, consisting of stannous chloride ($SnCl_2.2H_2O$) and thio-urea ($CS(NH_2)_2$) in required molarities was sprayed on to the substrate kept at a temperature 375 ± 5˚C with a spray rate of 2 ml/min. Total volume of the solution sprayed was 30 ml and the thickness of the films was 0.8 µm. The detailed report on the deposition and characterization of SnS film was presented in the previous chapter.

Incorporation of Sn was now achieved by diffusing the Sn metal layer deposited over SnS thin films. For this, thin layer of Sn having thickness of a few nanometer was deposited using vacuum evaporation technique (pressure during evaporation was ~$2x10^{-5}$ Torr) and subsequent annealing of the Sn/SnS bilayer system at 100^0C by using a radiant heater (500W Halogen lamp) for 30 minutes resulted in complete diffusion of the metal. Diffusion concentration was changed by varying the mass of the

metal used for evaporation. The Sn diffused samples were named as SnS:1Sn, SnS:3Sn, SnS:6Sn, SnS:9Sn and SnS:15Sn corresponding to 1 mg, 3 mg, 6 mg, 9 mg and 15 mg of Sn metal evaporated. Thickness of the Sn layers was calculated using the equation,

$$m = \frac{m}{2\pi\rho r^2} \quad \text{----------} \quad (4.1)$$

where, r is the distance between the vapor source (Mo- boat) and the target, ρ is the density and m is the total amount of the metal (Sn) evaporated [28]. Using Eq. 4.1, the thickness of the Sn layers were 1.21 nm, 2.46 nm, 3.63 nm, 4.84 nm and 9.08 nm respectively corresponding to the evaporation of 1 mg, 3 mg, 6 mg, 9 mg and 15 mg of Sn metal. Since the thickness of the metal layer was quite low, the samples were named using the quantity of Sn used for evaporation.

4.2.2 Results and discussions

SnS samples when coated with Sn and annealed, visibly it was found that the Sn layer diffused almost completely. The variations in structural and opto-electronic properties of SnS films with Sn diffusion are described in the following sub-sections.

4.2.2.1 Thickness measurement

Thickness of the films was not affected with Sn diffusion. All the samples under the study including the pristine film were about 800 nm thick. Roughness of the films, which can be considered as a vital parameter governing the performance of thin film photovoltaic devices, also remained more or less same with Sn diffusion. From the measurements done using stylus profiler, the root mean square value of surface roughness of the samples was measured to be 47 nm.

4.2.2.2 Structural characterization

Figure 4.1 shows x-ray diffractograms of pristine and the Sn diffused set of samples. The 'd' values coincided well with those of SnS in standard JCPDS data card (39-0354). The samples were crystallized in the Herzenbergate orthorhombic phase, with preferential orientation along (1 1 1) plane. From the XRD pattern, it is also clear that the incorporation of Sn neither caused any change in the structure of SnS nor resulted in the formation of new compounds. However, higher quantity of Sn diffusion (from 9 mg onwards) resulted in formation of Sn_2S_3 phase in the samples. Table 4.1 summarizes the details of XRD patterns (comprising experimentally obtained 2θ and d-value with corresponding JCPDS reference card number). Variation in grain size (calculated using Debye Scherrer formula) of the samples with Sn diffusion is given in Figure 4.2. All the Sn diffused samples were having smaller grains than the pristine samples. Among the diffused samples SnS:6Sn (with the thickness of Sn layer 3.63 nm) had the maximum grain size.

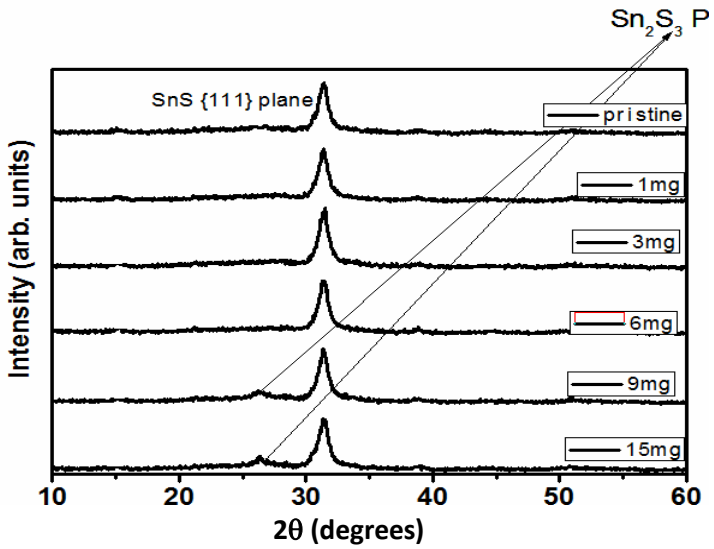

Figure 4.1: XRD pattern of pristine and samples SnS:1Sn to SnS:15Sn.

Table 4.1: Experimentally observed 2θ and d-values in the XRD pattern.

Sn-Binary sulphide phase	2θ value (degrees)	d-value (Å)	Lattice parameters (Å)	Plane	JCPDS Reference No.
SnS	31.52	2.836	a= 4.329 b=11.19 c=3.983	(1 1 1)	39-0354
Sn_2S_3	26.60	3.348	a= 8.864 b=14.02 c=3.747	(1 1 1)	14-0619

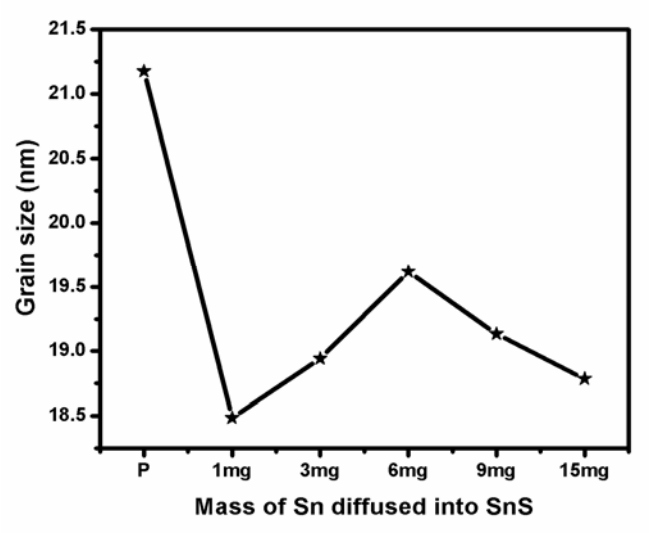

Figure 4.2: Variation in grain size of the pristine and the Sn diffused samples.

4.2.2.3 Optical Studies

Optical absorption spectra were recorded in the wavelength region 350 - 1900 nm and the results are depicted in Figure 4.3. It is clear from the figure that, there were no humps in the absorption spectra corresponding to the possible 'free carrier absorption' due to metal residues, if any, present in the sample.

In order to determine the optical band gap, $(\alpha h\nu)^2$ vs hv graph was plotted (Figure 4.4). Linearity of the plot confirmed the direct band gap of SnS films. Optical band gap is the decisive parameter, which makes SnS an ideal candidate with maximum theoretical photovoltaic conversion efficiency [4]. As evident from Figure 4.4, the band gap remains unaltered (1.33 eV) with Sn diffusion retaining the potential of the material to have maximum photovoltaic conversion efficiency. It was also observed that absorption edge was not sharp for the Sn diffused samples and there was absorption in long wavelength region. This might be caused by the introduction of shallow donor levels due to Sn diffusion [29].

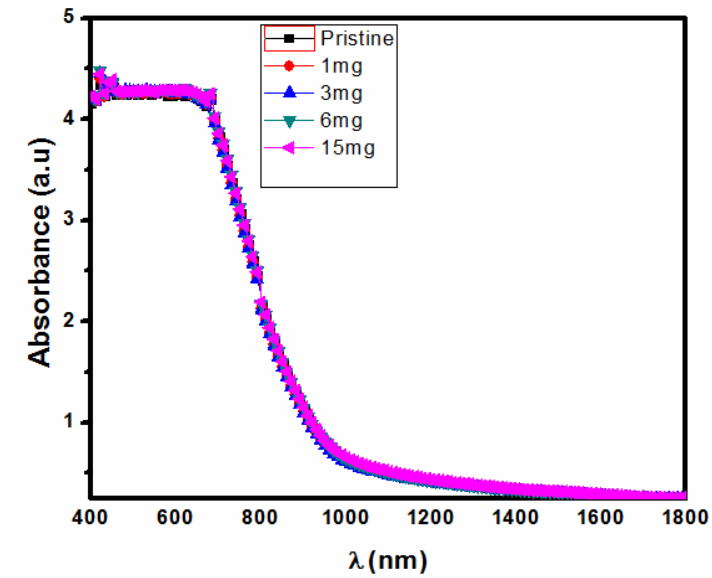

Figure 4.3: Absorption spectra of the pristine and the Sn diffused samples.

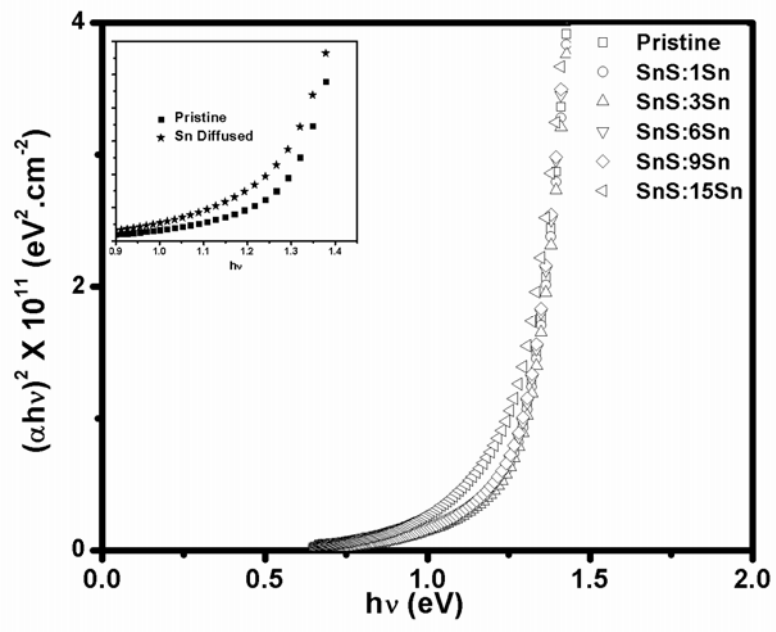

Figure 4.4: (αhν)² vs hν plot of the pristine and the samples SnS:1Sn to SnS:15Sn. In the inset, a magnified view showing the difference in absorption at higher wavelength of the pristine and a Sn diffused sample is given.

4.2.2.4 Electrical Studies

4.2.2.4.1 Resistivity measurements

Variation of electrical resistivity of the samples with Sn diffusion is depicted in Figure 4.5. Resistivity was found to be the lowest for SnS:6Sn (2 Ω.cm), which is about an order smaller than that of the pristine sample. This resistivity value is lower than that of the Ag doped SnS films reported by Devika *et al.* [30]. Moreover, we could get this without altering the optical band gap of the material.

4.2.2.4.2 Photosensitivity measurements

Photosensitivity is an important parameter as far as the materials for photovoltaic applications are concerned [31]. It is a measure of increase in conductivity of the samples on illumination. Photosensitivity

measurements were taken using two-probe method, by applying a potential difference in the range 1-2 volts across the Ag electrodes and it was calculated using the equation $(I_L-I_D)/I_D$, where I_L is illuminated current and I_D is the dark current. Among these samples, photosensitivity was maximum for SnS:6Sn with photocurrent magnitude approximately twice as that of the dark current. This value is comparable with the high photosensitivity obtained in SnS films by Sb - doping [18]. Interestingly, this was the sample with the lowest resistivity. Usually photosensitivity tends to be higher for samples which are highly resistive. The anomalous behaviour in photosensitivity of the samples may be due to the creation of shallow donor levels due to Sn diffusion. These donor levels play several roles in enhancing the minority carrier concentration. The first one is the direct creation of electrons (which are the minority carriers here) by the donors due to thermal excitation and this would naturally enhance the minority carrier density. The second possibility is the excitation of electrons from the valence band to the donor level and again from the acceptor level to the donor level. This is a sort of 'pumping' of electrons to the donor levels using sub-band gap energy photons and takes place in addition to the conventional band-to-band excitation (1.33 eV). From the donor level the thermal energy available at room temperature is sufficient to excite these electrons to the conduction band. Hence, it is assumed here that these three processes may result in an enormous enhancement of the minority carrier density and hence the photocurrent. Now the enhancement of dark current is also caused by the combined effect of acceptors and donors i.e. both electrons (minority) and holes (majority) contribute to the dark current. All these make the sample extremely suitable for photovoltaic applications.

Such anomalous behavior in photosensitivity has been observed earlier for Ag doped In_2S_3 films [32]. The variation of Photosensitivity and Resistivity of the pristine and the Sn diffused sample is plotted in Figure 4.5.

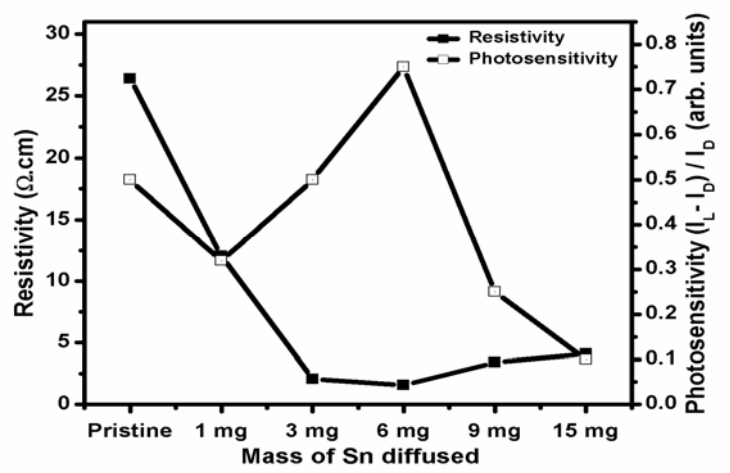

Figure 4.5: Plot showing variation of resistivity and photosensitivity of pristine and the Sn diffused samples.

4.2.2.4.3 Hall measurements

Hall measurements performed on the samples revealed p-type electrical conductivity. Variation of carrier concentration, mobility and Hall coefficient for pristine and the Sn diffused samples are tabulated in Table 4.2. As expected, carrier concentration increased with increase in the doping concentration. The decrease in mobility of the carriers in the diffused sample is probably due to enhanced probability of collision as carrier density is increased [33]. Maximum carrier concentration is obtained for SnS:6Sn with reasonably good mobility.

Table 4.2: Data obtained from Hall measurements.

Sample Specification	Mobility μ ($cm^2/V.s$)	Resistivity ρ (Ω.cm)	Carrier density N ($x10^{15}/cm^3$)
Pristine	1390	22	1.09
SnS:3Sn	37.9	3.2	47.0
SnS:6Sn	43.0	2.1	50.0
SnS:9Sn	40.1	3.0	53.0
SnS:15Sn	30	4.9	57.0

4.2.2.5 Compositional studies

Employing Ar-ion sputtering, the depth profiles showing variation in concentration of S, Sn, O, and Na along the sample thickness were obtained using XPS technique. At the end of sputtering, the glass substrate was exposed. From the XPS spectra (Figure 4.6 & 4.7), it is clear that the peak heights of S and Sn remain constant throughout the thickness (800 nm) of the sample, indicating the same chemical concentration of the constituent species throughout the thickness of the film. A shift in the S and O peak is observed in the surface layers of the pristine sample (Figure 4.6) which may be due to the formation of Sn-O-S in the surface [34]. But as evident from the XPS of the Sn diffused film (Figure 4.7), there is no shift in the binding energies of S and Sn. Even in the surface layer, the binding energies correspond to that of SnS. Also from the depth profile it is clear that Sn has been distributed uniformly throughout the depth of the film. So the enhancement in conductivity obtained due to the Sn diffusion may be due to the removal of highly resistive Sn-O-S contaminant layer from the surface by the formation of SnS layer.

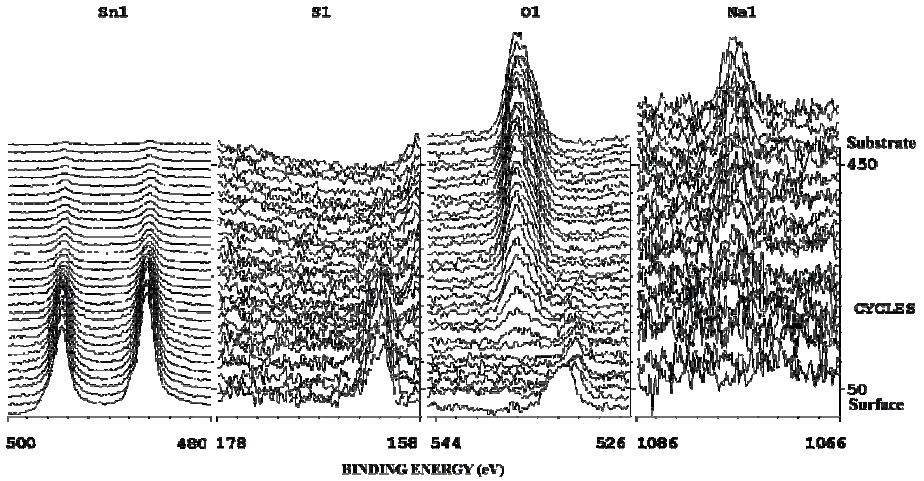

Figure 4.6: XPS depth profile of the pristine SnS films BE of Sn, S, O and Na are shown.

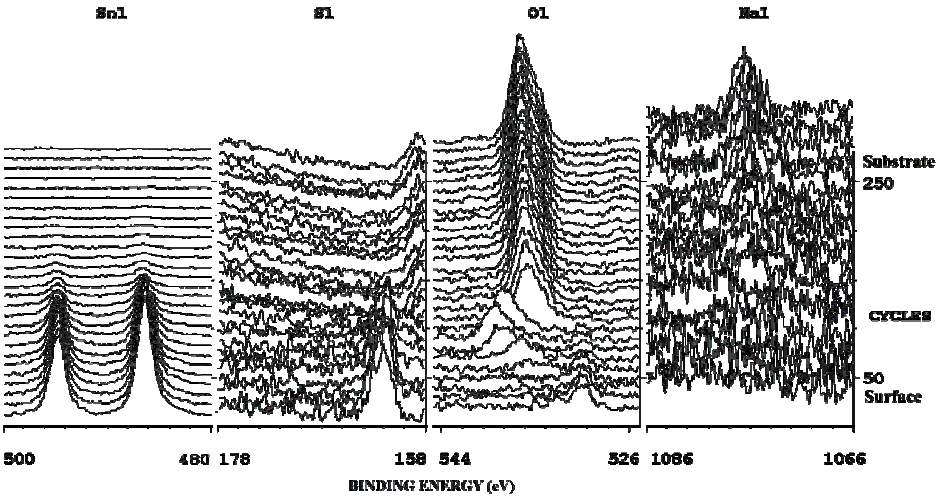

Figure 4.7: XPS depth profile of 6mg Sn diffused SnS films BE of Sn, S, O and Na are shown.

4.2.3 Conclusions

Innovative ex-situ Sn diffusion process has been employed to reduce the resistivity of the SnS films prepared using CSP technique for photovoltaic applications. The unavoidable impurity phase Sn-O-S from

the surface, formed in CSP technique, was removed completely through the diffusion of Sn. Carrier concentration was also found to be enhanced by an order. SnS:6Sn sample, with 3.63 nm thick Sn layer diffused in to the SnS matrix, was found to be optimum for obtaining crystalline single phase films having lowest resistivity together with highest photosensitivity. The major advantage of this technique is that we could obtain low resistive (resistivity ~ 2 Ω.cm) as well as highly photosensitive samples through Sn diffusion, keeping the other suitable properties of the material for photovoltaic application remaining unaffected.

4.3 pH Variation studies

Improving crystallinity and opto-electronic properties without giving any post-depositional treatments are very vital for a material to find its application in the photovoltaic technology. Especially for SnS films, not much reported works are available in literature on improvement of conductivity and crystallinity of the material. We could obtain low resistive SnS thin films by employing an innovative technique called "exsitu Sn diffusion" as explained in the preceding section. But this process involves post deposition treatments which are not much attractive from industrial point of view for device level applications. Here we intend to develop highly conducting and crystalline SnS thin films without employing post depositional treatments.

pH of the precursor solution can affect the structural and optoelectronic properties of the thin films developed out of chemical routes [36]. This parameter is very vital in CSP as well since it directly affects the reaction cross section of the precursors on the substrate during the pyrolytic reduction and hence may strongly affect the stoichiometry and grain growth.

The role of pH on the material properties of ZnO thin films deposited using CSP technique have been studied by M. Caillaud *et al.* in the year 1993 [35]. Kumar *et al.* had reported the effect of pH of starting-solution on the growth of Cu_2ZnSnS_4 thin films deposited by spray pyrolysis [36]. Structural and morphological variation of spray pyrolysed $CuAlO_2$ thin films with precursor pH was reported by Madhav Singh *et al.* [37].

In the present work, we varied pH of the precursor solution and investigated structural, compositional, optical and electrical properties of the films with an aim to see whether the as deposited optimum pH sample become more suitable for photovoltaic applications.

4.3.1 Experimental Details

SnS thin films were deposited on soda-lime glass substrates using CSP technique. The spraying solution contained equal volumes of 0.1M aqueous solution of stannous chloride and 0.2 M aqueous solution of thiourea (TU). Total volume of solution was 30 ml and the pH of the as-prepared solution was 0.8. Temperature of the glass substrate was kept at 375±5˚C, while the spray rate was 2 ml/min. The complex compound formed in the solution while mixing metal chloride and TU is of the form [38,39].

$$SnCl_2{:}TU \;::\; 1{:}2 \;\rightarrow\; [Sn(TU)_2]Cl_2.H_2O \qquad (4.2)$$

where, 1:2 stands for the ratio of the cationic precursor to anionic precursor solution. On the substrate, pyrolytic reduction of these complexes takes place resulting in the formation of Sn_xS_y thin films along with gaseous byproducts.

The film thus obtained had a thickness of ~ 0.8 μm with 30 Ω.cm resistivity. Magnitude of the optical band gap of this pristine (pH0.8) SnS film was 1.33 eV. Other minute details of the deposition and characterization of SnS films could be found in the previous chapter. The pH was varied from 0.8 to 3.2 by adding 0ml, 1ml, 2 ml, 5 ml, 7.5 ml, 10 ml and 20 ml of 0.1 M NH_4Cl. The samples prepared using these modified solutions were named as pH0.8, pH1.0, pH1.3, pH2.0, pH2.3 and pH3.2 respectively. pH of the precursor solution after adding different volumes of NH_4Cl and the sample nomenclature is given in Table 4.3.

Table 4.3: Amount of NH_4Cl added, the corresponding pH of the precursor solution and the sample nomenclature.

Amount of NH_4Cl	pH value of the precursor solution	Sample name
0ml	0.8	pH0.8
2ml	1.0	pH1.0
5ml	1.3	pH1.3
7.5ml	2.0	pH2.0
10ml	2.3	pH2.3
20ml	3.2	pH3.2

4.3.2 Results and Discussions

All the films deposited were having a thickness of around 800 ± 30 nm irrespective of the pH of the precursor solution. But the root mean square value of roughness of the films measured using the surface profilometer slightly increased from 40 nm to 65 nm with the increase in pH.

4.3.2.1 Structural Analysis

XRD patterns of the samples (depicted in Figure 4.8) indicate that the films are having pure SnS phase, crystallized in Herzenbergate orthorhombic structure, with preferential orientation along (1 1 1) plane. Details of XRD patterns (comprising experimentally obtained and actual *d* values with the corresponding JCPDS reference card number) are provided in Table 4.4.

Grain size of the films was calculated from the peak at $2\theta=31.53°$ using the Debye–Scherer formula, $D=0.9\lambda/(\beta\cos\theta)$, where D is the diameter of the crystallites forming the film, λ is the wavelength of X-rays (CuKα line), β is the full width at half maximum (in radians) and θ is the Bragg angle. The Bragg angle and full width at half maximum of each XRD peak were determined by fitting a Gaussian distribution to the experimental values. Grain size variation of the samples deposited using precursors with different pH is depicted in Figure 4.9. It is evident from Figure 4.8 & 4.9 that the crystallinity of the samples improves with the increase of pH of the precursor till an optimum value of pH and thereafter, it starts deteriorating. The sample pH2.0 is found to be most crystalline.

The grain size is essentially controlled by the initial nucleation and coalescence of the islands. Therefore, the optimum pH might have helped either the formation of larger nuclei or the coalescence of more number of nuclei to form larger grains.

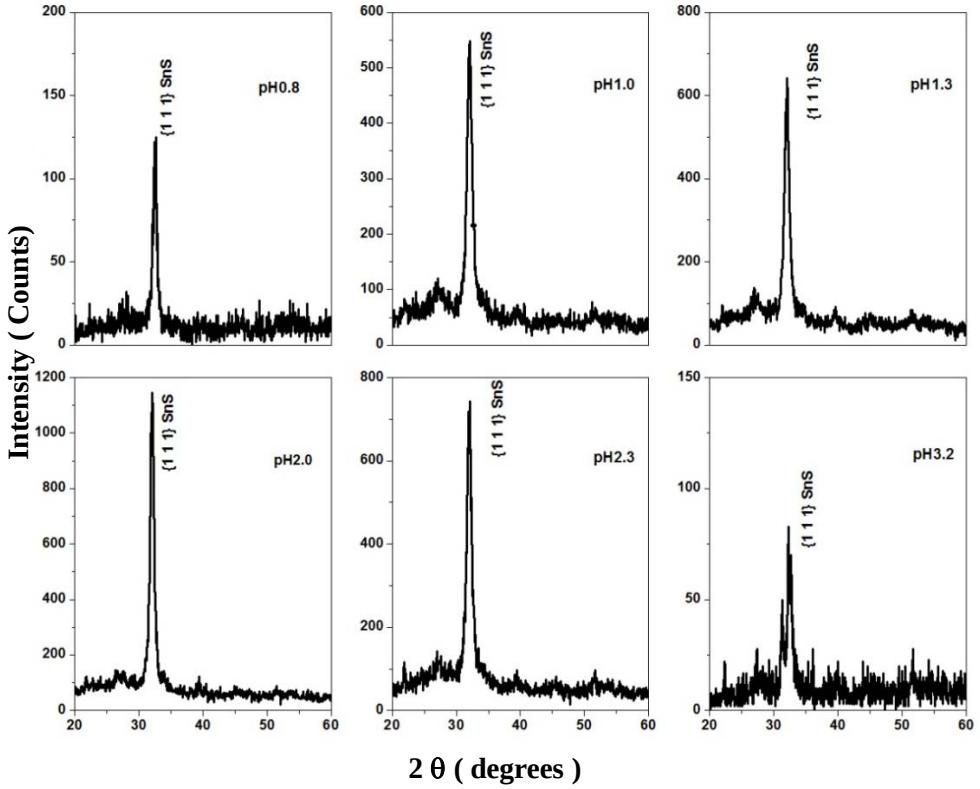

Figure 4.8 : XRD pattern of the pH0.8, pH1.0, pH2.3, pH2.0, pH2.3 and pH3.2.

Table 4.4: Experimentally observed 2θ and d-values from the XRD pattern, plane, lattice parameters and the corresponding JCPDS reference No.

Sn binary sulphide phase present	Observed values from XRD		Lattice parameters (Å)	Plane	JCPDS card reference No.
	2θ (degree)	d value (Å)			
SnS	31.53	2.836	a=4.329 b=11.19 c= 3.983	(111)	39-0354

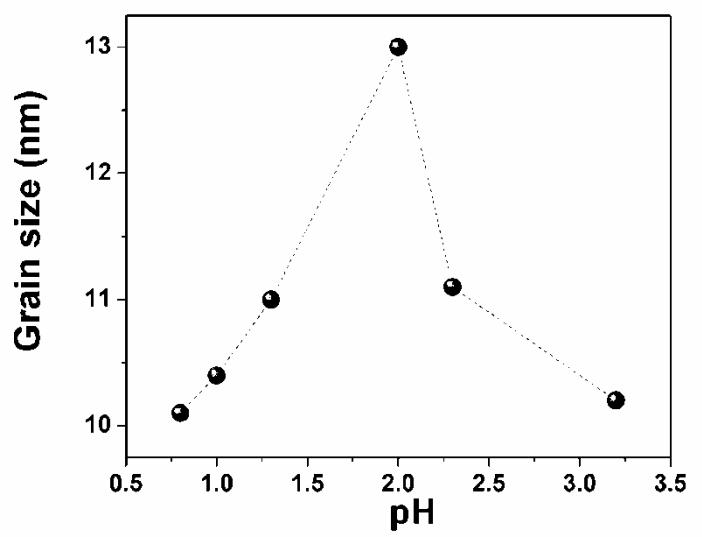

Figure 4.9: Variation in Grain size of the samples with respect to pH.

4.3.2.2 Optical Properties

Absorption spectra of SnS films prepared using precursors of different pH value are shown in Figure 4.10. It is clear from the plot that, there is no additional absorption peak present in any of the samples apart from the one corresponding to band edge absorption. In order to estimate the optical band gap of these film Tauc plot (Figure 4.11) was then drawn by taking $(\alpha h\nu)^2$ on Y-axis and $h\nu$ on X- axis. Band gap of the films decreased slightly till sample pH2.0 and further increase in the pH resulted in films with higher band gap. The reduction in band gap till the optimum pH value could be due to the improvement in crystallinity of the films.

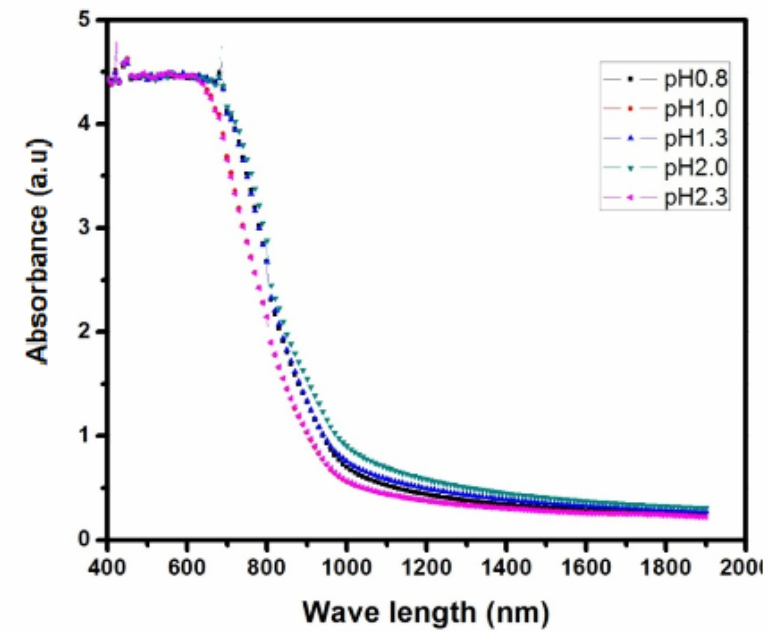

Figure 4.10: Absorption spectra of the pH varied samples.

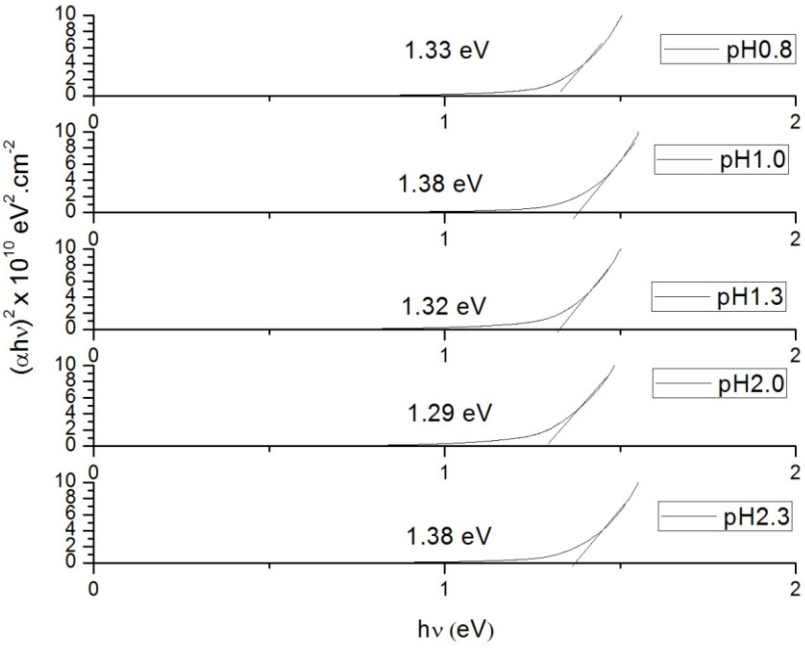

Figure 4.11: $(\alpha h\nu)^2$ versus $h\nu$ plot of the pH varied samples.

4.3.2.3 Morphological and compositional analysis

Figure 4.12 Shows the SEM image of the pristine (pH0.8) and the 'pH-varied' samples. All the films were uniform without any pin holes or cracks, and having an interesting 'needle like' grain structure. There is not much variation in morphology with respect to pH variation, except in the increased roughness at higher pH value.

Effect of pH of precursor on the surface morphologies and grain growth in the films can be understood by knowing the role of pH in the formation of complex in the precursor solution. Rate of reaction and hence reaction cross section of anionic and cationic precursor is mainly determined by the pH of the precursor solution due to the common ion effect [40]. Caillaud *et al.* investigated the influence of pH of the solution on the thin film deposition and found that the growth rate depended on the pH [35]. Formation of basic salts, adsorption compounds, or precipitates slowed down the growth at higher and lower pHs and hence there will be an optimum pH at which the reaction cross section is maximum for the formation of SnS by pyrolytic reduction. In our case this optimum pH is found to be 2.0 and is obtained by adding 7.5 ml NH_4Cl to the precursor solution.

Figure 4.13 shows variation in atomic percentage of Sn, S and Cl with respect to pH of the precursor solution as obtained from Energy Dispersive x-ray (EDAX) measurements. Variations in atomic percentage of Sn and Cl show an interesting 'mirror like' resemblance. This may be due to 'Charge Compensation' mechanism (as Cl goes into S site, there is a reduction of a negative charge and Sn concentration should accordingly get reduced to compensate this). It is evident from Figure 4.13 that pristine (pH0.8) film is almost stoichiometric and on increasing pH of the

precursors, these films initially become slightly 'S' rich. But at still higher pH, a retracing effect is observed, eventually making sample pH3.2 again nearly stoichiometric.

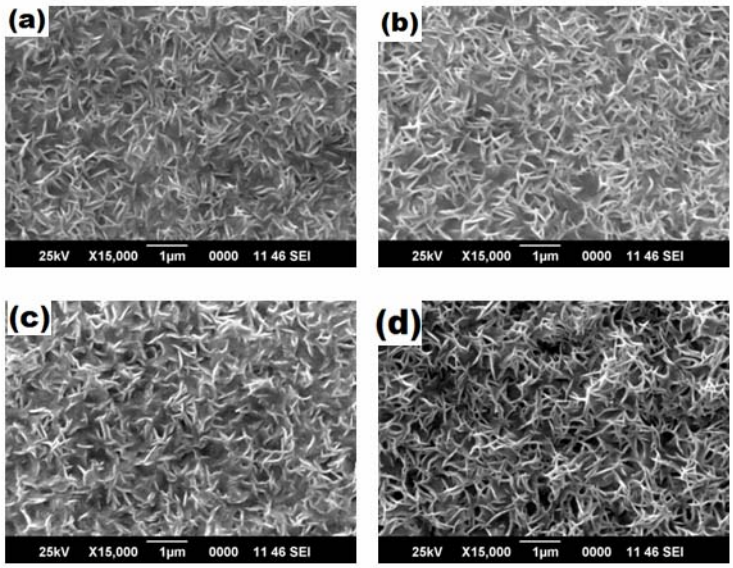

Figure 4.12: SEM image of the (a) pH0.8, (b) pH1.3, (c) pH2.0 and (d) pH3.2.

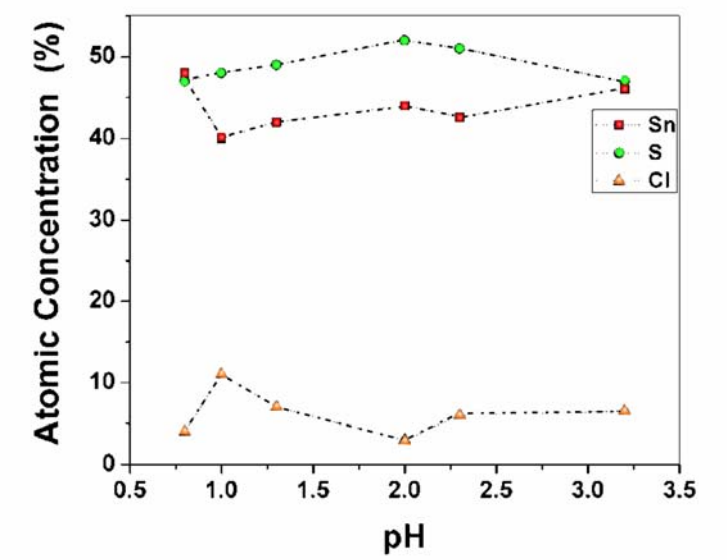

Figure 4.13: variation in atomic percentage of Sn, S and Cl with respect to pH of the precursor solution measured using EDAX.

4.3.2.4 Electrical conductivity studies

Variation in resistivity and photosensitivity of the samples is depicted in Figure 4.14. Resistivity of the samples decreased with increase in pH of the precursor solution till sample pH2.0; however further increase in pH resulted in slight increase of resistivity. Resistivity of sample pH2.0 was found to be almost three orders less than that of the pristine (pH0.8) sample. This value is found to be the lowest resistivity ever reported for SnS thin films. Interestingly the photosensitivity of the material, (defined as the ratio of increase in conductivity on illumination to the dark conductivity), exhibited an anomoulous behaviour with pH variation. Photosensitivity was maximum for the lowest resistive sample. The correlation between the crystallinity and photosensitivity indicates that grain boundaries in SnS films do not favor the lifetime of the photogenerated carreirs, unlike in $CuInSe_2$ films reported earlier [41]. Therefore the loss of photogenerated carriers in grain boundaries will be less and that explains the enhanced photosensitivity of the sample deposited at optimum pH. This is quite similar to the observation we made from ex-situ Sn diffusion as well described in the above section. Usually, higher photo sensitivity correlates to higher resistivity due to the fact that carriers that are photo-generated, do not undergo recombination when the dark resistivity is higher. However, in the present case, (at the optimum pH value) photosensitivity as well as conductivity is high making the samples very useful in photovoltaic device applications.

Sn vacancies in SnS films are reported to be the cause for acceptor levels and hence the p-type conductivity of the films [42]. The EDAX measurements clearly revealed that, as the pH increases, the material is becoming deficient in Sn concentration, which can increase density of

defect level due to Sn vacancies, providing more carriers and thus enhances the conductivity. However, as the pH goes above the optimum value (pH=2.0), the resistivity increases since Sn concentration is also increased after the optimum pH. Main advantage of the present study is that films with this superior property are achieved without employing any post deposition treatments.

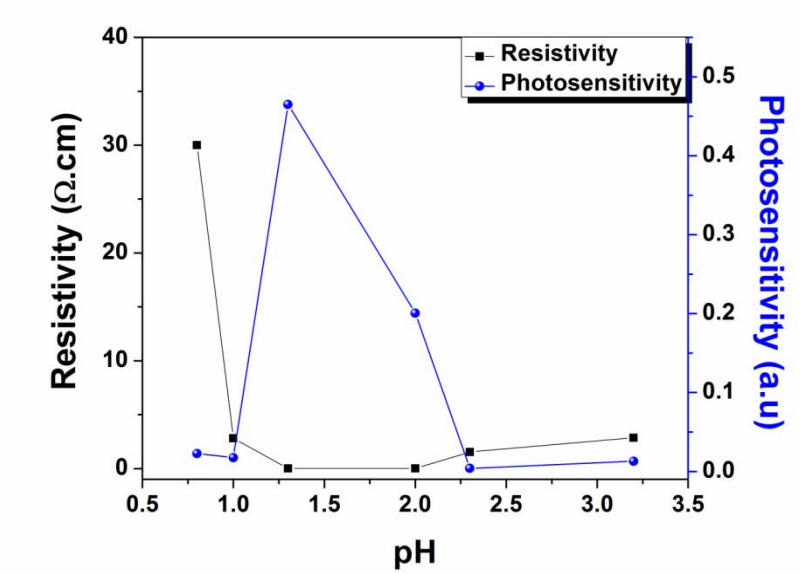

Figure 4.14: Variation in Resistivity and Photosensitivity of the samples with pH of the precursor solution.

4.3.3 Conclusions

The significance of pH of the precursor solution in determining the structural, morphological and optoelectronic properties of SnS film prepared using CSP technique is evident from this study. It is observed that the crystallinity of the films has a definite correlation with pH of the precursor solution and an optimal pH exists for the optimal crystallinity. The crystallinity of the films was best for pH of 2.0 and the electrical conductivity was also maximum for this pH. The lowest resistivity that could be obtained

by controlling the pH is about three orders lower than that of the pristine sample. Upto the best of our knowledge, this is the lowest value of resistivity achieved so far for pristine SnS thin films. This film exhibited maximum photosensitivity as well. Band gap of the films can be engineered by controlling the precursor's pH. Most importantly, these superior properties can be achieved without employing any post deposition treatments and hence it is quite useful for low-cost thin film photovoltaic technology.

References

[1] J. M. Chamberlain, M. Merdan J. Phys. C: Solid State Phys. **10** (1977) L571.

[2] C. S. Ferekides, U. Balasubramanian, R. Mamazza, V. Viswanathan, H. Zhao, D. L.Morel, Sol. Energy **77** (2004) 823.

[3] R. W. Miles, K. M. Hynes, I. Forbes, Prog. Cryst. Growth Charact. Mater. **51** (2005) 1.

[4] J. J. Loferski J. Appl. Phys. **27** (1956) 777.

[5] M. Parenteau, C. Carlone, Phys. Rev. **41** (1990) 5227.

[6] Alwyn George Davies, Keith Pannell, Tin chemistry: fundamentals, frontiers, and applications, John Wiley and Sons, Great Britain (2008).

[7] Akkari, M. Regima, C. Guasch, N. K. Turki, Advanced Materials Research **324** (2011) 101-104.

[8] Gao, H. Shen, L. Sun, Z. Shen, Mater. Lett. **65** (2011) 1413-1415.

[9] S. Cheng, H. Zhang, Micro & Nano Letters **6** (2011) 473 – 475.

[10] V. Dhanasekaran, T. Mahalingam, Jin Koo Rhee, J. P. Chu, Journal of Advanced Microscopy Research **6** (2011) 126–130.

[11] B. Ghosh, S. Chowdhury, P. Banerjee, S. Das, Thin Solid Films **519** (2011) 3368 -3372.

[12] Z. A. Jahangirli, Russ. J. Phys. Chem. A, **85** (2011) 1394–1397.

[13] K. T. R Reddy, N. K. Reddy, R. W. Miles, in: Proceedings of 14th Int. Photovoltaic Science and Engineering Conference Bangkok Thailand 627 (2004).

[14] H. Noguchi, A. Setiyadi, H. Tanamura, T. Nagatomoto , O. Omoto, Sol. Energy Mater. Sol. Cells **35 (**1994**)** 325.

[15] M. T. S. Nair, D. Avellaneda, S. Messina, P. K. Nair Mater. Res. Soc. Symp. Proc. **974 (**2007**)** CC10.

[16] Y. Yang, S. Cheng, S. Lai, Adv. Mater. Res. **60–61 (**2009) 105–109.

[17] G. E. Yan-hui,Y Y Guo , W. M. Shi, Y. H. Qiu, G. P. Wei, J. Shanghai Univ. (Engl. Edn) **11 (**2007**)** 403–406.

[18] Y. Guo, W. Shi, G. Wei G, in: Proceedings of ISES Solar World Congress Johannesburg I–V Edited by Y Goswami, Y Zhao 1337(2009).

[19] R. A. Smith, Semiconductors, Cambridge University press USA (1978).

[20] N. K. Reddy, K. T. R. Reddy, Mater. Chem. Phys.**102 (**2007**)** 13.

[21] P. Pramanik, P.K. Basu, S. Biswas Thin Solid Films **150** (1987)269.

[22] A. Tanˇusevski Semicond. Sci. Technol. **18** (2003)501.

[23] M. T. S. Nair, D. Avellaneda, S. Messina, P. K. Nair, Mater. Res. Soc. Symp. Proc. **974** (2007) CC10.

[24] Y. Yang, S. Cheng, S. Lai, Adv. Mater. Res. **60–61** (2009)105.

[25] G. E. Yan-hui, Y. Y. Guo, W. M. Shi, Y. H. Qiu, G. P. Wei, J. Shanghai Univ. (Engl. Edn) **11** (2007) 403–6.

[26] Y. Guo, W. Shi, G. Wei, in:*Proceedings of ISES Solar World Congress* vol I–V Edited by Y. Goswami and Y Zhao Johannesburg 1337 (2009).

[27] J. Nelson, The Physics of Solar Cells Imperial College Press London (2003).

[28] A. Goswami, Thin Film Fundamentals New Age International (P) Ltd New Delhi (1996).

[29] M. Mathew, G. Manju, C. S. Kartha, K. P. Vijayakumar, Y. Kashiwaba, T. Abe, Sol. Energy **84** (2010) 888.

[30] M. Devika, N. K. Reddy, K. Ramesh, K. R. Gunasekhar, E. S, R. Gopal, K. T. R. Reddy, J. Electrochem. Soc. **153** (2006) G727.

[31] T. T. John, S. Bini, Y. Kashiwaba, T. Abe, Y. Yasuhiro, C. S. Kartha, K. P. Vijayakumar, Semicond. Sci. Technol. **18** (2003) 491.

[32] M. Mathew, R. Jayakrishnan, P. M. Ratheesh Kumar, C. S. Kartha, K. P. Vijayakumar, J. Appl. Phys. **100** (2006) 033504.

[33] O. Oda, Compound Semiconductor Bulk Materials and Characterization World Scientific Singapore (2007).

[34] P. K. Nair, M. T. S. Nair, R. A. Zingaro, A. Edward, Meyers, Thin Solid Films **239** (1994) 85.

[35] Frédéric Caillaud, Agnès Smith, Jean-François Baumard, Journal of the American Ceramic Society **76** (1993) 998–1002.

[36] Y. B. Kishore Kumar, G. Suresh Babu, P. Uday Bhaskar, V. S. Raja, Phys. Status Solidi A **206** (2009) 1525–1530.

[37] M. Singh, A. R. Rao, V. Dutta, Materials Letters **62** (2008) 3613–3616.

[38] M. Krunks, T. Leskelä, I. Mutikainen, L. Niinistö, Journal of Thermal Analysis and Calorimetry **56** (1999) 479-484.

[39] M. Krunks, J. Madarász, T. Leskelä, A. Mere, L. Niinistö, G. Pokol **72** (2003) 497-506.

[40] J. Barman, J. P. Borah, K. C. Sarma Chalcogenide Letters **5** (2008) 265–271.

[41] Y. Yan, C. S. Jiang, R. Noufi, Su-Huai Wei, H. R. Moutinho, M. M. Al-Jassim, Phys. Rev. Lett. **99** (2007) 235504.

[42] Yu Wang, Hao Gong, B. Fan, G. Hu, J. Phys. Chem. C **114** (2006) 3256-3259.

Chapter 5

UNVEILING DEFECT LEVELS IN SnS THIN FILMS EMPLOYING PL TECHNIQUE AND MODELING OF ENERGY BAND SCHEME

Contents

5.1 Introduction

Defects and grain boundaries play a major role in determining the optoelectronic properties of semiconductor materials. To exploit the immense latent potential of a material for photovoltaic applications, an extensive analysis of the defect levels becomes mandatory which has not been discussed and reported in the case of SnS. Once the defect levels are identified, we can tune the opto-electronic properties of the material by purposefully manipulating the nature as well as density of these defect states.

Photoluminescence (PL) is a very efficient, non-destructive, contactless and standard technique used to characterize and evaluate quality of surfaces and interfaces as well as to probe defect levels within the material [1-4]. This technique requires very little sample manipulation or environmental control. Because the sample is excited optically, electrical contacts and

junctions are not required and highly resistive materials pose no practical difficulty. PL spectrum provides the transition energies, which can be used to determine electronic energy levels. PL intensity gives a measure of the relative rates of all the possible radiative recombination. Variation of the PL intensity with external parameters like temperature and applied voltage can be used to characterize further the underlying electronic states and bands [5,6].

Study of luminescence process can show the content as well as the behaviour of defects and impurities in semiconductors. PL spectrum and its dependence on irradiation intensity and device temperature can deliver important information for device characterisations. In particular, excitation energy/ intensity dependent PL spectra can deliver important information such as the band gap or wavelength of maximum gain, composition of the compound semiconductors, impurity level determination and also the different recombination mechanism. By exciting the samples with multiple wavelength excitation sources, we can even distinguish the surface and bulk contributions. Gracia-Gracia *et al.* used such an approach to study the surface layer of chemically etched CdTe [7].

Dangling bonds on a semiconductor surface or interface give rise to electronic states within the band gap. These mid-gap states fill up to the Fermi level with electrons that originate in the bulk of the material. Accumulation of charge at the surface creates an electric field – a depletion region – that leads to the bending of the valance and conduction band edges. According to a simple dead-layer model, 'electron hole pairs' (EHPs) that are generated in this region are swept apart by the electric field, prohibiting radiative recombination [8].

Intensity of incident light controls a critical property of the PL experiment. When the excitation intensity is low, the generated carrier density will be low, and the PL measurements are dominated by discrete defect and impurity sites at interface and within the bulk of the material. Recombination at these energetically favoured sites is frequently referred to as Shockley-Read-Hall (SRH) recombination. Shape of radiative efficiency curve in the SRH and radiative recombination transition region depends on the distribution of surface states that participate in recombination. If the distribution consists of a discrete set of states with similar energetic positions within the gap, complete saturation of the SRH recombination process will lead to a PL efficiency slope of unity. Efficiency curves with slops less than one indicates that the surface state distribution is continuous. Moreover, an increasing number of surface states are participating in recombination as the quasi-Fermi levels moves through the band gap. Hence the variation in the slope of the efficiency curve with increase in excitation can be used to map the surface state distribution within the gap. Since its development in 1991, photo luminescent surface state spectroscopy (analysis of the excitation intensity dependent PL signal) has been applied to a wide number of semiconductor systems [8].

Komiya *et al.* [9] measured excitation intensity dependent PL signal from a series of InGaAsP/InP double hetero structures. Although the PL signal was usually linear with excitation power, some samples showed super linear dependence under intermediate excitation, indicating the transition between non-radiative and radiative recombination regimes. Lack of such a transition in the other samples suggested that radiative

recombination dominated at all excitation levels, which gave an upper limit for interface recombination velocity.

In-situ PL has been used to assess InP surface during various cleaning etching steps, oxidation, ambient gas flow, plasma exposure and heating. In some cases laser induced interactions were found to alter the etch rates, surface morphology and surface contamination [10]. Timoshenko *et al.* [11] extended the in-situ PL technique to evaluate electrochemical treatments of indirect semiconductor surfaces, where pulsed excitation is required to obtain required signal.

PL intensity is an indicator of interface quality; measurement of PL signal vs. position provides information on the spatial uniformity of interface properties. Non-destructive and environment-insensitive features of PL makes this application particularly useful in the evaluation of substrate surface where detection of electrically active features may help to control problems in epitaxial devices. One of the first demonstrations of this approach was made by Krawczyk *et al.* [12] in an investigation of InP surface treatments. By coupling the excitation in one end of an optical fibre and scanning the the wave length in other end relative to a focusing objective, they achieved resolution of the order of a few microns. They observed wide variation in the PL signal on a microscopic scale.

In the characterisation of discrete low-energy states, quantitative analysis of the decrease in PL intensity with temperature helps to measure depth of a trap. Plotting the log of the PL intensity vs. reciprocal of the temperature, one can calculate the activation energy for exciting carriers out of the trap from the slope. These graphs, often referred to as Arrhenius plots, have been used to study interface alloy formation in ZnSe/CdSe

quantum Wires [13]. Temperature is also an important parameter in carrier dynamics. At the lowest temperature, excitons dominate radiative transitions and thermal energy in this regime leads to difficulties in momentum conservation. Because photons have small momentum, only low momentum exciton can directly recombine. Rising temperatures confound recombination by increasing the fraction of exciton with excessive momentum. Beyond this regime, the excitons themselves begin to dissociate and the oscillator strength of free carriers is usually much smaller than that for excitons. In this case recombining carriers must have equal and opposite momentum, a condition that decreases in likelihood as the average energy increases. In contrast, non-radiative recombination processes tend to accelerate with increasing temperature. In particular, non-radiative interface recombination usually involves thermally activated multi-photon events [14].

The fundamental limitation of PL analysis is its reliance on radiative events. Materials with poor radiative efficiency, such as low-quality indirect band gap semiconductors, are difficult to study via ordinary PL. Similarly, identification of impurity and defect states depends on their optical activity. Although PL is a very sensitive probe of radiative levels, one must rely on secondary evidence to study states that couple weakly with light.

The interesting structural, optical and electrical properties of SnS thin film making it suitable for optoelectronic, and photovoltaic applications have been elaborated in detail in the previous chapters. This IV–VI layered compound semiconductor has got a distorted NaCl-type orthorhombic crystal structure [15]. In particular, this type of

material is of interest in solar energy conversion due to the inventive arrangement of the structural lattice with cations and anions. The layers of cations are separated only by van der Waals forces, which provide intrinsically a chemically inert surface without dangling bonds and surface states. As a result, there is no 'Fermi level pinning' at the surface of the semiconductor. This fact leads to considerably high chemical and environmental stability [16]. It could support the fabrication of highly mismatched solid-state junctions without interface states. The estimated theoretical light conversion efficiency from Loferski Diagrams [17] for this compound is higher than 24%. These properties emphasize that SnS is a good absorber material to absorb major part of the electromagnetic spectrum. In spite of possessing the aforementioned qualities, reported photovoltaic conversion efficiencies [18-20] with this material are quite low as compared to the theoretical predictions. Defects and grain boundaries in the film are vital in determining the optoelectronic properties of any material. This chapter is dedicated to unveil the energy levels of various defects / impurities in the energy gap of SnS thin films and their origin.

In the present study, PL technique was used for defect level analysis considering its immense potential in the field.

PL analysis was carried out using an indigenously developed setup. He-Ne laser (Melles Griot; 632.8 nm, 15 mW) with a spot size of 0.6 mm was used to excite the sample. For low temperature PL measurements, the sample was mounted on the cold finger of liquid helium cryostat (Janis Research Company CCS 100/202) and cooled down to 12 K. The temperature was controlled to an accuracy of ±1 K

using Lakeshore temperature controller (321 Auto tuning). Low temperature PL measurements of all samples were restricted to the range 12 K- 200 K. Variation of PL intensity was studied by varying the excitation power from 4 to 12 mW/cm^2 with the help of neutral density filters. For all PL measurements, SnS samples of area 1 cm × 1 cm were used. PL spectra were recorded using spectrophotometer (Ocean Optics NIR512) having thermoelectrically cooled InGaAs array detector and interfaced to the computer via custom made software "OOI base 32". A brief account on the theory behind the technique and the experimental setup has been described in chapter 2.

5.2 Results and discussions

Some of the opto-electronic and structural properties of the pristine SnS films have been recalled in Table 5.1. A thorough analysis of the sample was done using PL.

Table 5.1: The physical properties of the pristine SnS film.

Sl. No	Property	Value
1	Band gap	1.33 eV
2	Absorbance	10^5 / cm
3	Thickness	800 nm
4	Structure	Herzenbergate orthorhombic crystal structure with prominent orientation along (1 1 1) plane.
5	Sn/S ratio	1.05
6	Morphology	Needle-like

5.2.1 Unveiling the position of defect levels

Room temperature PL spectrum of the SnS thin film is depicted in Figure 5.1. Two emissions could be recorded- one at 1.09 eV and another low energy peak, which can be resolved in to two distinct emissions at 0.75 eV and 0.76 eV respectively.

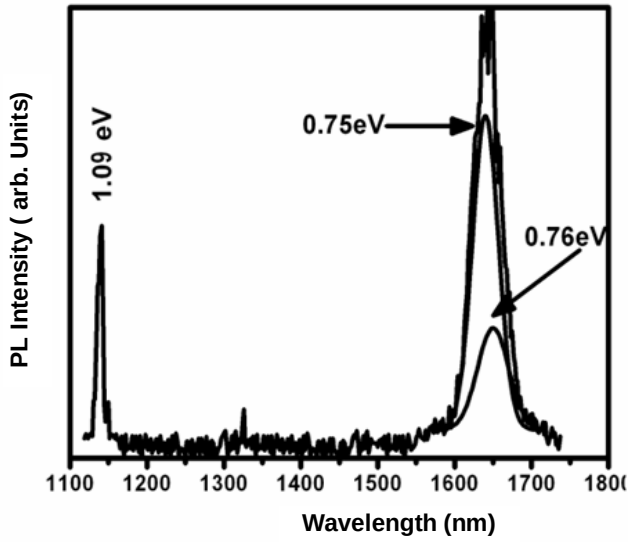

Figure 5.1: Room temperature PL spectra of SnS film.

To begin with, we focus on the emission at 1.09eV. This emission might probably be due to a transition from

1) a shallow donor to an acceptor,
2) conduction band (C.B) to acceptor or
3) a donor to valence band (V.B).

Type of radiative recombination, (i.e., whether it is due to Donor-Acceptor pair (DAP) transition, or free to bound transition), can be realized by studying the variation of PL intensity with excitation power. PL intensity (I) is found to obey a power law, given by

$$I=I_0P^{\gamma} \quad \text{——————————————————————————————} (5.1)$$

where I_0 and γ are constants and P is the excitation intensity per unit area. Slope of log (*I*)-log (*P*) plot gives the value of γ. From Figure 5.2, value of γ was estimated to be 0.73±0.02. Empirically, $\gamma < 1$ corresponds to 'free to bound' exciton or DAP recombination, $\gamma = 1$ for free to bound transitions and $1 < \gamma < 2$ for free or bound excitonic transitions. Thus, γ=0.73±0.02 indicates that the transition is DAP type [21, 22].

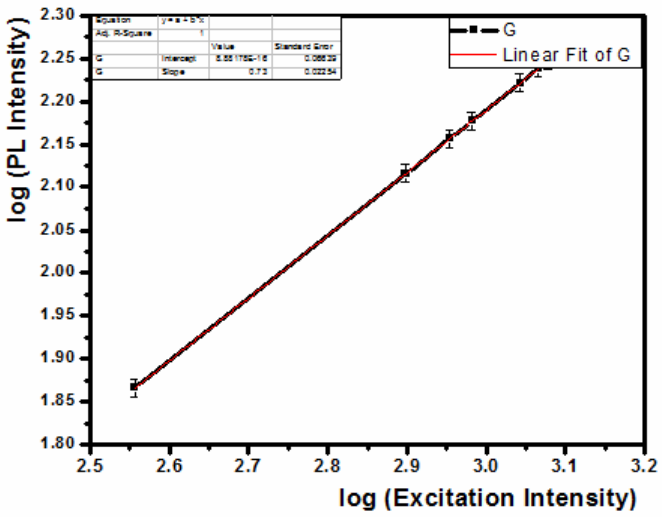

Figure 5.2: Variation of log(PL intensity) with log(excitation intensity).

The spectral resolution being high at liquid helium temperatures, low temperature PL measurements were performed on the sample and the emission at 1.09 eV was closely observed. PL spectrum of SnS thin film at different temperatures is shown in Figure 5.3.

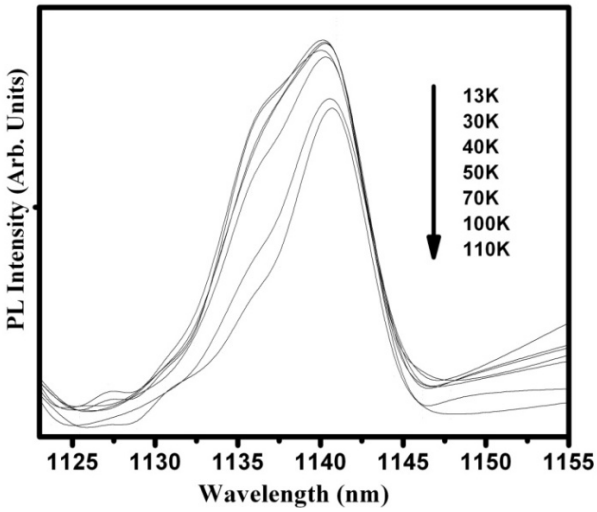

Figure 5.3: PL spectra of the pristine SnS sample at different temperatures.

Arrhenius plot or the plot between logarithmic value of integrated PL intensity and 1000/T can be used to calculate the PL quenching energy. The curve can be fitted using the relation

$$I(T)=I_0/(1+C\exp(-\Delta E/KT)) \quad \text{----------} \quad (5.2)$$

where I (T) is the PL intensity at temperature T, C is a measure of the capture cross section and ΔE is the activation energy [23].

In Figure 5.4 experimental fitting of the curve was done using Eq. (5.2) and the activation energy (ΔE) of the donor impurity obtained was 20 meV. Thermal ionization of the defect may be the reason for quenching of the emission at elevated temperature.

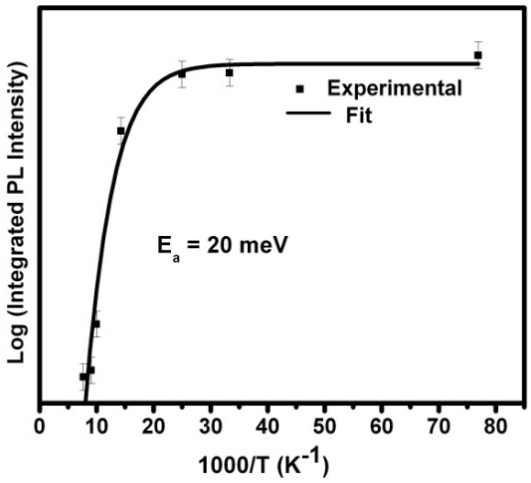

Figure 5.4: Arrhenius plot for calculation of activation energy.

Energy of the donor-acceptor pair (E_n) is related to the band gap (E_g) and depths of the donor and acceptor levels from conduction band and valence band, E_D and E_A respectively as [24]

$$E_n = E_g - (E_D + E_A) \quad \text{----------} \quad (5.3)$$

E_A can be obtained as 0.22 eV. Earlier reports on evaporated and PECVD deposited samples claim the presence of a deep acceptor level in the range 0.26 - 0.34 eV, from dark conductivity studies [25, 26]. It is generally observed that the activation energy very much depends on the thickness and preparation techniques [27]. Our observations related to the emission at 1.09 eV are consistent with the earlier reports. Band gap of the films (1.33eV) and the activation energy of the donor (20meV) prove that the emission at 1.09 eV is from a donor at 20 meV to an acceptor at 0.22 eV.

Based on our observations an energy band diagram for SnS film can be modelled partially as depicted in Figure 5.5.

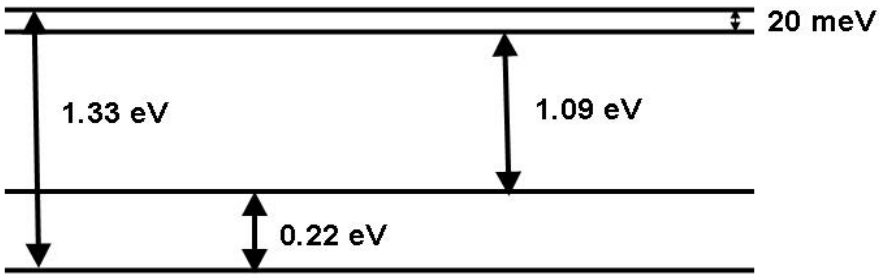

Figure 5.5: A crude band diagram modelled for SnS thin film.

Having obtained a schematic of the position of defects in the band gap, the next task is to identify the origin of these defects. Once the cause of these defect levels get revealed, it is easy to engineer the material so as to have the optimum properties for selection as an absorber layer in thin film solar cells.

5.2.2 Determination of origin of various energy levels

5.2.2.1 Identification of the Acceptor level

The particular crystal structure of SnS always allows lot of intrinsic cationic vacancies. The ionic radius of S (1.84 Å) is much larger than that of Sn (0.69 Å, for group VI coordination), which does not allow the formation of S interstitials [28]; instead Sn vacancies are possible in the lattice. Such Sn vacancies which are normally present in the lattice have been recognised as predominant acceptors in SnS thin films [29]. Our observations and the activation energy obtained for the acceptor level are quite consistent with earlier reports. Therefore, the acceptor level at 0.22 eV is assigned to Sn vacancies [25, 26].

5.2.2.2 Identification of the Donor level

The donor levels possible in this material may be created either due to S vacancies, or due to the presence of Sn^{2+} or Sn^{4+} ionized states of Sn [30].

In order to understand the origin of the donor level, detailed PL analysis was performed on the Sn diffused samples where, we purposefully have changed the Sn concentration in the material. Detailed description of the technique employed for the tin diffusion and the properties of the thus obtained sample has been elaborated in section 2.1.2 of the previous chapter.

Employing X-ray Photoelectron Spectroscopy (XPS), we have ensured that the evaporated thin layer of Sn has diffused uniformly throughout the depth of the film. There was neither any X-ray reflection peak corresponding to elemental Sn in the XRD pattern, nor any change in the optical band gap with respect to Sn diffusion (these results have been discussed in chapter 4).

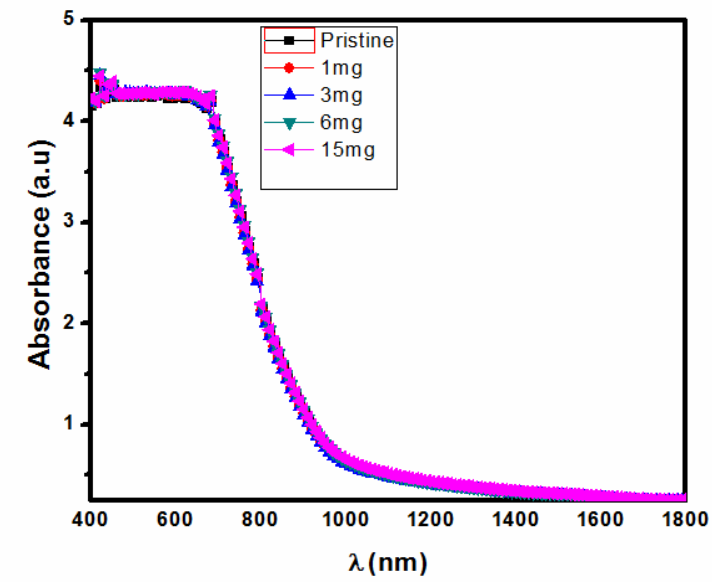

Figure 5.6: Absorption spectra of pristine and Sn-diffused samples.

Absorption spectra of the pristine and the Sn diffused samples are given in Figure 5.6. It is clear from the figure that there were no humps in the

absorption spectra corresponding to the possible free carrier absorption due to metal residues, if any, present in the sample.

PL spectra of the pristine as well as Sn diffused samples in the region 1120 nm – 1145 nm are shown in Figure 5.7. It can be seen that apart from the peak at 1.09 eV, there is another peak at 1.095 eV (1134 nm) gaining prominence with Sn diffusion. This emission (at 1.095 eV) has been analyzed in detail so as to understand role of Sn diffusion in SnS films. As with the emission at 1.09 eV, the variation in PL intensity of the emission at 1.095 eV of the optimum Sn diffused sample (SnS:6Sn) was recorded by varying the excitation intensity.

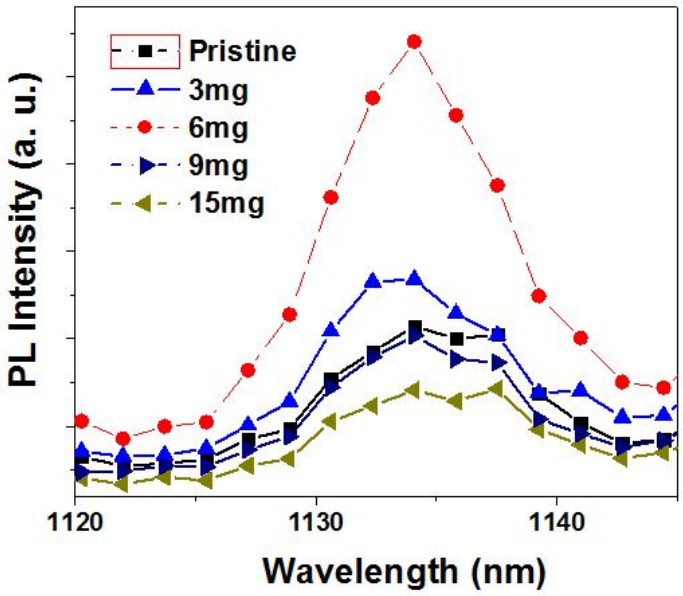

Figure 5.7: PL spectra of the pristine and the Sn diffused samples.

Figure 5.8 shows the PL signal intensity as a function of the excitation intensity of the SnS:6Sn sample, where it follows a linear

relationship. As for the previous case, performing a linear fit yielded the value of γ 0.80±0.02 indicating that this emission is a DAP transition.

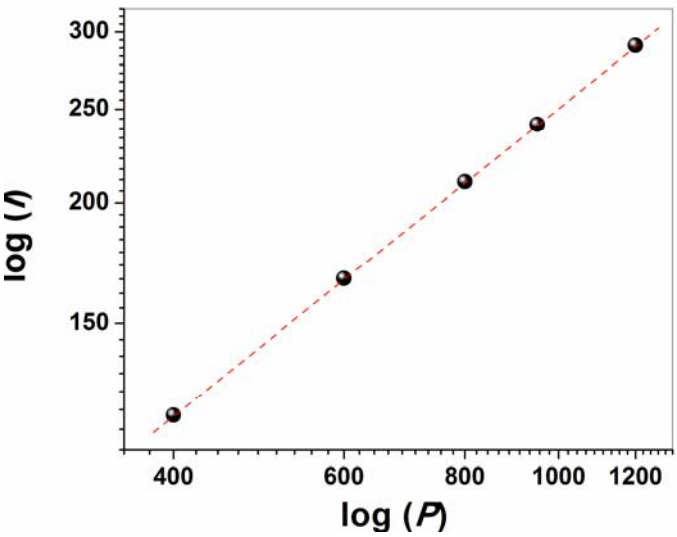

Figure 5.8: Variation of log(PL intensity) with log(excitation intensity).

In order to determine the position of the donor level in the band gap of the SnS film, temperature dependent PL analysis was carried out on the samples by first cooling it down to 12 K using the closed cycle He cryostat. Temperature of the sample was then raised at the rate of 2°C/min and recorded the PL spectra concentrating the emission at 1.095 eV at regular temperature intervals. Figure 5.9 shows the Arrhenius plot from which the activation energy was found to be 15±0.03 meV, i.e., lying 5 meV above the donor level at 20 meV.

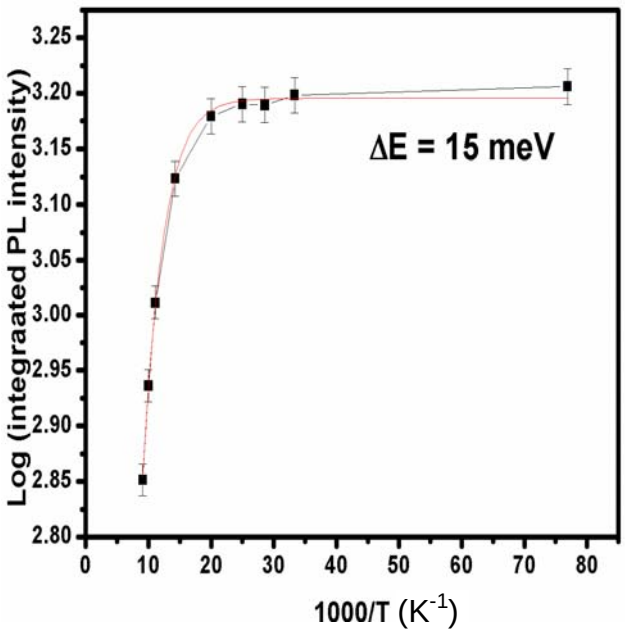

Figure 5.9: Arrhenius plot for the emission at 1.095 eV of SnS:6Sn sample.

This indicates that the two donor levels are there; one lies at 15 meV and the other at 20 meV below the conduction band minimum. Donor levels in SnS are due to the sulfur vacancies in SnS. The donor level created by sulfur vacancy in SnS is denoted by D_{Sn}^{2+} and that created by sulfur vacancies which otherwise bonded to Sn^{4+} ionized state is denoted by D_{Sn}^{4+}. Ghosh *et al.* has reported that D_{Sn}^{4+} has larger ionization energy than D_{Sn}^{2+} [31]. This conclusion has been supported by the following facts as well.

Variation of intensities of the two PL emissions (at 1.09 eV and 1.095 eV) with variation in Sn concentration in the material has an interesting trend. The intensity of the 1.095 eV emission, which is hardly present in the pristine film, increases with increase in the Sn concentration till SnS:6Sn and with further increase of the Sn concentration, it starts decreasing. This trend indicates that increase of Sn concentration beyond a certain threshold causes certain phase

change in the film. It has been reported earlier that as-prepared SnS films will contain traces of SnS_2 and Sn_2S_3 phases (in amorphous form) [32]. *Ex situ* Sn diffusion leads to the replacement of these impurity phases (SnS_2 and Sn_2S_3) by SnS phase as per the following reactions [33].

$$Sn + SnS_2 \rightarrow 2\,SnS$$

$$Sn + Sn_2S_3 \rightarrow 3\,SnS$$

In either of these reactions, both SnS_2 and Sn_2S_3 have Sn in 4^+ ionized states whereas in SnS, Sn is in the 2^+ state. Since the as-deposited SnS films contain intrinsic traces of SnS_2 and Sn_2S_3 phases, both Sn^{4+} and Sn^{2+} states are present in these films which give the two PL emissions at 1.09 eV and 1.095 eV respectively.

On diffusing Sn into SnS films, intensity of the emission at 1.095 eV increases as the SnS phase increases (due to enhancement of Sn^{2+} state); this continues till all the Sn^{4+} states are converted into Sn^{2+} as indicated in the reactions given above. Figure 5.7 shows that the SnS sample with 6 mg of Sn diffused (SnS:6Sn) has the highest PL peak at 1134 nm.

Employing XPS, we have already shown that the transition of SnS to Sn_2S_3 takes place at larger Sn concentrations (previous chapter). In light of this, the reduction of the PL intensity of the peak at 1.095 eV at larger Sn concentration can be explained as the phase transition from SnS to Sn_2S_3 and we can attribute the emission at 1.095 eV to be due to the transition from the donor level at 1.315 eV (D_{Sn}^{2+}) to the acceptor level at 0.22 eV (V_{Sn}).

5.2.2.3 Determination of origin of Trap level

The as-deposited SnS thin films exhibit another strong emission at 0.75 -0.76 eV. Figure 5.10 shows the PL emission from SnS film before and

after vacuum annealing. Interestingly, the emission vanished upon post-deposition annealing in vacuum (pressure~$2x10^{-5}$ Torr) at 150°C for 90 minutes. This indicates the removal of oxygen present in the sample, by vacuum annealing and hence the emissions may be due to the transition to strong trap level in the band gap due to the presence of oxygen.

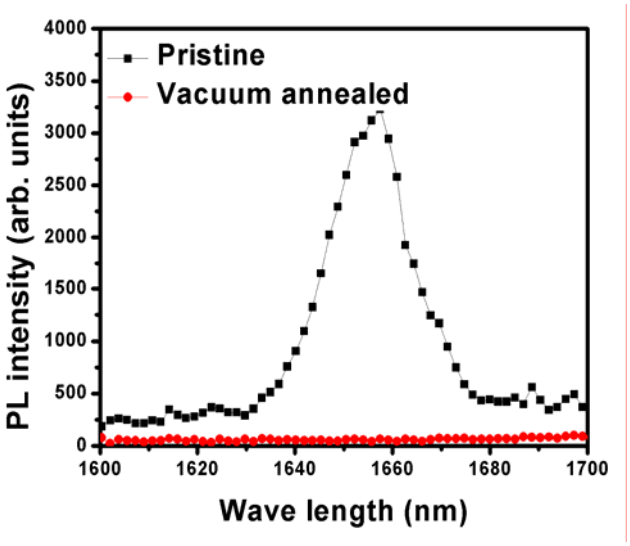

Figure 5.10: Room temperature PL spectra of the SnS sample before and after vacuum annealing.

The trap level may be due to oxygen sitting in the interstitial position or in the vacant lattice sites. PL emissions of pristine as well as Sn diffused samples were taken to probe this defect. Figure 5.11 shows PL spectra of the pristine and the Sn-diffused set of samples in the range 1600 nm to 1700 nm. It is clear that the intensity of PL emission decreased with increase in concentration of Sn diffused. So it is evident that oxygen may be sitting in the vacancy of Sn ($^{O}V_{Sn}$) and this has been reduced considerably with diffusion of Sn.

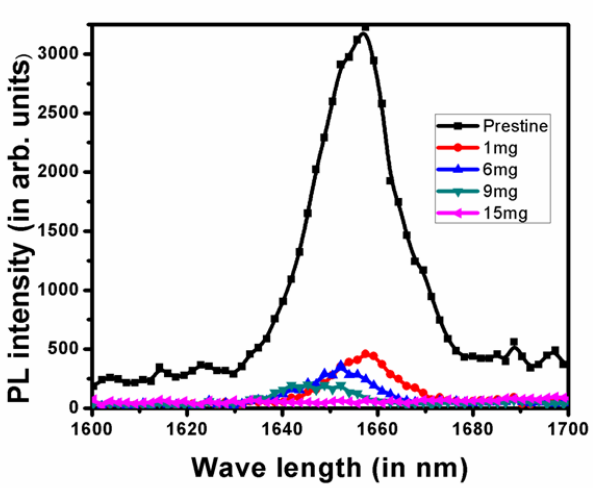

Figure 5.11: PL spectra of pristine and Sn diffused samples (SnS :1Sn to SnS:15Sn).

5.2.3 Determination of Work function

Kelvin Probe Atomic Force Microscopy (KPFM) image of the sample (Figure 5.12) was used to map the local surface potential of the sample, which is used to extract the work function of the sample [34]. Information regarding the work function of the material (separation between vacuum level and the Fermi level) is quite vital to model its energy level scheme.

With the platinum work-function of 5.1 eV, the surface potential calculated on the SnS grain was observed to be ~ 0.175 V. Based on the simple estimation of local surface potential difference, $\Delta SP = (\varphi_{tip} - \varphi_s)/e$, the work function of SnS films φ_s was calculated to be 4.92 eV, which means that the Fermi level of the material lies 4.92 eV below the vacuum level.

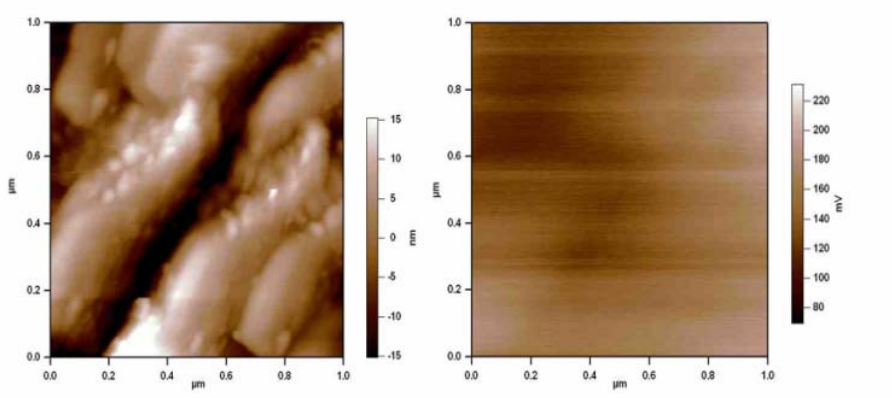

Figure 5.12: (Left) AFM topography of SnS pristine film deposited on glass substrate. Image size was 1 µm × 1 µm. (Right) KPFM topography of SnS pristine film, average surface potential was measured as 0.175 V, from which, the work-function of SnS was estimated as 4.92 eV.

5.2.4 Modelling of comprehensive energy band scheme

With the help of the present study and also using the data from the earlier reported works [35, 36] a comprehensive band diagram for the SnS can be modelled as depicted in Figure 5.13.

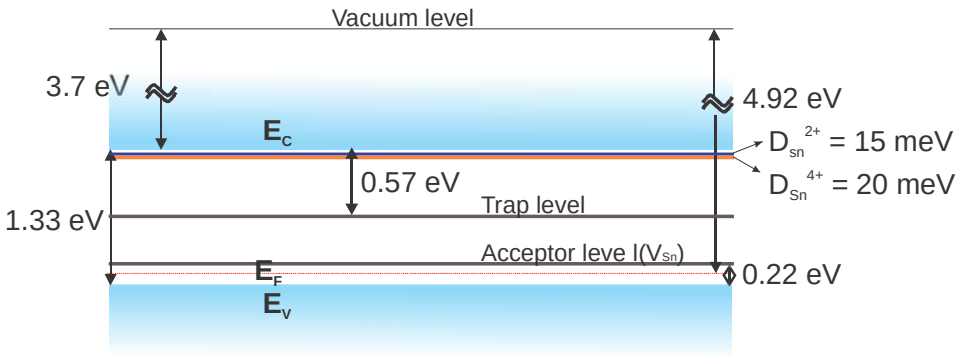

Figure 5.13: The proposed band diagram of the SnS thin films showing the different defect levels.

This model helps in explaining the properties exhibited by SnS films.

Generally it is observed that only highly resistive film exhibit high photosensitivity. But the Sn-doped films showed higher photosensitivity compared to that of the pristine sample, even though their resistivity was quite low. This anomaly in the photosensitivity can be well explained using the band diagram as given below. Enhanced photosensitivity of Sn diffused sample must be due to the enhancement in minority carrier (electrons) concentration. In p type SnS, production of electrons in conduction band occurs through (1) thermal excitation from the donors, (2) pumping of electrons from the acceptor level at 0.22 eV and (3) the usual band to band excitation. But in the case of the Sn-diffused samples, it has been observed that the trap level present at the mid band gap region (due to the presence of oxygen) has been removed as evident from the reduction in intensity of PL emission at 0.75-0.76 eV (Figure 5). Thus Sn diffusion should have considerably reduced the trapping and / or recombination of minority carriers, leading to very high photo current and hence high photo sensitivity.

5.3 Trial on junction fabrication

The major aim of developing SnS thin films by cost effective and easily scalable deposition means is to use it for thin film solar cell application as an absorber layer. This section demonstrates the potential of SnS films developed in the present work in forming hetero junction with various window layers.

We used two different materials; 1) In_2S_3 and 2) SnS_2, in order to fabricate photovoltaic junction with SnS. In_2S_3 have been selected considering its wider band gap, n-type conductivity, non toxicity and the

easiness of deposition. To the best of our knowledge, nobody have so far investigated or fabricated In_2S_3/SnS heterojunction. Moreover, the deposition conditions for this material intended for fabrication of with the intension of using it as window layer for CIS based cells have previously been optimized in our lab. Now as far as SnS_2 is concerned, it possesses many superior optoelectronic properties described in chapter 1 because it belongs to the 'tin chalcogenide family'. We also could obtain almost single phase SnS_2 as a side result while optimizing substrate temperature and atomic ratio of precursor solution for the deposition of SnS thin films. Therefore, we thought of using this SnS_2 also as the window layer to fabricate hetero junction with SnS.

Superstrate configuration was used for the cell fabrication. i.e., illumination was through the substrate-side which in turn imposed the condition that the substrate must be transparent as well as conducting. Hence, ITO coated glass was used as the substrate. Junction was fabricated by depositing In_2S_3 (or SnS_2) layer first and SnS layer over that, (both through CSP method), on ITO coated glass. Silver electrodes were then coated using vacuum evaporation.

Interestingly we could observe that for the ITO/InS/SnS, open-circuit voltage (V_{OC}) increased and short circuit current density (J_{SC}) decreased with the increase in the thickness of the absorber layer. A moderate performance (177 mV, 1.1 mA/cm^2) was achieved when the absorber layer thickness is 800 nm. The major problem with these cells was the very high value of the series resistance (~7535 Ω.cm^2). Since there is little report about heterojunction formed by thin films of In_2S_3 and SnS, it is not possible to compare our results. However, these results obtained here

open the opportunity to study this kind of junctions. More detailed analysis must be done in order to understand the electrical transport trough the device and, at the same time, to improve the quality of these diodes for better performance. Also proper contact electrodes have to be selected so as to reduce the series resistance.

Trial junction was also fabricated using SnS_2 window layer. The main advantage here is that, we could deposit both the window and the absorber layer sequentially using the same precursor solution by adjusting the substrate temperature. The only thing we have to do is just to change the substrate temperature (460^0C for SnS_2 and 375^0C for SnS).

In this case also we could fabricate p-n junction with knee voltage greater than 800 mV. We could also obtain clear photovoltaic shift on illumination in the fourth quadrant of the graph. The V_{oc} and J_{sc} values of the device were 185 mV and 0.84 mA/cm^2 respectively.

5.4 Conclusions

Presence of donor and acceptor levels of SnS films have been successfully unveiled using PL technique. The two nearby donor levels are identified as due to sulfur vacancies in SnS (with activation energy of 15 m eV) and that in other binary sulfides of tin whose oxidation state is 4+ (with activation energy of 20 meV) which may present as inevitable contaminant in SnS. Origin of the emission at 0.75 eV & 0.76 eV has been attributed to transition from CB to the mid band gap trap level created by O_2 contaminant. A detailed band diagram for SnS has been proposed in this work outlaying the different donor and acceptor levels. Anomalous properties exhibited by Sn-diffused SnS films have been successfully explained in this chapter with the help of the proposed energy level

scheme. Certain defects may come handy for photovoltaic applications and hence unveiling the defects present in SnS films is highly relevant as it is used as absorber layer in thin film solar cells. The immense potential of PL technique in analyzing the different defect levels present in the material was also established through the present work.

The feasibility of SnS absorber layer developed in the present work, for fabricating photovoltaic junction has been demonstrated successfully. Trial junctions were fabricated with the structure, ITO/n-type Window layer/p-SnS/electrode. The work was found to be promising as we could obtain photovoltaic shift when illuminated with white light.

References

[1] T. H. Gfroerer, Photoluminescence in analysis of surfaces and interfaces, Encyclopedia of analytical chemistry Editted by R. A. Mayers John Wiley & Sons Ltd. Chichester (2000) 9209.

[2] R. Jayakrishnan, K. G. Deepa, C. S. Kartha, K. P. Vijayakumar, J. App. Phys **100** (2006) 046104.

[3] D. R. Vij, Luminescence of solids Plenum Press New York (1998).

[4] Elliot, Phys. Rev. **108** (1957) 1384.

[5] Zott, K. Leo, M. Ruckh, H. W. Schock, Appl. Phys. Lett. **64** (1994) 1027.

[6] R. Jayakrishnan, Defect analysis of semiconductor thin films for photovoltaic applications using photoluminescence and photo-conductivity Ph.D thesis Cochin University of Science and Technology 2008.

[7] Garcia-Garcia, J. Gonzalez-Hernandez, Mendoza-Alvarez, E.L Cruz, G. Contreras-Puente, J. Appl. Physics **67** (1990) 3810.

[8] J. Hollingsworth, R. Sites, J. Appl. Physics **53** (1982) 5357.

[9] A. Komiya, I. Yamaguchi, Umebu, Solid state Electronics **29** (1986) 235.

[10] H. J. Frtenk, W. Kulisch, R. Kassing, in: Proceedings of SPIE **1144** 250 (1989).

[11] V. Yu. Timoshenko, J. Rappich, Dittrich, Appl. Surf. Sci. **123/124** (1998) 111.

[12] S. K. Krawczyk, M. Garrigues, H. Bouredoucen, J. Appl. Phys. **60** (1986) 392.

[13] Z. Zhu, H. Yoshihara, T. Yao, J. Cryst. Growth **138 (**1994) 619.

[14] L. W. Molekamp, H. F. J. Van't Blik, J. Appl. Phys. **64** (1988) 4253.

[15] P. Pramanik, P. K. Basu, S. Biswas Thin Solid Films **150** (1987) 269.

[16] N. K. Reddy, Y. B. Hahn, M. Devika, H. R. Sumana, K. R. Gunasekhar, J. Appl. Phys. **101** (2007) 093522.

[17] J. J. Loferski, J. App. Phys. **27** (1956) 777.

[18] K. T. R. Reddy, N. K. Reddy, R. W. Miles, in: proceedings of the 14th international photovoltaic science and engineering conference, Bangkok, Thailand, 627 (2004).

[19] H. Noguchi, A. Setiyadi, H. Tanamura, T. Nagatomoto, O. Omoto, Sol. Energy Mater. Sol. Cells **35** (1994) 325.

[20] M. Sharon, K. Basavaswaran, Sol. Cells **25** (1998) 97.

[21] Y. Miyamoto, K. Tanaka, M. Oonuki, N. M. Oritake, H. Uchiki, Jpn. J. Appl. Phys. **47** (2008) 596.

[22] S. Ozaki, S. Adachi, J. App. Phys. **100** (2006) 113526.

[23] Dingle, J. Appl. Phys. **81** (1997) 1442.

[24] K. Tanaka, Y. Miyamoto, H. Uchiki, K. Nakazawa, H. Araki, Phys. Status Solidi A **203** (2006) 2891.

[25] H. Noguchi, A. Setiyadi, H. Tanamura, T. Nagatomoto, O. Omoto, Sol. Energy Mater. Sol. Cells **35** (1994) 325.

[26] A. S Juarez, A. Tiburcio-Silver, A. Ortiz, Thin solid films **480-48**1(2005) 452.

[27] M. Devika, N. K. Reddy, D. S. Reddy, S. V. Reddy, K. Ramesh, E. S. R. Gopal, K. R. Gunasekhar, V. Ganesan Y. B Hahn, J. Phys. Condens. Matter **19** (2007) 306003.

[28] Yu Wang, Hao Gong, B. Fan, Guangxia Hu, J. Phys. Chem. C **114** (2010) 3256.

[29] M. Ristov, G. Sinadinovski, I. Grozdanov, M. Mitreski, Thin Solid Films **173** (1989) 53.

[30] R. A. Castro, S. A. Nemov, P. P Seregin, Electronic and Optical Properties of Semiconductors **40** 898 (2006).

[31] B. Ghosh, R. Roy, S. Chowdhury, P. Banerjee, S. Das, Appl. Surf. Sci. **256** (2010) 4328.

[32] W. Martienssen, H. Warlimot (editors) Springer Hand book of condensed matter and materials data vol 1 Springer publications Germany (2000).

[33] V. Piacente, S. Foglia, P. Scardala J. Alloys Compounds **177** (1991) 17.

[34] D. S. H. Charrier, M. Kemerink, B. E. Smalbrugge, T. de Vries, and R. A. J. Janssen, ACS Nano 43, (2010) 541.

[35] M. Ichimura, Solar Energy Mater. Sol. Cells **93** (2009) 375-378.

[36] A. R. H. F. Ettema, R. A. de Groot, C. Hass, T. S. Turner, Phys. Rev. B: Condens. Matter **46** (1992) 7363.

Chapter 6

CONCLUSIONS & FUTURE OUTLOOK

Contents

6.1 Summary and general Conclusions

This Thesis concerned with a novel compound semiconductor material, that has a great potential for use in photovoltaic energy system. SnS has been identified as one of the best absorber layer material for heterojunction thin film solar cells. The favorable electrical and optical properties make this metal chalcogenide most promising in the field. SnS belongs to IV–VI group that exhibits orthorhombic structure. It has a suitable optical band gap of 1.33 eV and large absorption coefficient of over 10^4 cm^{-1}, above the band gap energy. In addition, it has the added advantage of abundant constituent elements. SnS grenerally do not pose any health and environmental hazards. However, the reported data indicates that physical characteristics of this material have not been studied extensively in relation to their photovoltaic application.

The thesis mainly concentrates on the development of SnS thin films having optimum properties for absorber layer in thin film solar cells. Deposition parameters were fully optimized for obtaining phase-pure, device quality SnS thin films out of CSP technique. Several properties of the films like dark conductivity, photoconductivity/photosensitivity and

band gap were engineered by in-situ and ex-situ means. Detailed defect level analysis of the SnS thin films were performed by using photoluminescence technique. An energy band structure for SnS thin films has been suggested, outlaying the origin of various defect levels. In order to demonstrate the potential of the developed SnS thin films, some initial trials on fabrication of photovoltaic junctions were also performed using In_2S_3 and SnS_2 as the window layers and these studies indicated positive results. The proposed aim of the thesis was accomplished in three different phases.

In the first phase, the deposition parameters were optimized for fabrication of stoichiometric SnS films that can be used as p-type, direct band gap absorber layer with very high absorption coefficient. Band gap engineering of phase-pure SnS thin film was done in the temperature region 350°C–400°C. This can avail us the flexibility to use both low and high band gap SnS films in PV applications. Interestingly n-type SnS films could be obtained when content of cationic precursor is higher than that of the sulfur precursor in spray solution. As the deposition temperature is same for the deposition of both n and p-type SnS films, it is possible to have sequential deposition of n and p-type layers for possible fabrication of SnS homojunction. Highly photosensitive SnS films which had high photocurrent value, can also find application as smart material.

The second phase was dedicated in enhancing the opto-electronic properties of the SnS films. An innovative ex-situ Sn diffusion process was employed to reduce the resistivity of SnS films. The unavoidable impurity of Sn–O–S phase on the surface was removed completely through the diffusion of Sn. Carrier concentration was also found to be enhanced by an

order. SnS:6Sn sample, with a 3.63 nm thick Sn layer diffused into the SnS matrix, was found to be optimum and it had the lowest resistivity together with the higher photosensitivity. The major advantage of Sn diffusion technique is that we could obtain low-resistive (resistivity ~2 Ω.cm) as well as highly photosensitive samples Sn diffusion, without affecting other photovoltaic properties of the material (Eg. Optical b and gap).

Since ex-situ Sn diffusion involves post deposition treatments which in general is not suitable for device level applications, our next aim was to enhance the opto-electronic properties through an in-situ process. For this, the significance of pH of the precursor solution in determining the structural, morphological and optoelectronic properties of SnS film was evaluated. It was observed that the crystallinity of the films has a definite correlation with pH of the precursor solution and an optimal pH exists for the optimal crystallinity. Crystallinity of the films was best for a pH of 2.0 and the electrical conductivity was also maximum for this pH value. The lowest resistivity obtained by controlling the pH was about three orders lower than that of the pristine sample. This film exhibited maximum photosensitivity as well. The band gap of the films can also be engineered by controlling pH of procures solution. Most importantly, these superior properties can be achieved without employing any post deposition treatments and hence it is quite useful for low-cost thin film photovoltaic technology.

The third and the final phase deals with the identification of the origin of various defects present in the sample. Presence of donor and acceptor levels of SnS films have been successfully unveiled using PL

technique. The two nearby donor levels are identified as due to sulfur vacancies in SnS (with activation energy of 15 meV) and that in other binary sulfides of tin whose oxidation state is 4þ (with activation energy of 20 meV) which may present as inevitable contaminant in SnS. Origin of the emission at 0.75 eV & 0.76 eV was attributed to transition from Conduction Band to the mid band gap trap level created by O contaminant. A detailed band diagram for SnS was proposed in this work outlaying the different donor and acceptor levels. Some of the anomalous properties exhibited by Sn-diffused SnS films have been successfully explained with the help of the proposed energy level scheme. Certain defects may come handy for photovoltaic applications and hence unveiling the defects present in SnS films is highly relevant as it is used as absorber layer in thin film solar cells. The immense potential of PL technique in analyzing the different defect levels present in the material was also established through the present work.

After the successful completion of the three phases of the research work, the feasibility of the developed SnS absorber layer, for fabricating photovoltaic hetero-junction was demonstrated by fabricating trial junctions with the structure, ITO/n-type Window layer/p-SnS/electrode. As the suitable window layers for the SnS based thin film solar cells, SnS_2 and In_2S_3 were chosen. Thickness of the SnS layer was varied. Substrate temperature was found to be more critical for depositing SnS_2 films over ITO. The work has been found to be promising as we could obtain photovoltaic shift when illuminated with white light.

6.2 Future Prospects

Natural progression of present research would be its application in solar cell fabrication. Obviously our next aim is to improve the performance parameters of the device. Optimization of the deposition conditions to deposit window layer of required thickness and conductivity, optimizing the thickness as well as photosensitivity of absorber layer and selection and optimization of the deposition condition of the contact electrode are the major areas in which we have to work on in future to fulfill our aim. Once these are completed, works have to be done to improve the efficiency of the device by modifying the interface properties and also to modify the spary system for depositing the cells through a 'line process'.

In the present work, we have used imported ITO coated glass for cell fabrication. Indigenous development of transparent conducting oxide layer like Al: ZnO or F:SnO_2 will help in the development of cost-effective and all sprayed solar cells. Another scope of the work is to try nano-crystalline SnS films in third generation photovoltaics by using it in quantum dot sensitized solar cells (QDSSC).

Present work is only a small step towards achieving a greater goal: *development of an efficient, eco-friendly and cost-effective 'all sprayed' thin film solar cell*. Lot of efforts has yet to be put forth for the fulfillment of such a vision and our group is continuing the research works in this direction, with a well focused aim, to make this initiative a reality.

.....ꕥ.....